공학박사학위논문

고분자 전해질막 연료전지의 3 차원 양극 유로 설계에 따른 성능 변화 연구

Studies on 3D Structure as Cathode Flow Channel of Polymer Electrolyte Membrane Fuel Cell with Geometric Parameter Changes

2022 년 8 월

서울대학교 대학원

기계항공공학부

최 성 훈

고분자 전해질막 연료전지의 3 차원 양극 유로 설계에 따른 성능 변화 연구

Studies on 3D Structure as Cathode Flow Channel of Polymer Electrolyte Membrane Fuel Cell with Geometric Parameter Changes

지도교수 김 민 수

이 논문을 공학박사 학위논문으로 제출함

2022 년 4 월

서울대학교 대학원

기계항공공학부

최 성 훈

최성훈의 공학박사 학위논문을 인준함

2022 년 6 월

위 원 장 : _____ **(인)**

부위원장 : _____ **(인)**

위 원 : _____ **(인)**

위 원 : _____ **(인)**

위 원 : _____ **(인)**

Abstract

Studies on 3D Structure as Cathode Flow Channel of Polymer Electrolyte Membrane Fuel Cell with Geometric Parameter Changes

Sung Hoon Choi
Department of Mechanical and Aerospace Engineering
The Graduate School
Seoul National University

Bipolar plate design in PEMFC can change performance, fuel efficiency, cell and stack duration and manufacturing costs. According to unique characteristics of chemical reaction along the fuel cell, geometric characteristics of flow channel have to be separately studied to develop highly efficient and durable fuel cell system. Starvation of reactants and severe water accumulation can be major causes operating failure and performance degradation. Therefore efforts for enhancing mass transfer capability with moderate pressure drop are necessary. Since water accumulation and dead-zone

formation are normally severe along the cathode flow channel, design of cathode flow channel was examined through experimental and numerical methods.

In this study, modification in flow channel design was investigated utilizing 3D printed structure as flow channel in unit fuel cell. Selecting two effective geometric parameters, channel width and bottom-rear channel depth, and simplifying curvature of complex design, various types of 3D structure were manufactured. To observe effect of modification separately, width varied and slope varied arrangements were tested individually, finding the best arrangement of each strategy. Combining two strategy into one arrangement, the best arrangement showed 13.0% higher maximum power density compared with uniform arrangement. Compared with 3D printed parallel flow channel which had the same structure-gas diffusion contact area, the best arrangement showed 39.4% higher maximum power density. Moreover, even if uniform arrangement of 3D structure showed 10.4% higher performance in unit cell. EIS data also showed that non-uniform arrangement had lower concentration loss.

To expose detail causes of performance enhancement, CFD analysis using ANSYS FLUENT was conducted along a single row of 3D structure. Replacing 3D structure near outlet to differently designed structure, various patterns tested

in experimental study were analyzed through CFD. Narrow channel width with thicker wall thickness showed lower contact resistance and enhanced overall velocity, however, narrowed interface between GDL and reactants flow lowered mass transfer though porous structure of GDL. Sloped structure separately enhanced velocity, especially perpendicular with GDL surface, efficiently enhancing mass transfer capability. Analysis with porous structure implied that velocity fluctuation along the channel and on surface of gas diffusion layer could enhance mass transfer. Comparing with experimental results, overall velocity could be positive with water removal and although current density distribution was not be measured in experiment, performance uniformity could be measured through CFD analysis and direction of arrangement was revealed to have significant effect to performance uniformity.

To suggest advanced non-uniform arrangement, CFD analysis for larger domain was performed. Geometry modification along the width direction targeting potential dead-zone formation was applied, reducing flow resistance at side of the active area by making difference in wall thickness. Firstly, through CFD analysis, uniformity enhancement through width direction varied non-uniform arrangement was confirmed. Finally, durability test with performance measurement was conducted. The results showed that arrangement with width and length direction non-uniformity showed the highest durability compared

with the other. Maximum power density decrease ratio was reduced from 12.4% to 8.6% and high frequency resistance increase ratio was reduced from 18.0% to 12.9% after 60000 cycles of accelerated stress test.

Keyword: Polymer electrolyte membrane fuel cell, Metallic bipolar plate, Non-uniform arrangement, CFD analysis, Performance enhancement, Durability test

***Identification number*: 2017-26437**

Contents

List of Figure

List of Tables

Nomenclature

ϕ	electric potential [V]
η	overvoltage [V]
W_{comp}	compression work [W]
ϵ_{comp}	compression efficiency
c_p	specific heat [J/kg-K]
T	temperature [K]
P	pressure [N/m^2]
κ	electrical conductivity [S/m]
J	volumetric transfer current [A/m^3]
ς	specific active surface area [1/m]
j	exchange current density per active surface area [A/m^2]
c	species concentration [$kmol/m^3$]
γ	concentration exponent
α	transfer coefficient
F	Faraday constant [C/mol]
R	Ideal gas constant [J/mol*K]
S	source term
M	molecular weight [kmol/kg]
K	intrinsic permeability [m^2]
s	volume fraction of liquid water
μ	viscosity [kg/m-s]
σ	surface tension [N/m^2]

θ_c	contact angle [°]
ε	porosity
C_r	condensation rate constant [1/s]
D	diffusion coefficient [m^2/s]
λ	water content
n_{drag}	osmotic drag coefficient
M_{mem}	equivalent weight of dry membrane [kg/kmol]
A	active area [m^2]
SR	stoichiometric ratio
ρ	density [kg/m^3]
H_c	thickness of flow channel [m]
H_D	thickness of gas diffusion layer [m]
u	velocity [m/s]
m_f	mass fraction

Subscript

cell	cell
open	open-circuit
act	activation
ohmic	ohmic
conc	concentration

0	reference
e	electric
ion	ionic
a	anode
c	cathode
react	reaction
L	latent
l	liquid water
wv	water vapor
sat	saturation
cap	capillary
R	reactants
*	catalyst layer

Chapter 1. Introduction

1.1. Background of the study

As global climate change has been intensified recently, enormous demands for clean energy conversion systems are emerging to reduce greenhouse gas emission such as carbon dioxide [1]. Sunlight generation, wind power, wind power and tidal power systems are one of the popular examples of environmental friendly electric power generating systems, however, proper storage means are needed to use electric power at anytime and anywhere. In this circumstances, hydrogen is one of the best methods to keep the electric energy [2].

For utilizing hydrogen gas to make electricity, polymer electrolyte membrane fuel cell (PEMFC) is being commercialized widely. From a small size of drone to off-grid energy system, PEMFC can be widely used due to its high efficiency, high-power density and low or zero emissions with moderate operating temperature and pressure range [3]. **Figure 1.1** shows how PEMFC operates.

PEMFC has various components such as membrane electrode assembly (MEA), gas diffusion layer (GDL), bipolar plate (BPP), gasket and end plate. Each of these component play a key role in generate electricity, transporting

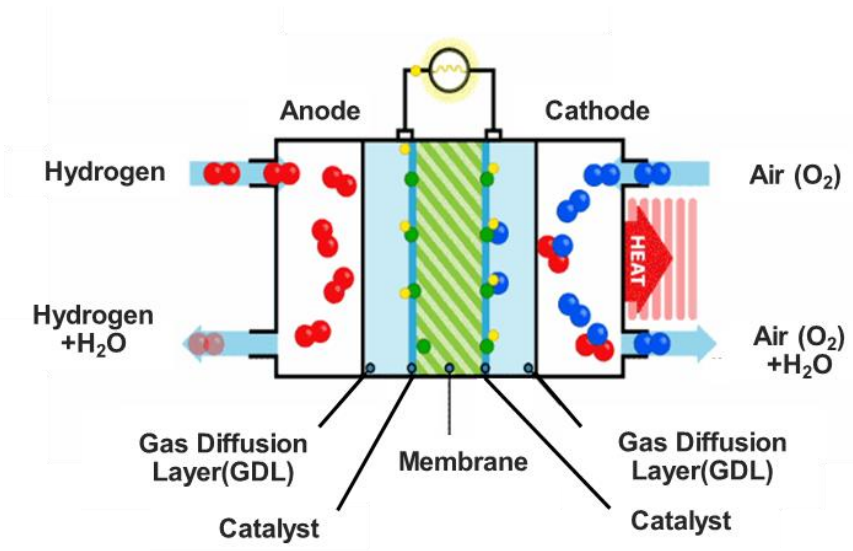

Anode $H_2 \rightarrow 2H^+ + 2e^-$

Cathode $O_2 + 4H^+ + 4e^- \rightarrow 2H_2O$

Over all $2H_2 + O_2 \rightarrow 2H_2O$

Figure 1.1 Schematic of the PEMFC

and distributing reactants and products, preventing flow leakage and supporting the structure of PEMFC. Material, design and sizes of these components can affect to PEMFC's performance, durability, manufacturing and operating costs. Since driving conditions of PEMFC can be varied under the specific circumstances, many researches have been undergone to develop ideal PEMFC, targeting various applications and driving conditions.

Securing high performance of PEMFC has been the most important issues to make hydrogen energy used wider. **Figure 1.2** shows I-V curve of two different PEMFCs which have different performance. Dashed line indicates poor performance since it shows lower voltage under the same current densities, compared with the solid line. When the current density rises, the voltage goes down. These characteristics are based on electro-chemical theory about fuel cell [4]. If the PEMFC was designed poorly, voltage would goes down faster. This voltage drop is called overvoltage losses. Therefore, decreasing overvoltage losses of PEMFC is the most important way to enhance performance of the PEMFC.

Overvoltage can be explained by Eq. (1.1).

$$\phi_{cell} = \phi_{open} - \eta_{act} - \eta_{ohm} - \eta_{conc} \qquad \text{Eq. (1.1)}$$

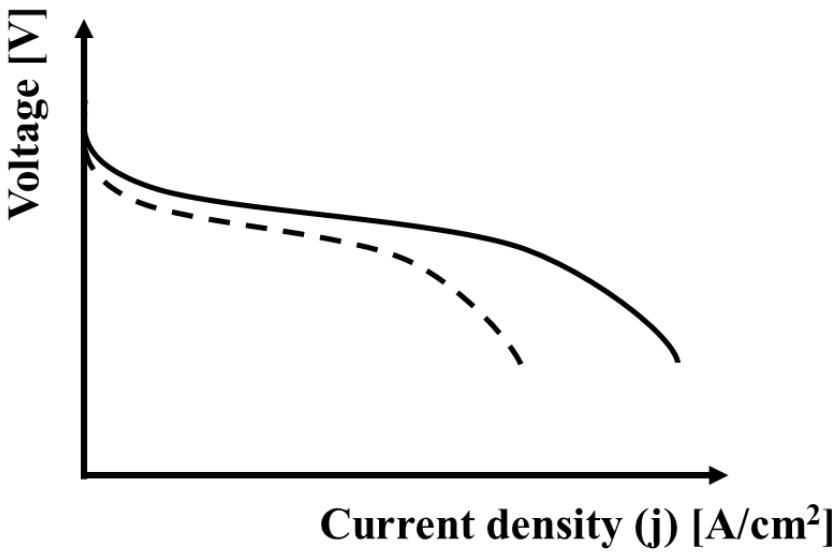

Figure 1.2 I-V curve of PEMFC

In Eq. (1.1), ϕ_{cell} is cell voltage and ϕ_{open} is open-circuit voltage, which is generated under zero current. Next, η_{act}, η_{ohm}, and η_{conc} represent activation loss, ohmic loss and concentration loss respectively. Activation loss is related with activation energy. For electrochemical reactions on catalyst surface, certain amount of energy is required to overcome the activation energy. To reduce activation loss, proper catalyst should be developed. Ohmic loss is related with charge transport. Conductors of fuel cell are not ideal, so they have intrinsic resistance. Therefore, through charge transport process, voltage loss can arise. In this case, reducing thickness of membrane and increasing electrical conductivity can be tried to alleviate the ohmic loss. Lastly, concentration loss is related with mass transfer of reactants and products such as hydrogen, oxygen and water. Along the flow direction, concentrations of reactants are reduced due to chemical reaction. Moreover, accumulated water, the products of electrochemical reactions, can lower reactants mass transfer to catalyst surface by blocking. Compared with the other overvoltage losses, concentration loss is mainly dominant under high current density operation. Thus, reducing concentration loss is directly connected with developing high performance PEMFC.

To overcome this issues, many researchers tried to develop ideal bipolar plates which include flow channel since geometric and configuration

characteristics of flow channel are strongly related with mass transfer of reactants and products [5]. According to mass transfer capability, reactant transport, water management, efficiency and even durability of PEMFC can be changed. As a result, developing ideal bipolar plate for PEMFC is one of the most important assignment to commercialize hydrogen energy more globally.

1.2. Literature survey

1.2.1. Conventional flow channel design

Understanding conventional flow channel design can be a good start to developing a novel flow channel design. There are three representative conventional flow channel: parallel, serpentine and interdigitated [6]. **Figure 1.3** shows their structures. Parallel channel has multi-channel structure but single inlet, targeting to distribute flow to each channel. It has simple design and shows low pressure drop, however, when poorly designed, severe flow non-uniform distribution can occur. Serpentine channel can overcome this disadvantage. With a single channel, reactant and product gas or liquid are forced to flow along the channel. Due to this characteristic, non-uniform distribution of inner flow can be solved, however, serpentine channel shows comparatively high pressure drop. Interdigitated flow channel shows the highest pressure drop among the conventional flow channel. Disconnected flow channel design force under-rib convection. Reactants gas have to flow under the rib, namely through gas diffusion layer. This can be effective in terms of removal water droplet through GDL.

Many studies about these conventional flow channel have been conducted so far for optimizing their geometry and configuration. Channel width, depth

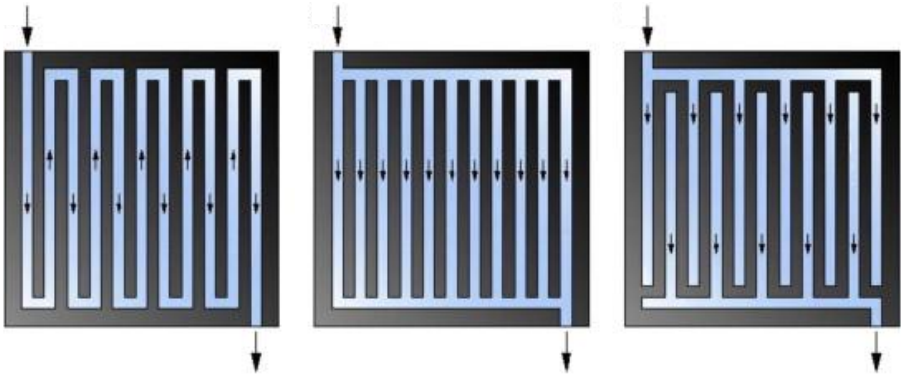

Figure 1.3 Design of conventional flow channel [6]

and length were varied and various configurations were studied by experimental and numerical methods. Bachman et al. [7] conducted experimental study, varying the length of parallel flow channel from 5 cm to 25 cm. Due to higher pressure drop along the longer channel, water flooding was predicted to be removed easier when the longer channel length was chosen. Chen et al. [8] inserted porous media along the parallel channel and performed experimental study. Although pressure drop became higher when porous media was inserted, two phase flow mal-distribution was alleviated. Targeting portable PEMFC, Henriques et al. [9] alerted cathode flow channel geometry for enhancing fuel cell efficiency. Applying transverse channel and depth varying structure, author experimentally verified that modified cathode flow channel geometry could enhance portable fuel cell efficiency up to 26.4%. Hossain et al. [10] numerically studied about optimal header design of parallel flow channel to reduce flow non-uniformity among the channel. Author showed that without proper header design, a large portion of flow can be concentrated on a few specified channel. Lim et al. [11] used ANSYS Fluent software to conduct numerical study about a relationship between fuel cell performance and a number of inlet and outlet. Applying additional inlet and outlet to conventional parallel flow channel, modified flow channel showed better reactant distribution. Atyabi et al. [12] introduced sinusoidal pattern to

conventional parallel flow channel. Through numerical study, the results indicated oxygen concentration uniformity on GDL-catalyst interface which means efficient distribution of reactants can be achieved by wavy structure. Similar study was conducted on larger scale. Saco et al. [13] numerically compared straight channel with zig-zag channel under scaled up (225 cm^2) active area. More uniform distributions of oxygen and water were observed, leading to performance enhancement. Most of the studies about parallel flow channel were targeted to overcome a critical weakness of structure, insufficient flow distribution capability. However, low pressure drop due to short flow length is obviously the best strength of parallel flow channel. Therefore, Vazifeshenas et al. [14] tried to utilize both parallel and serpentine flow channel's strength, designing compound flow channel which include parallel and serpentine channel structure.

Meanwhile, studies for serpentine flow channel have been performed widely. Basic serpentine type has single channel with rectangular cross section, however, various changes have been tried through experimental and numerical studies. Getting out of rectangular cross section, Freire et al. [15] discovered that under high humidity condition of inlet gas, trapezoidal cross section shape showed better performance. This experimental study implies that cross section shape of channel can affect fuel cell performance. Li et al. [16] showed that

wave structure which makes channel depth change along the channel periodically, could enhance mass transfer of reactants, increasing forced convection through GDL. Through numerical study, oxygen concentration at catalyst surface was increased and this result was verified through experiments. Similarly, Kuo et al. [17] also studied about wave structure along the serpentine flow channel. Instead, author mainly focused on enhanced heat transfer. Numerical analysis results showed that increasing Nusselt number, periodic wave structure could increase convective heat transfer rate. Porous media was combined with serpentine flow channel also. Instead of using single serpentine channel, Shimpalee et al. [18] increased a number of channel from 3 to 26. This numerical study concluded that the shorter path length showed more uniform current density distribution and less water accumulation. Compared with single serpentine channel, flow length could be decreased by increasing a number of channel. Marappan et al. [19] inserted porous media on rib region, allowing reactants flow through rib also. Performance could be increased due to additional water removal accumulated in the interfacial region of the GDL and rib surface. Through this study, we can figure out that not only water accumulation along the channel but also under the channel rib have to be considered to develop efficient flow channel. Therefore, Baik et al. [20, 21] invented serpentine channel with multi-hole structure. Through multi-hole

structure and sub-flow along this region, water accumulation in GDL was efficiently removed at both condition: air and oxygen supply system. Through experimental methods, size of the hole was optimized and changes of overvoltage under difference flow channel types were analyzed. In addition, numerical studies about geometrical characteristics of rectangular cross section and various arrangement of serpentine flow channel. Manso et al. [22] varied cross section aspect ratio, namely, channel width and depth were changed. The result indicated that models with high aspect ratio showed more uniform current distribution with higher maximum and minimum intensity values and temperature gradient was also comparatively low. Baz et al. [23] tried to enhance under rib mass transport via developing new configuration of serpentine flow channel. Current density and water content distribution were mainly explained. To reduce required pumping power, pressure drop was a key factor for evaluating newly developed serpentine flow channel.

Lastly, interdigitated flow channel has been continuously studied. Compared with parallel flow channel, interdigitated flow channel shows higher convection transport but lower diffusion transport [24]. Although interdigitated flow channels normally carry out better performance for its advantage in mass transport ability, relative high pressure drop is regarded as the biggest weakness. Under this characteristics, various experimental and numerical studies have

been conducted. Yan et al. [25] conducted experimental study on interdigitated, changing flow area ratio from 40.23 to 66.75%. Channel configuration was changed during alternation of flow area ratio and the result showed that increasing flow area ratio affected fuel cell performance in negative direction. However, this result cannot be considered as global principle among the other flow channel since interdigitated flow channel has its unique mass transport characteristics. Cooper et al. [26] tried to figure out a relationship between channel aspect ratio and performance of interdigitated flow channel through experimental study. The result showed that decreasing aspect ratio leaded better performance. This result was opposite with numerical study for serpentine flow channel [22]. Both studies considered water accumulation, therefore, difference between the results can be supposed to be occurred by type of the flow channel. What we can try is to find previous studies which compared two or more flow channel under varying geometric characteristics and driving conditions. Cooper et al. [27] compared parallel and interdigitated channel experimentally, changing channel-rib ratio and driving condition. Through this study, result indicated that each variable has difference dominance to fuel cell performance and this trend could be changed by the type of flow channel. From this study, we can conclude that optimized design of flow channel can be differed by driving condition. Chen et al. [28] changed width ratio between inlet and outlet

of interdigitated flow channel. The numerical result showed that narrower outlet channel width showed more uniform distribution of oxygen concentration and current density, leading better performance. This study is distinguishable compared with other studies related with interdigitated flow channel since it changed only outlet channel geometry. Lee et al. [29] suggested that position difference between inlet and outlet of interdigitated greatly affect to fuel cell performance. The result showed that counter-flow performed better compared with co-flow condition and channel-rib ratio showed remarkable impact with pressure drop. Finally, Mahmoudi et al. [30] analyzed GDL compression in interdigitated flow channel since under rib convection is the main mass transport along interdigitated flow channel. The result showed that compression of GDL by 35% caused a negligible performance loss in single-phase regions but not in two-phase regions since compression of GDL increased water accumulation through GDL.

Analyzing flow characteristics along the flow channels and modifying design of them, many researchers tried to overcome the weaknesses of conventional flow channel. Pressure drop, uniformity of oxygen and water, distribution of current density and temperature and velocity profile were observed to understand overall characteristics of flow channel. Under the different type of flow channel, optimized design and driving condition were

also changed. Although conventional flow channel designs have a limitation in modification, they are used in PEMFC up to now due to their simple design and manufacturing costs [31].

1.2.2. Advanced flow channel design

Although optimized conventional flow channels are used widely, creative attempts to invent new type of flow channel have been tried. Sauermoser et al. [32] introduced various unique design of flow channel. Pin-type, mesh-type, radial design, fractal type and bio-inspired flow channel were listed. Most of these trials were targeted to enhance fuel cell performance by elevating mass transfer capability. Jang et al. [33] conducted experimental and numerical study on spiral flow channels. The results indicated that spiral channel could produce secondary vortices and these could increase mass and heat transfer compared with conventional serpentine flow channel. Juarez-Robles et al. [34] changed a number of spiral channel and analyzed numerically. Reaction heat, current density and reactants distribution were observed and result indicated that four spiral channels performed the best. Instead, large number of spiral channel showed the worst performance since excessive entropy could be generated. Monsaf et al. [35] changed direction of flow along the spiral channel with variation of flow channel sizes. The result stated that when the reactants were injected from the external side of the spiral channel, the performance of fuel cell increased compared with the opposite direction. Briefly, channel configuration and geometric characteristics such as channel-rib width ratio, aspect ratio, flow direction and number of channel have been important issues

at developing spiral flow channel. Meanwhile, Arvay et al. [36] introduced various attempts mimicking nature to utilize it as a flow channel of PEMFC. Liu et al. [37] conducted numerical study comparing symmetric and asymmetric bionic flow channel under gravity. According to the flow channel pattern, liquid water distribution and pressure fluctuation were differed. In this case of study, gravity affected greatly to fuel cell performance, regardless of the version of bio-inspired flow channel. Since the nature can be categorized by animals and plants, Fan et al. [38] compared corn leaf pattern and human vein pattern as a flow channel of PEMFC. The result showed that animal prototypes performed better than plan prototypes in terms of maximum power density. As briefly explained, however, these types of flow channel still stick to rectangular cross-section shape.

Cross-section shape does not have to be rectangular and it can be changed along the flow direction. If manufacturing difficulties can be overcome, there are additional rooms which make researchers consider more unique and optimized flow channel. Preferentially, what kind of additional criterion can be considered at developing high-efficiency flow channel? Shen et al. [39] emphasized that velocity and concentration gradient perpendicular with GDL direction must be estimated. Previously mentioned, studies about wave-like flow channel highlighted forced convection through GDL, increasing reactants

concentration on catalyst layer [16, 17]. Han et al. [40] analyzed velocity profile difference between straight channel and wave-like channel numerically. Plus, 5.76% of performance enhancement was observed by experiments.

In the same manner, inserting baffle or blockage along the flow channel has been tried to enhance heat and mass transfer through fuel cell. Atyabi et al. [41] performed three-dimensional multiphase CFD analysis for observing the effect of honeycomb shaped blockage on flow channel. Similarly, Wang et al. [42] inserted novel dot matrix and sloping baffle along the flow channel improving oxygen supply to GDL. Number and sizes of slope baffle were changed and result found the best performed baffle pattern. Although the term 'blockage' and 'baffle' was used in two studies above to explain the honeycomb-like pin structure and dot matrix, they were more similar case with pin-type of mesh-type structure as it subscribed in previous study [32]. Instead, Heidary et al. inserted blockage between the conventional parallel channels using in-line and staggered patterns [43, 44]. Similar with interdigitated flow channel, blockage structure forced reactants to be transfer through GDL strongly. In terms of velocity and concentration gradient, flux toward GDL surface was strongly enhanced with high pressure drop. Using this pressure drop, in-line blockage pattern outperformed staggered pattern, forming pressure differentials between adjacent channels and this result was validated through

experimental and numerical researches. Further, Perng et al. [45] changed a shape of baffle from rectangular to trapezoid. For optimization, three different trapezoids with different angle were selected and distance between GDL surface and baffle was varied. The result proved that flow channel with larger angles and heights of trapezoid baffles caused enhanced mass transfer through catalyst layer.

If a distance between baffles and GDL surface becomes zero, namely, baffles totally block the flow and allow reactants flow only through GDL excessive pumping power might be needed like interdigitated flow channel. Therefore, studies with baffle which partially block the reactants flow have been researched so far. Houreh et al. [46] inserted partially blocked baffle with various shape: rectangular, triangle and circular. Compared with straight channel, velocity magnitude was dramatically increased at gap between GDL surface and baffles. This velocity acceleration could enhance water concentration distribution on membrane surface under the same humidifier. Plus, according to the shape of baffle, required pump power included at humidifier was not equal. Heidary et al. [47] focused a number of baffle and various evaluation criterion such as local Reynolds number, local Nusselt numbers and Darcy number. Porosity of GDL was also varied and result indicated that accelerated flow velocity could make liquid water be washed out

or evaporated. Also, increasing a number of baffle became useless in terms of local Nusselt numbers. Shen et al. [48] performed experimental study on single serpentine channel with baffle structure and tried to verify results of previous numerical studies. The case with baffle structures on both anode and cathode bipolar plates showed the best performance and result indicated that optimal intervals of baffle structure on anode and cathode side were different. Due to higher diffusion coefficient of hydrogen, baffle structure on cathode side was proved to be more efficient compared with anode side. Likewise, Yin et al. [49] focused on the height of the baffle structure. As the height increased, the result showed that pressure drop and mass transfer of oxygen were increased at the same time. Unlike previous studies which fixed the height of baffle along the channel, Tiss et al. [50] and Barati et al. [51] conducted numerical studies on single channel with baffle structure varying height of baffle gradually along the flow direction. Their results also concluded that velocity acceleration due to baffle structure could enhance the mass transport, increasing overall performance of the fuel cell.

Until recently, researchers developing flow channel of fuel cell normally considered reactants flow as a single stream. As fuel cell technology has been improved, some of the researchers started to apply additional flow or to invent a new type of flow channels which have sub-channel structures. Similarly with

multi-hole serpentine flow channel research, Wang et al. [52, 53] made additional fuel inlet in the middle of the flow channel in order to remove water accumulation more efficiently. The experimental results indicated that according to the position of additional inlet, sub-channel design could be either beneficial or disadvantageous. Further, through numerical study, optimum position of additional inlet and flow rate along the sub-channel were found. On the other hand, without adding supplementary channel, there was trial to separate reactants flow, improving water droplet dynamics along the channel. Niu et al. [54] and Fan et al. [55] suggested an innovative 3D cathode flow channel, targeting to separate water droplet which arises from GDL surface and hinder mass transfer of reactants. Using two-phase VOF model, numerical results found optimal geometric parameters of 3D baffle structures such as interval of baffle, width of baffle, slope angle and length. Compared with single straight channel with no additional structures, the new channel design showed better performance in terms of reactants mass transfer.

Previously mentioned, porous media was used as subsidiary material in conventional flow channel in order to overcome the weaknesses[8, 19]. Karthikeyan et al. [56] also derived performance enhancement by inserting carbon sponge into the rib region. However, porous media has come up as a representative flow distributor, replacing conventional flow channel design.

Tsai et al [57] conducted experimental study with metal foam, comparing several metal foam flow field designs. I-V curve and electrochemical impedance spectroscopy (EIS) curve indicated that unit cell with single metal foam zone showed weak convection at side corners. Instead, dividing the metal foams into multiple regions by adding rib between them showed better performance in terms of gas distribution and fuel utilization rate. Instead of considering channel width and depth, porosity and size of a pore can be the main geometric characteristics for porous media. Kozakai et al. [58] utilized bi-porous media as a flow distributor in order to improve gas diffusivity. Bi-porous media has a double peak in the pore size compared with simple porous media which has a single peak. Under low oxygen stoichiometric ratio driving condition, bi-porous media showed mass transfer enhancement due to separation between water and gas and this effect was brought by porosity difference. Similarly, Shin et al. [59] put metal foams with different cell sized in accordance with flow direction and relative position with inlet and outlet. Through several experiments, the results indicated that securing enough contact area near inlet region and increasing gas diffusion area could enhanced fuel cell performance. In other words, inserting a metal foam with low porosity or small size of cell at inlet region and inserting a metal foam with high porosity or big size of cell at outlet region could bring the highest performance. This result was

mainly due to water accumulation and fuel starvation at outlet region. Porous media can be used in special application also. Kang et al. [60] experimentally verified that metal foam could enhance the performance of open-cathode fuel cell, keeping membrane from dry out and removing water droplet along the channel efficiently. There was a optimal pore size of metal foam and the result was shown by I-V and EIS curve.

Even if the porous media has many advantages as a flow channel, there are a few weaknesses. Lack of flow guidance can generate dead-zone can create dead-zone which has poor mass transfer due to low velocity and severe water accumulation [61]. Combining the strengths of baffle structure and porous media as flow channel, 3D fine mesh was commercially introduced by Toyota Motors [62, 63]. 3D fine mesh is made of a lot of small repeated and staggered units having slope structure through GDL surface direction and flow guidance along up and down side of the units. With this invention, Toyota Motors succeeded in performance enhancement by increasing limiting current density up to 2.4 times. After this eye-opening progress several studies for figuring out detailed flow characteristics along the 3D fine mesh was conducted. Zhang et al. [64] and Bao et al. [65] explained several characteristics and advantages of 3D fine mesh structure as flow channel through numerical studies. First, there is no blockage like a rib of serpentine flow channel. When flooding along flow

channel is intensified, water droplet can escape to adjacent structure. This feature is similar with porous media like metal foam. Second, 3D mesh was designed to have baffle structure which can accelerate mass transfer through GDL. This feature accords with that of baffle structures. Finally, staggered arrangement of unit made air guidance toward both up and down and separated water and reactants flow. Although small contact area with GDL compared with conventional serpentine flow channel, the results stated that performance enhancement could compensate ohmic loss enough. Modification and simplification of 3D mesh structure were tried also. Cai et al. [66] substituted solid bottom rib with porous media to achieve uniform distribution of reactants concentration. Also, author adopted two evaluation criterions: performance evaluation criterion (PEC) and effective mass transfer coefficient (EMTC). Similarly, Shen et al. [67] simplified the 3D mesh structure and analyzed water droplet dynamic through flow channel, confirming performance enhancement in terms of reactants concentration distribution and current density. In short, various attempts to invent a new type of flow channel have been tried and optimized geometric parameters and proper analysis methods are continuously found through numerical studies.

1.2.3. Non-uniform design along active area

Every flow channel design mentioned above have their own features, however, there is one common ground. They can be considered as consecutive arrangements with equivalent unit of channel. In other words, straight structures of parallel, serpentine and interdigitated flow channel are repeated rectangular unit and baffle and porous structures can also be considered as uniform pattern. Plus, their optimization of geometric characterization were limited to uniform arrangement, namely, sizes of channel were fixed along the flow direction. When it comes to large scale fuel cell, that strategy can counter major barriers to maintain enhanced performance and the biggest reason of this difficulty is due to uneven flow distribution [68]. Even if previous studies mentioned at from 1.2.1 to 1.2.2 targeted uniform distribution of reactants, they have limitation at large scale fuel cell since mal-distribution along the flow channel becomes severe in large active area. Uneven flow distribution can be formed by poorly designed header and flow channel, insufficient operating pressure and dead zone. Uneven flow distribution can lead uneven chemical reaction, uneven water and heat production, generation of hot and dry spot, severe flooding and reactants blockage, higher mechanical stress and faster performance degradation [69]. Of course, these problems are not only due to increment of active area. Instead, the nature of fuel cell affects greatly to the

problems together [70]. From inlet to outlet, oxygen and hydrogen are continuously consumed and accumulation of water is normally concentrated near outlet. Therefore, reduction of mass transfer and reactants concentration are unavoidable even if novel flow channel can alleviate them. When water accumulation, so called ‘flooding’, goes severe, pores of GDL are filled with water droplet make porosity of GDL decrease. Therefore, porosity and mass transfer capability of GDL can be reduced by flooding, especially near outlet. This phenomena normally diminishes uniform distribution of reactants concentration on catalyst layer [71]. If excessive inlet pressure is imposed to overcome this problem, parasitic power consumption might exceed performance enhancement. Briefly, flow uniformity and low pressure drop are two main standards judging flow channel design whether it is good or bad [72].

Kahraman et al. [73] introduced incline flow channel design targeting to enhance mass transfer near the outlet. Normally, depth or width of channel have been decreased along the flow direction since reactants flow near outlet has to be forced through the GDL more strongly in order to alleviate imbalance. At the early stage of development, Liu et al. [74] studied numerically about reactant gas transfer and the fuel cell performance with a tapered channel. Tapered channel which cross-section area decreased continuously along the channel brought two effects: accelerating flow velocity near outlet and forcing

flow direction to the GDL surface. Reducing the depth of channel near outlet to 10% of inlet, performance enhancement at high current density driving region was distinguishable, however, pressure drop increment was inevitable. Fontana et al. [75] performed CFD analysis, applying non-uniform cross sectional area on both anode and cathode flow channel. Varying angles of inclination, the results indicated that current density and reactants consumption were increased, following increment of inclination angle. Similarly, the major problem of inclined channel was comparatively large pressure drop. Further, Mancusi et al. [76] numerical study of two-phase flow patterns along inclined flow channel, focusing on water droplet dynamics using VOF model. The results showed that performance enhancement effect of inclined flow channel was exposed strongly at high current density and high temperature condition. In terms of water droplet dynamics, results implied that there was optimal angles of inclination. For a rectangular channel and inclined channel with high ratio of inclination, the water in the channel was removed as slugs. On the contrary, for inclined channel with moderate ratio of inclination, slugs were still dominant but film patterns were also observed especially at outlet region. Formation of film patterns can cover the surface of GDL impeding mass transfer to catalyst layer. Therefore, optimal level of inclination has to be researched. Fontana et al. [77] additionally revealed about coalescence and detachment of water droplet through inclined

flow channel. As velocity increased near outlet, coalescence and detachment of droplet was firstly observed near the outlet and then formed slug or film formation according to initial velocity of flow. Regardless of the type of formation near the outlet, following water slug formed at middle and front of flow channel absorbed the water near the outlet. For this reason, inclined flow channel was revealed to be favor at water removal. Likewise, Akhtar et al. [78] observed droplet dynamics numerically, changing wettability of GDL and every side wall of flow channel. The result showed that combination between hydrophobic wall and hydrophilic GDL was in favor of water removal. Although these studies about water droplet dynamics give us a great insight in developing flow channel, the results can hardly said that they reflected realistic water behavior since most of these studies did not include non-uniform chemical reaction along the flow channel.

Different patterns of inclined flow channel have been introduced. Song et al. [79] suggested five types of incline pattern including curved and straight path and narrowing the average channel depth was shown to promote the reactants mass transfer to catalyst layer in both fuel cell and electrolytic cell modes. Instead of decreasing depth linearly, Min et al. [80] made numerical model for flow channel with a stepped depth change. The result additionally stated that the smaller number of step, the higher fuel cell performance was

estimated. In other words, comparing with linear depth reduction, discontinuous pattern showed better performance. Ferng et al. [81] compared two types of conventional flow channel, parallel and serpentine, with tapered slope modification. Compared with serpentine channel, parallel channel was proved to be more sensitive with depth variation.

Through experimental studies above results have been tested. Kumar et al. [82] conducted experimental study on single serpentine flow channel with decreasing depth along the flow direction. From I-V curve and Nyquist and Bode plot using EIS technique, the result showed performance enhancement at high current density region. Chowdhury et al. [83] tried opposite case of previous study. Through experimental study, author compared two cased: increasing and decreasing channel depth along the flow direction. Channel depth of inlet and outlet were changed and result indicated that both depth varying pattern showed better performance than normal straight channel. Even increasing channel depth showed performance enhancement due to water removal since flow resistance was relieved at large cross-sectional area. Shin et al. [84] also conducted experimental study on serpentine flow channel with depth varying, including variation of operating pressure. As same as the case with atmospheric pressure, pressurized experimental cases also showed performance enhancement decreasing channel depth along the flow direction.

Varying width along the flow direction has also been tried. Zehtabiyan-Rezaie et al. [85] proposed converging and diverging channel design including both increment and decrement of channel width. Mass flow rate difference between adjacent channels encouraged under rib convection, therefore the result proved performance enhancement. More detailed study about varying width pattern was performed by Wang et el.[86]. Under fully humidified condition, depth decreasing pattern outperformed width narrowing pattern. However, under 32% of relative humidity of inlet gas, width narrowing pattern showed better performance. Yan et al. [87] conducted numerical study on parallel channel, including either convergent or divergent width pattern. The result explained about why narrowing width showed negative effect to performance. Narrowing rib made interface between channel and GDL surface decrease, resulting mass transfer decline. Fixing channel width, Rahimi-Esbo et al. [88] derived width narrowing effect by reducing a number of channel near outlet. As a result, velocity acceleration could be gained without reducing channel-GDL interface area. The numerical result showed that reduce a number of channel in half performed the best, however, lack of concentration distribution and mass transfer comparison with the other cases made discussion obscure. A few researchers even tried to change channel depth. Wang et al. [89, 90] divided serpentine channel more than five sections and changed width and

height almost randomly. For instance, not only increasing or decreasing width and height, the sizes could be maximum at the middle or minimum at the inlet. Author preferentially found novel combination of depth change and then considered it as a default design in order to find the best combination of width change. The result suggested that diverging pattern near outlet is helpful to enhance performance, however, the numerical analysis was conducted on 0.81 cm^2 scale. Therefore, that result can hardly said that it can be applied in larger scale commonly.

Various incline patterns along flow channel can be considered as 'non-uniform' or 'gradient' pattern since they were invented to alleviate uneven flow distribution and designed not to be equal along the flow direction. Not only width and slope, other parameters have been deformed creatively, forming non-uniform pattern along the flow channel. Liu et al. [91] and Lei et al. [92] imposed slope structure on U-turn region of serpentine channel. The result showed that proper design of turning point at serpentine flow channel could enhance water droplet dynamics in favor of fuel cell performance. Perng et al. [93] combined baffle structure with tapered straight channel and performed numerical study using non-isothermal model. Yan et al. [94] and Chen et al. [95] adopted non-uniformity for wave channel, changing wavelength and height of unit along the flow direction. Bigger units with large wavelength and height

were positioned gradually near outlet, causing performance enhancement through velocity acceleration. Kang et al. [96] changed cell size of metal foam and inserted it unevenly along the flow direction. The case with the porosity of metal foam was gradually increased from inlet to outlet showed the highest maximum power density. Moreover, through EIS curve analysis, that type of non-uniform pattern of metal foam showed the smallest concentration overvoltage loss. This result was discord with other researches which suggested diverging flow channel near outlet to reduce flow resistance for water accumulation. It can be a hint stating that different types of flow channel have their own design strategy to lead performance enhancement.

Through sufficient review of previous researches, several points can be emphasized as follow:

- From conventional to newly developed flow channel, enhancing fuel cell performance have been targeted in terms of uniform distribution of reactants, mass transfer capability and pressure drop.
- In order to enhance mass transfer through GDL layer, velocity direction perpendicular to GDL has been important issue and this subject has been solved by baffle or slope structure.

- To overcome the nature of fuel cell, non-uniform or gradient pattern has been imposed and this can be important especially on large active area
- According to the type of flow channel, there can be individual strategy which can maximize fuel cell performance in various ways.
- On experimental studies, I-V curve and EIS curve analysis have been widely used
- On numerical studies, reactants concentration along channel, GDL and catalyst layer have been mainly discussed and pressure, velocity, current density, temperature and water droplet dynamic can be comprehensively discussed.

1.3. Objectives and scopes

In this study, non-uniform 3D structure patterns to enhance mass transfer and to improve fuel cell performance are analyzed through experimental and numerical study. Considering the molar concentration and velocity of reactants flow tend to be decreased from inlet to outlet, specific design parameters of 3D structure can be changed according to its position on active area.

In chapter 2, 3D structure was designed inspired by 3D fine mesh. For manufacturing by metal 3D printer, complex design of 3D fine mesh was simplified. Also, two design parameters were selected to control non-uniformity. Several non-uniform patterns were chosen on the basis of theory and previous studies. Unit cell performances with various patterns of flow channel were experimentally measured by I-V and EIS curve. Since water accumulation is normally intense on the cathode side, 3D structures were inserted at the cathode side and anode side was designed as parallel flow channel. Comparing among conventional parallel flow channel, uniformly designed 3D structure and non-uniformly arranged 3D structure, geometry parameters which were favor of fuel cell performance were revealed.

In chapter 3, effects of geometry changes on 3D structure as flow channel in fuel cell were numerically studied to obtain insights in development high efficiency fuel cell. For discussion solely on geometrical changes in length

direction and for reducing computing time, single row of 3D structure was selected as numerical domain. Comparing between uniformly arranged and non-uniformly arranged 3D structure, changes in flow characteristics which are related with performance of fuel cell were examined. The objects of this chapter was to explain experimental results in chapter 2 and to obtain ideas to invent non-uniform arrangement strategy for fuel cell with larger active area.

In chapter 4, possible non-uniform patterns along the width direction were studied. When a scale of fuel cell becomes large, design of header, manifold, configuration and specific geometric parameters give impact on fuel cell performance compared with small scaled fuel cell. If header of reactants supply system is not ideal and water droplet accumulation is under consideration, formation of dead-zone along the flow channel is inevitable. Assuming that side and near outlet region are vulnerable with dead-zone formation, strategy targeting mass transfer enhancement on that area was discussed. In this progress, experimental and numerical results from chapter 2 and 3 were utilized. Finally, through experimental durability tests, flow uniformity along the advanced non-uniform arrangement of 3D structure was examined.

In chapter 5, a research conclusion of this study was written with various insights and limitation which could be obtained through the whole study.

Chapter 2. Experimental study on PEMFC with non-uniformly arranged 3D structures

2.1. Introduction

At previous studies, advantages of 3D fine mesh structure were introduced. Staggered and repeated arrangement of unit structures with baffle design is the main geometric characteristic of 3D fine mesh, however, it was hard to be manufactured in laboratory scale since various types of 3D structure had to be made to diverse non-uniform arrangements of flow channel. Moreover, excessively complex curvature and too low wall thickness had to be simplified to be manufactured. Maintaining the main geometric characteristic of 3D structure, metal 3D printer was utilized to overcome this difficulty.

In this chapter, various non-uniform patterns made by metal 3D printer were examined. Selecting channel width and slope intensity as the variables, comparisons with the conventional parallel flow channel and uniform arrangements of 3D structures were performed. Basic and the biggest assumption in selecting possible arrangements was that accelerating flow velocity via narrower channel and steeper tapered structure could enhance fuel cell performance by efficient water removal near outlet. The best-performed patterns for width, slope and combined non-uniform arrangements were

obtained and reverse arrangements for each cases were tested to verify the basic assumption. I-V curve, EIS curve, channel volume comparison and pressure analysis were conducted. This chapter were published at International Journal of Hydrogen Energy[1]

[1] Choi, Sung Hoon, et al. "Experimental study on non-uniform arrangement of 3D printed structure for cathodic flow channel in PEMFC." *International Journal of Hydrogen Energy* 47.2 (2022): 1192-1201.

2.2. Preparation for experiment

2.2.1. Designing and manufacturing 3D structures

Figure 2.1 shows the schematic of main idea in this study. Accelerating velocity can help water accumulation to be removed and adding tapered structure to flow channel can accelerate flow velocity toward GDL, enhancing reactants mass transfer. These two objects of design can be necessary especially near outlet since water accumulation, called flooding, which can be concentrated in that region. Moreover, fuel starvation can occur even without flooding near outlet since lowered reactants concentration is unfavorable with concentration gradient driven diffusion. Therefore, if design parameters can be designed differently along the flow direction, performance can be enhanced compared with uniformly designed flow channel. If velocity acceleration and baffle structure are imposed uniformly from inlet to outlet, namely, if more packed structures are equally arranged regardless of the position, pressure difference can be increased unnecessarily. The main assumption of this study is that velocity and mass transfer capability manipulation can enhance the performance of fuel cell.

According to previous studies on 3D fine mesh, around 0.1 mm of wall thickness was utilized [62-65]. To manufacture fine flow channel with

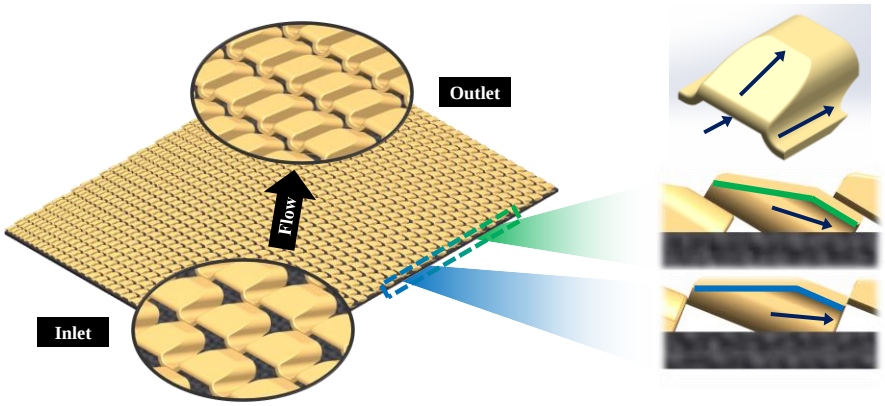

Figure 2.1 Idea sketch of 3D structure arrangement

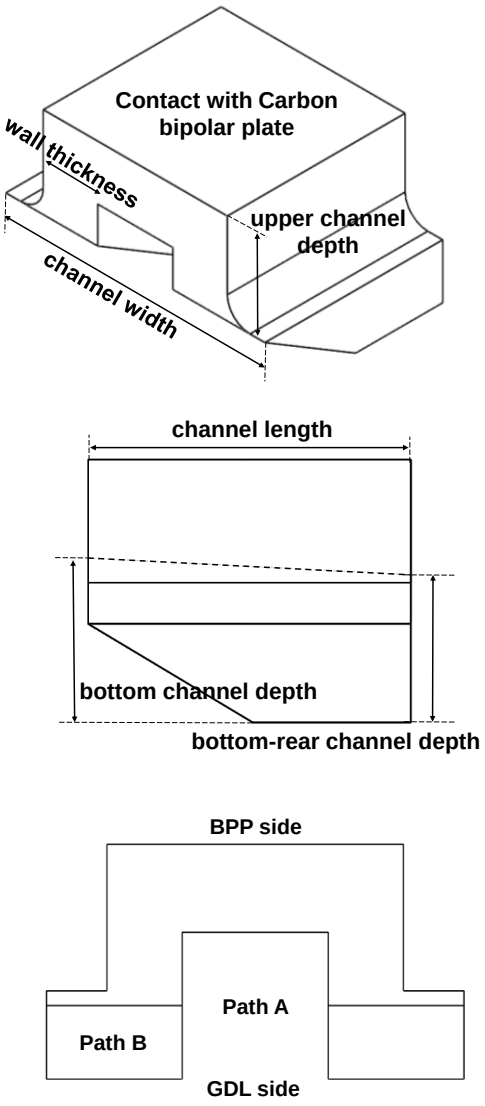

Figure 2.2 Layout of unit structure

complex geometry in laboratory circumstances, simplification of unit structure was conducted. Wall thickness should be smaller than 0.6 mm due to its manufacturing limitation. Also, detailed curvatures in small sizes could not be realized through metallic 3D printer. **Figure 2.2** shows simplified geometry of 3D structure. Channel wall thickness was fixed to 0.6 mm and both upper and bottom channel depths were set to 1.0 mm. Channel width and bottom-rear channel depth were selected as variable parameters, which could reduce the cross sectional area of the flow channel and add sloped structure. 3D structures were inserted in unit fuel cell, between GDL and carbon BPP. Therefore, to minimize an effect of contact resistance on fuel cell performance, total contact area between 3D structure and carbon BPP was fixed. Considering conventional flow channel depth has a range of 0.6 to 1.0 mm, sloped structure could be made by decreasing bottom-rear channel depth. **Figure 2.3** shows an example of 3D structure insertion on carbon BPP with 20 cm^2. Channel width of unit structure was determined depending on the number of channels along width direction on the active area. Plus, tapered baffle structure was made by decreasing bottom-rear channel depth for reinforcing flow direction to GDL. If so, various unit numbers and degrees of tapered structure could be examined whether they are appropriate or not.

Considering mass transfer through GDL, volume of 3D structure, contact

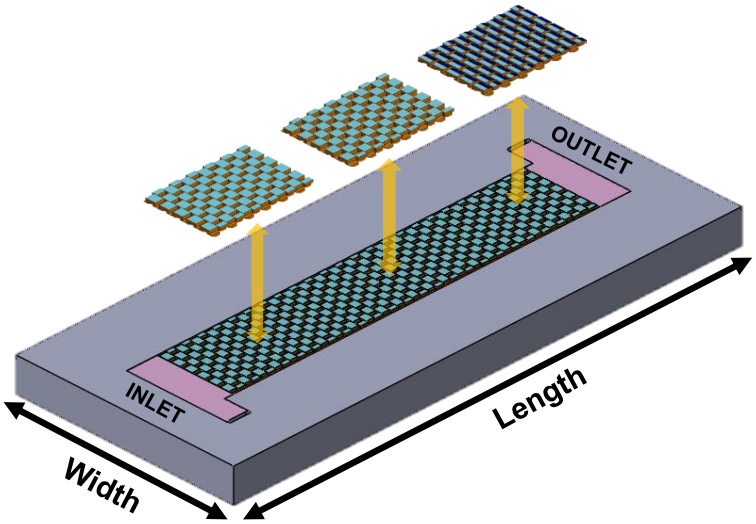

Figure 2.3 Plan of 3D structure arrangement insertion

area with GDL, intensity of slope and volume fraction of inclined flow path were expected to affect performance of flow channel. First, flow velocity could be changed with volume of structure. If the volume of structure increased, overall velocity was predicted to be increased also. Wall thickness was fixed to 0.6 mm, therefore, increasing a number of unit along width reduced width of channel and 'path A' in **Figure 2.2**, leading growth of volume of structure. Second, contact area with GDL was affected by the width of 'path B' and this could be changed depending on a number of unit. Third, volume of inclined flow path included volume of path B which was applied basically to all type of unit structure. Plus, volume of 'path A' which could be considered as inclined flow path when bottom-rear channel depth was decreased. Supposing there is no inclined structure along 'path A', volume of inclined flow path was affected by width of 'path B'. Plus, width of path A had to be on proper range of channel width of previous studied channel. According to literature survey, channel width between 0.5 mm and 1.5 mm was utilized. Finally, intensity of slope could be controlled by bottom-rear channel depth and it should not be smaller than 0.6 mm because of the thickness of structure. Considering unintended manufacturing error, minimum bottom-rear channel depth was limited by 0.8 mm. Apart from intensity of slope, volume of structure, contact area with GDL and volume fraction of inclined flow path

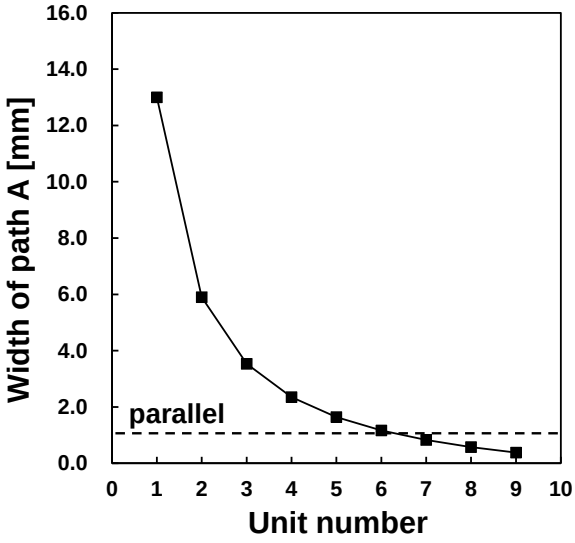
16.0
14.0
12.0
10.0
8.0
6.0
4.0
2.0
0.0
Width of path A [mm]
parallel
0 1 2 3 4 5 6 7 8 9 10
Unit number

(a)

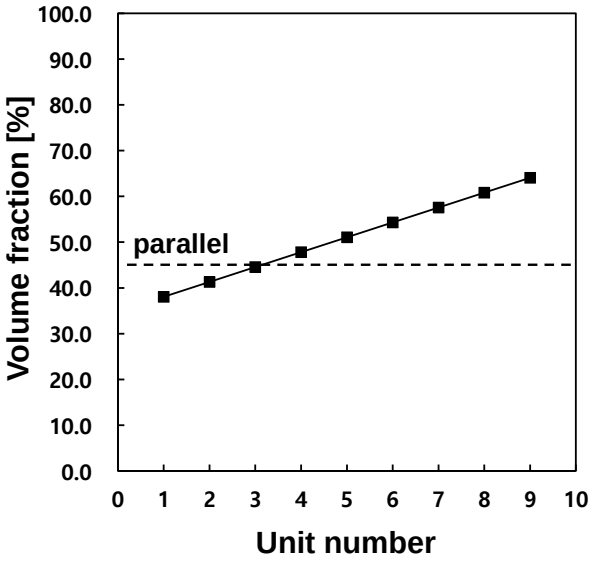
100.0
90.0
80.0
70.0
60.0
50.0
40.0
30.0
20.0
10.0
0.0
Volume fraction [%]
parallel
0 1 2 3 4 5 6 7 8 9 10
Unit number

(b)

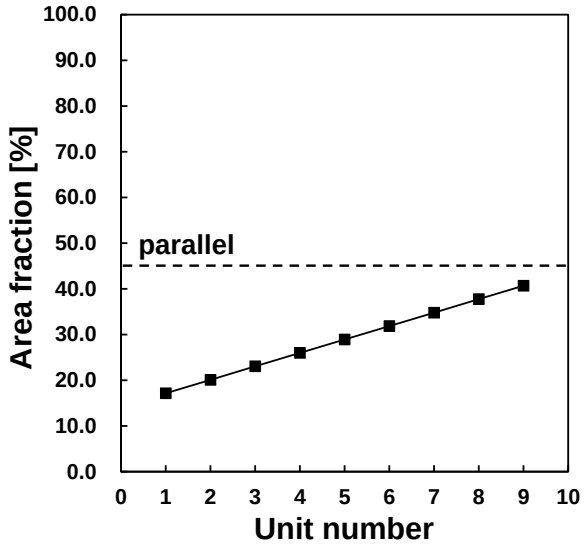

(c)

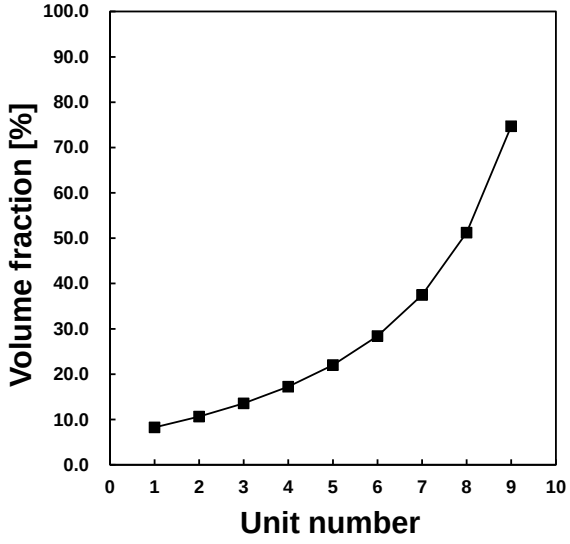

(d)

Figure 2.4 Geometric parameters change with unit number; (a) width of path A, (b) volume fraction of structure, (c) GDL-structure contact area ratio, (d) volume fraction of inclined structure

were changed by a number of unit along width. **Figure 2.4** shows that geometry variations according to a number of unit along width direction. In this study, typically designed graphite parallel flow channel and 3D printed parallel flow channel were used as references. Graphite parallel flow channel had 10 straight parallel channels with 1 mm of width and 0.9 mm of rib width. Therefore, volume fraction of BPP (rib) was 45% and ratio of contact area was 45% also. 3D printed parallel flow channel had 7 straight parallel channels with 1.8 mm of width and 1.0 mm of rib width. To be in appropriate range of channel width, unit number of six, seven and eight were selected. Applied with the unit number of seven to 3D structure, it had the same volume fraction of BPP and ratio of contact area with 3D printed parallel flow channel. Comparing with a graphite parallel channel, volume fraction of structure was slightly high and contact area was slightly low**.** This characteristics trend with a number of unit was covered in detail at chapter 3. **Figure 2.5** shows both sides of a single structure, manufactured by 3D printer.

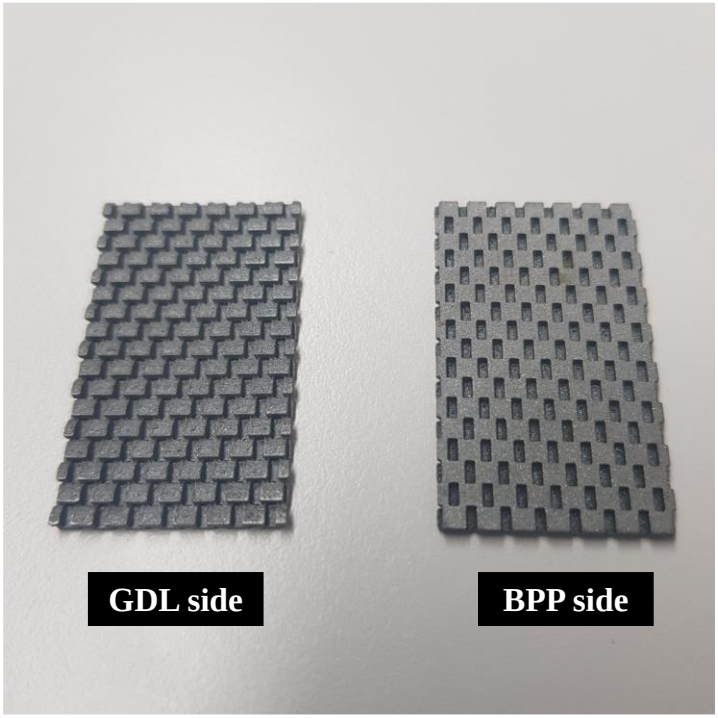

Figure 2.5 Two sides of 3D printed structure

2.2.2. Arrangement of 3D printed single structures

Figure 2.6 shows how 3D printed flow channels were inserted on carbon-based cathode BPP of unit cell. Instead of selecting square-shaped BPP, rectangular BPP with active area of 20 cm^2 (2 cm of width and 10 cm of length) was chosen to focus mass transfer along the flow direction from inlet to outlet, minimizing convection along the width direction. Three 3D structures could be inserted along the length direction and the same or different types of single structure could be mixed. Plus, a single structure was formed by repeatedly arranging one equal unit structure. **Table 2.1** shows geometric parameters about unit structures in nine different single structures. Previously mentioned, a number of channel units along the width direction decided channel width. Therefore, SS-7(0) indicates 7 unit structures were arranged in width direction in single structure and no reduction of bottom-rear channel depth was applied. Meanwhile, 17 unit structures were arranged in the length direction regardless of the type of single structure. SS-7(10) indicated that bottom-rear channel depth was decreased to 0.9 mm, namely 10% of reduction from the original depth to make sloped structure. Three kinds of channel width and bottom-rear channel depth variations were set respectively and combination of these could be formed. In summary, nine types of single structure and 729

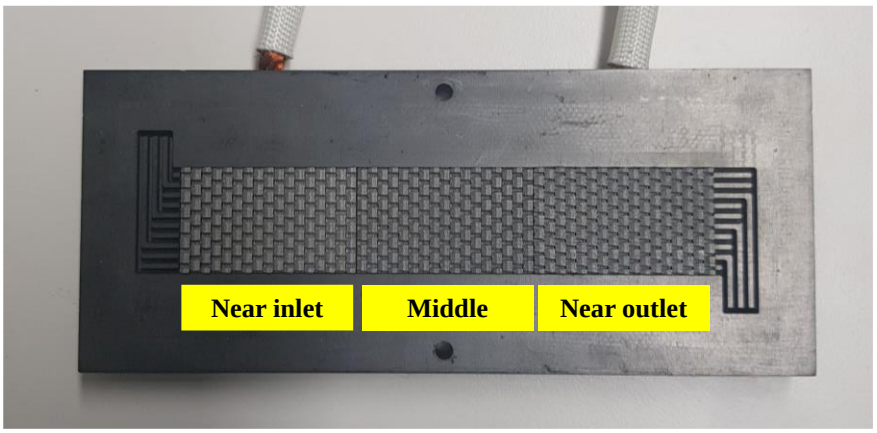

Figure 2.6 3D printed structure on carbon BPP

Table 2.1 Properties of 3D printed single structures

Type	Channel width of single unit [mm]	Bottom-rear channel depth [mm]
SS-6(0)	3.33	1.0
SS-6(10)	3.33	0.9
SS-6(20)	3.33	0.8
SS-7(0)	2.86	1.0
SS-7(10)	2.86	0.9
SS-7(20)	2.86	0.8
SS-8(0)	2.50	1.0
SS-8(10)	2.50	0.9
SS-8(20)	2.50	0.8

* SS – ‘number of unit structure in width direction’ (‘decrease ratio of bottom-rear channel depth’)

single structure arrangements could be suggested. Mentioned above, mass transfer resistance due to flooding effect is normally severe near the outlet of cathode. Therefore, appropriate arrangements of single structures could be sorted which had narrower and steeper single structure near the outlet. **Table 2.2** shows eight representative arrangements through this process. For comparison, performance measurement was conducted with four uniform arrangements (666, 777, 888, 777(10-10-10)) and four non-uniform arrangements (678, 667, 778, 777(0-10-20)). If the fuel cell with specific non-uniform arrangement showed the best performance, reverse arrangement of it should be tested to verify the main assumption. Therefore, performance measurements for reverse arrangements of some cases were also conducted. After showing a sole effect of width and slope arrangement on the performance of unit cell, the best arrangements with changing both width and slope could also be tested.

Table 2.2 Arrangements of 3D printed single structures

Type	Near inlet	Middle	Near outlet
666	SS-6(0)	SS-6(0)	SS-6(0)
777	SS-7(0)	SS-7(0)	SS-7(0)
888	SS-8(0)	SS-8(0)	SS-8(0)
777(10-10-10)	SS-7(10)	SS-7(10)	SS-7(10)
678	SS-6(0)	SS-7(0)	SS-8(0)
667	SS-6(0)	SS-6(0)	SS-7(0)
778	SS-7(0)	SS-7(0)	SS-8(0)
777(0-10-20)	SS-7(0)	SS-7(10)	SS-7(20)

2.2.3. Experiments on single cell

Figure 2.7 shows a diagram of equipment setup for experiments. In this study, current-voltage curve (I-V curve) and EIS curve with electric loader (PLZ664WA, Kikusui) were measured to characterize performance of unit cell. Hydrogen gas with purity of 99.999% and ambient air were utilized. Bubbler type humidifier was used to adjust relative humidity of inlet gases. Thermocouples (T-type, Omega) were used to measure temperature of reactant gas and cell. Sigracet 39BB was used as GDL, which is non-woven carbon paper with 5 wt% of PTFE microporous layer. This porous media has 315 μm thickness and majority portion of pore sizes is between 10 and 100 μm [97]**.** PTFE coated glass fabric with 235 μm thickness was used as gasket which is 80 μm thinner than GDL to prevent leakage of gas properly. Catalyst layer was treated as 0.45 mg/cm^2 for both sides of Nafion 211 MEA (VINA Tech). Incornel 718 was selected as 3D printing material. In this study, EOS M series 3D printer was used. This equipped 400 W scale Yb-fiber laser and had 7.0 m/s scan speed and 100 μm of laser focus diameter. During laser processing, stacking unit was controlled by 40 μm and size of metal power was 15 to 45 μm. Since metallic single structures were inserted between GDL and carbon BPP, we added carbon cloth (1071 HCB, AvCarb) between 3D printed structure and carbon BPP to reduce contact resistance and compress GDL

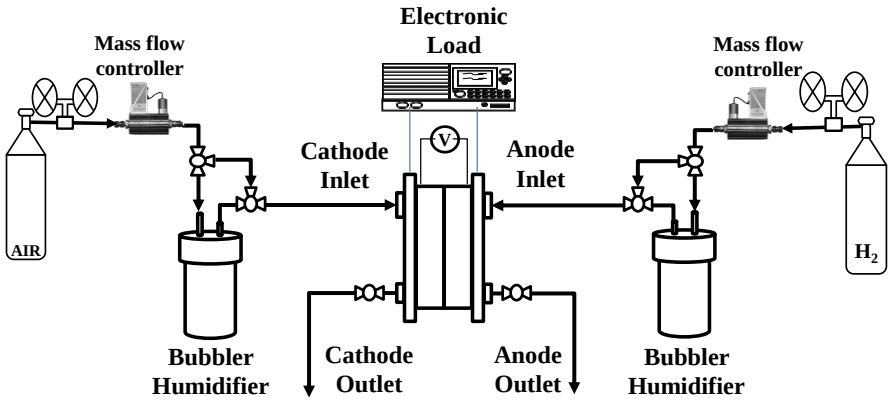

Figure 2.7 Experimental setup

sufficiently. Additional surface processing was not applied. **Table 2.3** lists experimental driving conditions. Inlet gas of anode side was not humidified and inlet gas of cathode side was fully humidified to solely focus on mass transfer reduction by flooding effect of cathode side at high current density driving condition. All the I-V curve consisted of 2 minutes duration in constant current driving starting from 3.2 A with 1.6 A interval. Data during 30 seconds of both beginning and end of every constant current were removed to measure in steady state. Average of the last three I-V curve data was calculated which could be considered as reliable data. Lastly, EIS measurements were conducted for comparing mass transfer resistance between the best-performed arrangement and the reference arrangements.

Table 2.3 Experimental conditions

Parameter	Value
Temperature of the inlet gas [K]	333
Temperature of the cell [K]	333
Relative humidity (anode/cathode) [%]	0 / 100
Stoichiometric ratio (anode/cathode)	1.5, 2
Operating pressure (anode/cathode) [bar]	1, 1

2.3. Results and discussion

2.3.1. Effect of width non-uniformity on the single cell performance

I-V curves of various arrangements with width variation are shown in **Figure 2.8**. Among the uniform arrangements, the unit cell with 777 pattern performed the highest maximum power density. Therefore, ingle structure SS-7(0) could be selected as a default, three single structures could be varied in order to realize non-uniform arrangements. Change in channel width could be maximized selecting 678 pattern. Taking account of water accumulation near the outlet side, 667 and 778 patterns could be selected too. As shown in **Figure 2.8**, the unit cell with non-uniform arrangements (red marks) performed better compared with that of uniform arrangements (black marks). 778 pattern showed 12.5% and 13.7% higher maximum power density, compared with 777 and 888 patterns, respectively. For validation of the main assumption, the unit cell with reverse arrangement (877) was tested additionally (gray marks). Result shows 19.2% of maximum power density drop is obtained. The only difference between 778 and 877 pattern was the direction of arrangement. Contact area between GDL and 3D structure arrangements and total channel volumes of the two arrangements were equal. Result showed that enhancing mass transfer by accelerating flow velocity was more efficient near the outlet.

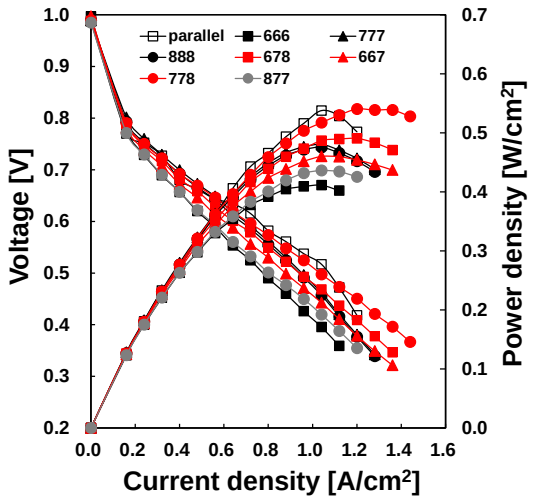

Figure 2.8 I-V and I-P curve at various arrangements with width changes

Figure 2.9 shows the trend between maximum power density and channel volume fractions of various arrangements. Even though 3D structure did not have the same geometrical characteristics with metal foam and conventional flow channel, channel volume fractions of structures were checked, since aspect ratio or porosity of flow distributor have been an important design factor in previous studies. With increasing channel volume fraction or with increasing pressure drop tended to enhance fuel cell performance in previous studies. However, 778 and 877 pattern had the same channel volume fraction but showed a noticeable performance difference. Results indicated that not only the general characteristics of flow channel but also the non-uniformity of channel arrangement could affect fuel cell performance. Of course, 778 pattern and 877 pattern had the same GDL-structure contact area and volume fraction of inclined structure.

Although a positive effect of non-uniform arrangements was shown, 778 pattern did not largely outperform the graphite parallel flow channel. According to I-V curve, severe ohmic resistance due to large contact resistance could be observed. Comparing with graphite, metallic materials normally have larger contact resistance with carbon-based GDL. Therefore, carbon cloth could be inserted to reduce contact resistance. For checking the effect of carbon cloth, **Figure 2.10** shows the comparison results.

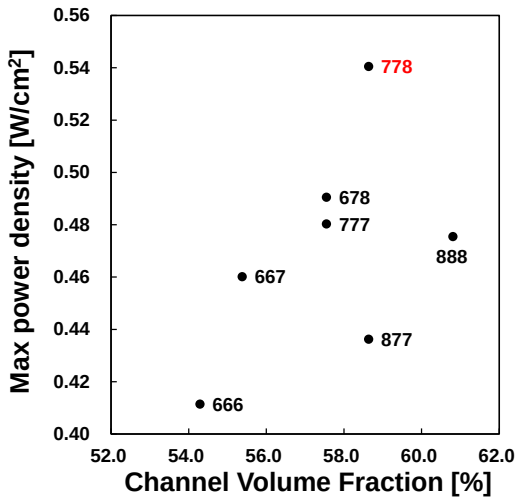

Figure 2.9 Maximum power density at various channel volume fraction of 3D structure arrangements with width changes

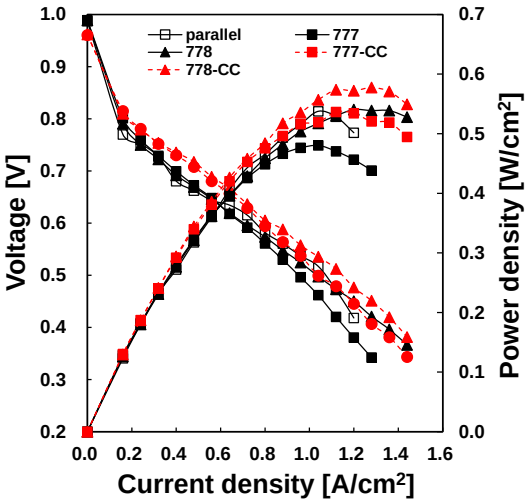

Figure 2.10 I-V and I-P curve at various arrangements with width changes including carbon cloth insertion

The unit cell with 778 pattern increased by 6.8% via inserting carbon cloth, meaning 7.4% of maximum power density enhancement comparing with that of graphite parallel flow channel**.** Also, the unit cell with 777 pattern reached a similar maximum power density with that of graphite parallel flow channel. Under carbon cloth insertion, comparing between 777 and 778 pattern, 7.6% of performance enhancement was possible by adding non-uniformity on flow channel. Therefore, it could be said that carbon cloth insertion was favor of reduction of contact resistance.

Although the performance reduction due to large contact resistance could be solved, effect of advanced geometric characteristics and non-uniform arrangement could hardly evaluated under comparison with different materials. To judge the effect of geometric characteristics on fuel cell performance separately, 3D printed parallel flow channel could be considered. 3D printed parallel flow channel was designed to have the same contact area with 777 pattern. **Figure 2.11** shows performance comparison with 3D printed parallel flow channel. 10.4% of performance enhancement could be observed with 777 pattern comparing with 3D printed parallel flow channel. In summary, performance enhancement by geometric characteristics and arrangements of 3D structure were be confirmed.

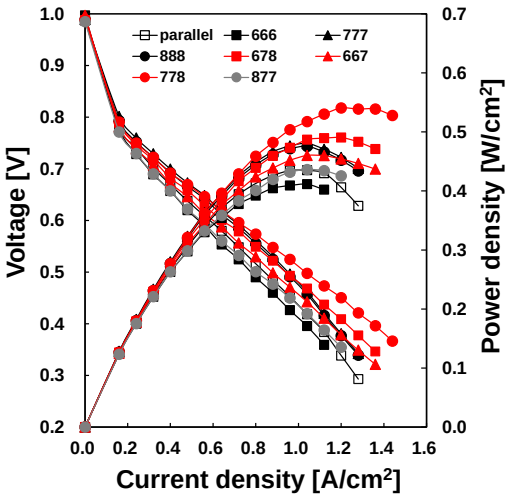

Figure 2.11 I-V and I-P curve at various arrangements with width changes including carbon cloth insertion (compared with 3D printed parallel channel)

Relative high pressure drop was observed in experiments with relatively high volume fraction of 3D structure such as 888. Regarding the whole system efficiency, not only performance of PEMFC cell, compressor power of fuel supply system have to be considered in evaluation. When increase in pumping power exceeds power enhancement of fuel cell, non-uniform arranged 3D structures can't be said as good any longer. Work of compressor can be calculated as follow [98]:

$$W_{comp} = c_p \frac{T}{\epsilon_{comp}} \left[\left(\frac{P}{P_0} \right)^{0.286} - 1 \right] \qquad \text{Eq. (2.1)}$$

where ϵ_{pump} indicates efficiency of compressor. Applying 0.9 as efficiency of compressor, **Figure 2.12** shows required work for driving fuel cell with 3D structure arrangements. Considering the maximum power density was bigger than 10 W, extra power consumption could be neglected. One thing can be highlighted in these results that applying dense structure can't always enhance performance, just wasting extra power consumption.

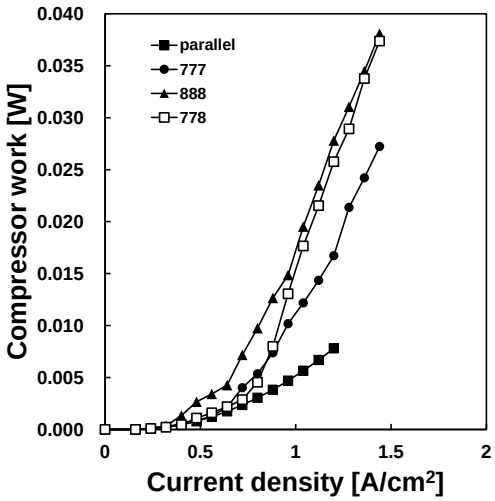

Figure 2.12 Additional compressor work in operating fuel cell with 3D structures; width changes

2.3.2. Effect of slope non-uniformity on the single cell performance

Figure 2.13 shows I-V curves of a unit cells with various slope arrangements. SS-7(0) was selected as a standard single structure based on previous results, therefore, three references, 777, 777(10-10-10) and 3D printed parallel flow channel were selected. The unit cell with 777(0-10-20) pattern showed the highest maximum power density and this was 11.3% higher than that of 777 pattern. However, its reverse arrangement, 777(20-10-0) pattern, also performed 10.8% higher maximum power density than that with 777 pattern. This results indicated that direction of slope non-uniformity showed minor impact on the performance of fuel cell. Reducing bottom-rear-channel depth, sloped structure was originally intended to enhance flow velocity through GDL direction. Therefore, if sloped single structure like SS-7(20) was arranged near the inlet, chemical reaction could be expected to be accelerated neat the inlet. Higher oxygen molar concentration can be expected near inlet, therefore, more efficient performance enhancement in terms of flow reinforcement could be expected. Plus, since water accumulation is not intense near the inlet, enhancing mass flux of humidified air through GDL and MEA near inlet can be expected to affect fuel cell performance positively. On the other hand, if sloped structure was positioned near the outlet, lowered performance due to insufficient concentration of oxygen and excessive

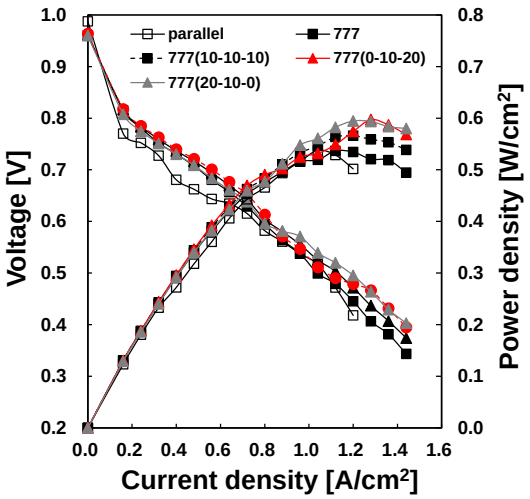

Figure 2.13 I-V and I-P curve at various arrangements with slope intensity changes including carbon cloth insertion

accumulation could be expected to be alleviated. For further information, detailed difference among various arrangement direction are discussed in the next chapter.

Comparing with the unit cell with 777 and 777(10-10-10) pattern, sloped structure in 3D structures could improve fuel cell performance. Plus, 777(0-10-20) arrangement showed 37.3% higher maximum power density compared with 3D printed parallel flow channel. As same as width non-uniform arrangements, pressure analysis result for slope cases are shown in **Figure 2.14**.

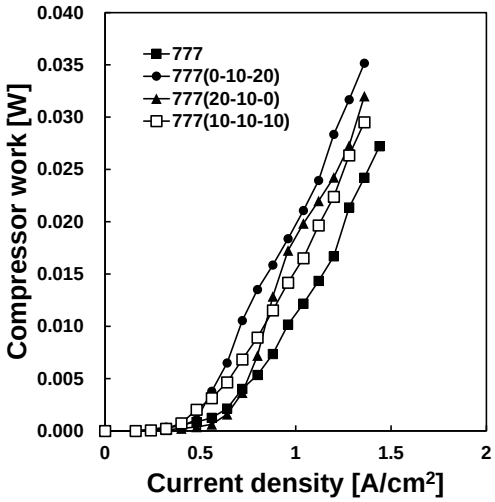

Figure 2.14 Additional compressor work in operating fuel cell with 3D structures; slope intensity changes

2.3.3. Mixed non-uniform arrangements

Figure 2.15 shows I-V curves of unit cell with mixed arrangements. The best arrangements in previous experiments were 778 and 777(0-10-20). Therefore, they could be mixed and be tested to find the best non-uniform arrangement. Even though dramatic performance enhancement was not observed, the unit cell with 778(0-10-10) pattern showed the best performance, 5.0% higher maximum power density than that of 778 pattern. 778(0-0-20) pattern was also tested since it had the similar volume fraction with that of 778(0-10-10). Compared with uniform arrangement, 777, the unit cell with 778(0-10-10) pattern showed 13.0% higher maximum power density. The best case was not 778(0-10-20), therefore, SS-8(20) could be considered as too dense structure to distribute inner flow efficiently. As a result, a unit cell with 778(0-10-20) arrangement showed 2.2% lower maximum power density compared with 778(0-10-10), even though they shared the same assumption and had similar channel volume fraction. Finally, the unit cell with 778(0-10-10) pattern performed 39.4% higher maximum power density than that of 3D printed parallel flow channel.

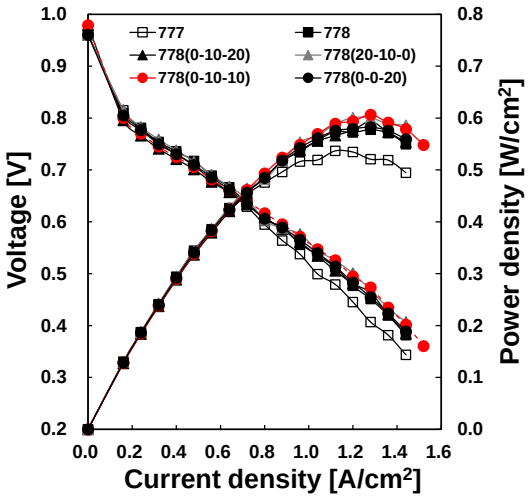

Figure 2.15 I-V and I-P curve at various arrangements with both width and slope intensity changes including carbon cloth insertion

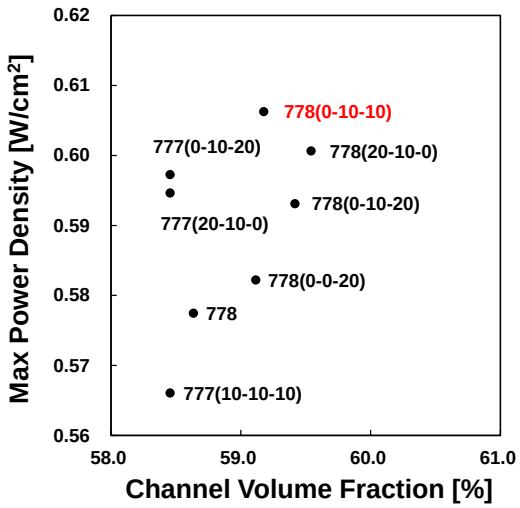

Figure 2.16 Maximum power density at various channel volume fraction of 3D structure arrangements with width and slope changes

Figure 2.17 shows results of EIS measurements for the unit cell with 778(0-10-10) arrangement and reference. The right arc of EIS represents the mass transfer resistance which can be measured at high frequency. According to **Figure 2.17**, the unit cell with non-uniform arrangement showed a smaller mass transfer resistance compared with that of the reference case. The results showed that velocity manipulation near outlet could help to remove accumulated water, enhancing mass transfer and alleviating concentration resistance in high current density driving condition. Lastly, pressure analysis results for mixed non-uniform arrangement is presented in **Figure 2.18**.

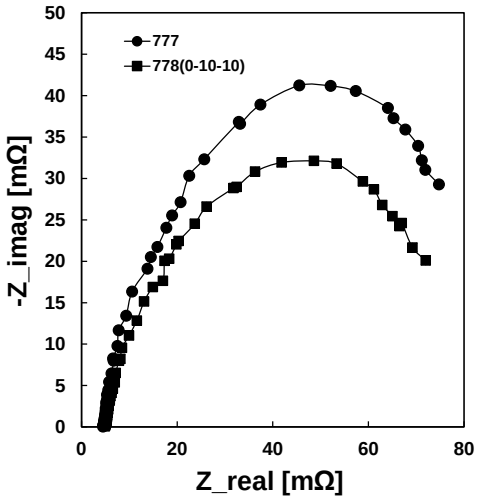

Figure 2.17 EIS curve of unit cell with uniform arrangement and mixed arrangement at 1.2 A/cm^2

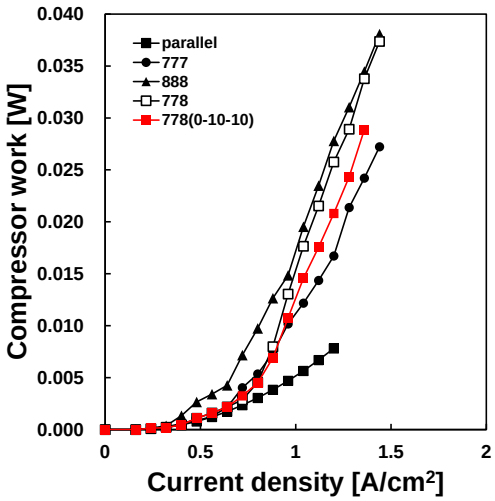

Figure 2.18 Additional compressor work in operating fuel cell with 3D structures; width and slope intensity changes

2.4. Summary

In this study, positive impact of non-uniformly designed flow channel on performance enhancement in PEMFC was experimentally studied. Motivated by 3D fine mesh, structure design was simplified and two parameters (channel width and bottom-rear channel depth) were chosen to apply non-uniformity along the active area. This strategy was targeted to accelerate flow velocity near the outlet and to reinforce flow direction through GDL, enhancing mass transfer of oxygen. Varying channel width and applying sloped structure were conducted on simplified 3D structure. Since poor mass transfer due to flooding effect is normally intense near the outlet, narrower and steeper structure was positioned near the outlet. To validate this strategy, reverse arrangements of the best cases were tested and discussion based on channel volume fraction and EIS data was conducted. The following conclusions can be drawn.

- Among width varying arrangements, the unit cell with 778 pattern showed the best performance. With carbon cloth, maximum power density increased by 7.6% by narrowing channel width near the outlet.
- The reverse arrangement of 778 showed 19.2% lower performance. This results showed that mass transfer enhancement by accelerating flow velocity was more efficient near the outlet.
- Among slope varying arrangements, the unit cell with 777(0-10-20)

pattern showed the highest maximum power density, but reverse arrangement of it did not show noticeable performance drop. Results showed that sloped structure brought positive impact on performance regardless of the position.

- Among mixed arrangements, the unit cell with 778(0-10-10) pattern showed the best performance. The performance with this pattern performed 39.4% and 13.0% higher maximum power density than that of 3D printed parallel flow channel and the standard uniform arrangement (777) respectively. Through EIS data, smaller concentration loss could be observed with the non-uniform arrangement.
- With the high possibility, according to the performance reduction with SS-8(20), optimum design parameter could be found to maximize fuel cell performance.

Chapter 3. Computational fluid dynamics analysis on 3D structures at various scales

3.1. Introduction

Although experimental study on non-uniform arrangements of 3D structures was conducted, detailed causes that can explain performance enhancement were needed. For flow channel of PEMFC, plenty of numerical studies using computational fluid dynamics (CFD) tools have been conducted. In this chapter, three dimensional CFD using ANSYS FLUENT for 3D structures was explained. Reviewing mathematical equations of PEMFC module of ANSYS FLUENT was firstly conducted. Then, grid test and model validation were conducted. Simple analysis on straight arrangements of unit structures along length direction was performed for comparison with conventional parallel flow channel. Unique characteristics of 3D structure as flow channel were explained and effects of geometric variables which were selected in chapter 2 were studied. Velocity and concentration related indexes were compared to figure out which flow characteristics affected to fuel cell performance.

Forming non-uniform arrangements which were similar with experiments, various trends between structure geometries and flow characteristics were

observed according to position on active area such as inlet, middle and outlet. Through experiments, current density distribution was not considered as fuel cell performance, only observing integral current density. Thanks to CFD tool, current density distribution could be observed and evaluating 3D structure arrangements in terms of current density uniformity was possible.

3.2. Preparation for CFD analysis

3.2.1. Numerical models

Three dimensional, two phase, non-isothermal and steady state model could be built on CFD. Although various formulas and boundary conditions were specified, some assumptions for numerical study were needed to simplify model. Generally, simplified boundary conditions were conducted through various studies [75]. Here are assumptions used in this study.

- The model operated in steady state
- Incompressible and ideal fluid condition were used
- Wall temperature was fixed to operation temperature
- Porous media (GDL, catalyst and membrane) were homogenous and isotropic.
- Contact resistance was neglected
- Droplet dynamic through flow channel was not considered.
- Tafel equation was used instead of Butler-Volmer equation since operation at relative high current density was planned.
- Gas crossover through membrane was neglected.
- Flow regime through fuel cell was considered as laminar.

Governing equations were based on computational study of Tao et al. [99]

and re-arranged in terms of fuel cell module in ANSYS FLUENT. Two equations for electric potential which drives chemical reaction through fuel cell are as follows:

$$\nabla \cdot (\kappa_e \nabla \phi_e) + J_e = 0 \qquad \text{Eq. (3.1)}$$

$$\nabla \cdot (\kappa_{ion} \nabla \phi_{ion}) + J_{ion} = 0 \qquad \text{Eq. (3.2)}$$

where κ is electrical conductivity (S/m), ϕ is electric potential (V) and J is volumetric transfer current (A/m^3) and subscripts e and ion indicate electric and ionic respectively. Electrons transfer through fuel cell components except membrane and protons transfer through membrane. Therefore, Eq. (3.1) can be applied to BPP, GDL and catalyst layer, namely, except membrane. On the other hand, Eq. (3.2) can be applied to membrane. Except for membrane domain, volumetric transfer current is negative value of anodic volumetric transfer current and positive value of cathodic volumetric transfer current. For membrane, volumetric transfer current has positive value of anodic volumetric transfer current and negative value of cathodic volumetric transfer current.

Each volumetric transfer current can be calculated as follows:

$$J_a = (\varsigma_a j_a^0)\left(\frac{c_{H_2}}{c_{H_2}^0}\right)^{\gamma_a}\left(e^{\alpha_a F \eta_{a,act}/RT} - e^{-\alpha_c F \eta_{a,act}/RT}\right) \qquad \text{Eq. (3.3)}$$

$$J_c = (\varsigma_c j_c^0)\left(\frac{c_{O_2}}{c_{O_2}^0}\right)^{\gamma_c}\left(-e^{\alpha_a F \eta_{c,act}/RT} + e^{-\alpha_c F \eta_{c,act}/RT}\right) \qquad \text{Eq. (3.4)}$$

where ς is specific active surface area (1/m), j is exchange current density

per active surface area (A/m^2), c is species concentration (kmol/m^3), γ concentration exponent, α is transfer coefficient, η_{act} is activation overpotential, F is Faraday constant (C/mol), R is gas constant and T is temperature. And subscripts a, c and 0 indicate anode, cathode, and reference value respectively. Eq. (3.3) and Eq. (3.4) are Butler-Volmer equations, however, in relative high current density, they can be simplified to Tafel equation.

$$J_a = (\varsigma_a j_a^0)\left(\frac{c_{H_2}}{c_{H_2}^0}\right)^{\gamma_a}\left(e^{\alpha_a F\eta_{a,act}/RT}\right) \quad \text{Eq. (3.5)}$$

$$J_c = (\varsigma_c j_c^0)\left(\frac{c_{O_2}}{c_{O_2}^0}\right)^{\gamma_c}\left(e^{-\alpha_c F\eta_{c,act}/RT}\right) \quad \text{Eq. (3.6)}$$

In this study, current density over 1 A/cm^2 was selected as driving condition since reactants starvation and water accumulation near outlet were the main area of interest. Therefore, using Tafel equation instead of Butler-Volmer equation was appropriate. And then, species volumetric sources on catalyst layer and conservation of current can be expressed as follows:

$$S_{H_2} = -\frac{M_{H_2}}{2F}J_a \quad \text{Eq. (3.7)}$$

$$S_{O_2} = -\frac{M_{O_2}}{4F}J_c \quad \text{Eq. (3.8)}$$

$$S_{H_2O} = \frac{M_{H_2O}}{2F}J_c \quad \text{Eq. (3.9)}$$

$$\int J_a dV = \int J_c dV \quad \text{Eq. (3.10)}$$

where S is source term of species (kg/m^3-s) and M is molecular weight (kg/kmol). Eq. (3.10) indicates current conservation since a sum of electrical current is equally produced on catalyst layer at both anode and cathode side.

Source of heat can be expressed as follows:

$$S_h = h_{react} - J_{a,c}\eta_{a,c} + I^2 R_{ohm} + h_L \qquad \text{Eq. (3.11)}$$

where h_{react} and h_L are enthalpy change in electrochemical reaction and phase change of water respectively, $J_{a,c}\eta_{a,c}$ indicates product of transfer current and the overpotential on catalyst layer and $I^2 R_{ohm}$ is heat generation due to ohmic resistivity.

For water transport modeling on GDL and catalyst layer, liquid water condensation rate can be expressed as follows:

$$S_w = \nabla \cdot \left(\rho_l \frac{K s^3}{\mu_l} \frac{dP_{cap}}{ds} \right) \qquad \text{Eq. (3.12)}$$

$$S_w = \begin{cases} (1-s) C_r \dfrac{P_{wv} - P_{sat}}{RT} M_{H_2O} & if \;\; P_{wv} - P_{sat} > 0 \\ s C_r \dfrac{P_{wv} - P_{sat}}{RT} M_{H_2O} & if \;\; P_{wv} - P_{sat} < 0 \end{cases} \qquad \text{Eq. (3.13)}$$

$$P_{cap} = \frac{\sigma cos\theta_c}{\left(\frac{K}{\varepsilon}\right)^{0.5}} (1.417s - 2.12s^2 + 1.263s^3) \;\; if \;\; \theta_c > 90^\circ \qquad \text{Eq. (3.14)}$$

where K is intrinsic permeability (m^2, reciprocal term of viscous resistance in ANSYS FLUENT), s is volume fraction of liquid water, μ_l is liquid water viscosity (kg/m-s), σ is surface tension (N/m^2), θ_c is contact angle and ε is porosity. P is pressure (N/m^2) and its subscripts wv, sat and cap indicate

water vapor, saturation and capillary respectively. C_r is set to 100 s^{-1} as default value, which means condensation rate constant.

Instead of using multicomponent diffusion correlations, approximated dilute method was utilized for diffusion in fuel cell. Diffusivity (m^2/s) of species i can be expressed as follow:

$$D_i = \varepsilon^{1.5}(1-\mathrm{s})^{\gamma_s} D_i^0 \left(\frac{P_0}{P}\right)^{\gamma_p} \left(\frac{T}{T_0}\right)^{\gamma_t} \quad \text{Eq. (3.15)}$$

where subscripts s, p and t of exponent γ are liquid water volume fraction, pressure and temperature respectively. Reference values of exponents, pressure and temperature can be differed by modifying user defined functions in ANSYS FLUENT.

For PEMFC, water and proton transfer through membrane. Correlations about water balance and ionic conductivity on membrane can be expressed as follow:

$$\kappa_{ion} = \beta(0.514\lambda - 0.326)^{\omega} e^{1268\left(\frac{1}{303}-\frac{1}{T}\right)} \quad \text{Eq. (3.16)}$$

$$W_{drag} = 2n_{drag}\frac{j}{2F} \qquad (n_{drag} = 2.5\frac{\lambda}{22}) \quad \text{Eq. (3.17)}$$

$$W_{back\ diffusion} = -\frac{\rho_{mem}}{M_{mem}} D_{mem}(\lambda)\frac{d\lambda}{dz} \quad \text{Eq. (3.18)}$$

$$W_{total} = 2n_{drag}\frac{j}{2F} - \frac{\rho_{mem}}{M_{mem}} D_{mem}(\lambda)\frac{d\lambda}{dz} \quad \text{Eq. (3.19)}$$

where β and ω are constants and λ is water content. n_{drag} and M_{mem}

are osmotic drag coefficient and equivalent weight of dry membrane. On membrane, electric-osmotic drag force make water transfer from anode to cathode side. On the other hand, due to water concentration difference between both side (normally much higher at cathode), back diffusion occurs that make water transfer from cathode to anode. Therefore, sum of water transfer through membrane can be sum of Eq. (3.18) and Eq. (3.19). Diffusivity of water on membrane is function of water content. As water content on membrane and operating temperature increase, ionic conductivity of membrane can be increased also according to Eq. (3.16).

Mass flow rate boundary conditions can be obtained as follows:

$$\dot{m}_{O_2} = \frac{jA \times SR_c}{4F \times M_{O_2}} \quad \text{Eq. (3.20)}$$

$$\dot{m}_{H_2} = \frac{jA \times SR_a}{2F \times M_{H_2}} \quad \text{Eq. (3.21)}$$

where SR indicated stoichiometric ratio, can be differed by driving condition. According to relative humidity (RH) of anode and cathode side, total mass flow rate boundary conditions can be differed.

Before starting calculation, several material properties and constants had to be decided. Min et al. [100] conducted parameter study that revealed sensitivity between input parameters and numerical results. According to the results, transfer coefficient of cathode affected greatly to I-V curve and volumetric

transfer current density affected moderately, compared with other parameters. Porosity of GDL affected well to I-V curve, however, exceeding porosity over 0.6 did not change fuel cell performance noticeably. Fortunately, parameters which are considered hard to be measured directly like porosity of catalyst layer, diffusion coefficient and permeability of GDL had small impact to I-V curve in case these properties are in proper range. Therefore, transfer coefficient was selected as primary validating parameter and volumetric transfer current of anode and cathode side were selected as secondary. Specific active surface area (surface/volume ratio in program) was fixed and anode reference exchange current density had 10^3 times larger than cathode [101]. All the constants and properties needed from Eq. (3.1) to Eq. (3.21) and modified properties are listed on Table 3.1

Table 3.1 Properties in numerical equations

Parameter	Value	Reference
ς [1/m]	200000	[99]
j_a^0, j_c^0 [A/m^2]	5000, 5	Validation
$c_{H_2}^0$ [kmol/m^3]	5.64×10^{-3}	[99]
$c_{O_2}^0$ [kmol/m^3]	3.39×10^{-3}	[99]
$k_{BPP}, k_{catalyst}, k_{mem}$ [W/m-K]	150, 1, 0.95	[99]
$\kappa_{BPP}, \kappa_{GDL}, \kappa_{catalyst}$ [S/m]	20000, 5000, 5000	[102]
γ_a, γ_c	0.5, 1	-
$\gamma_s, \gamma_p, \gamma_t$	2.5, 1.0, 1.5	-
α_a, α_c	0.6	Validation
$K_{GDL}, K_{catalyst}, K_{mem}$ [m^2]	10^{-12},10^{-13}, 2×10^{-20}	[102, 103]
$\varepsilon_{GDL}, \varepsilon_{catalyst}, \varepsilon_{mem}$	0.5, 0.3, 0.5	[100]
$\theta_{c,GDL}, \theta_{c,catalyst}$ [°]	130	Measured
P_0 [Pa]	101325	-
T_0 [K]	300	-
$D_{H_2}^0$ [m^2/s]	9.15×10^{-15}	[100]
$D_{O_2}^0$ [m^2/s]	2.2×10^{-15}	[100]

$D_{H_2O}^0$ [m^2/s]	2.56 ×10^{-15}	[100]
ρ_{mem} [kg/m^3]	2719	-
M_{mem} [kg/kmol]	1100	-
β	1	-
ω	1	-
C_r [s^{-1}]	100	-

3.2.2. Model validation

Model validation in this study was not based on experimental results from other previous studies. Instead, a unit cell with single and long straight channel with 3D structure was made. Here is five steps of model validation:

1. Selecting key properties to focus on
2. Grid test for mesh independency
3. Experiment for model validation
4. Repeated calculation varying validation parameters
5. Geometry modification for SS-6(0) and SS-8(0)

The last step occurred since manufacturing thickness limitation from chapter 2 and further explanation about this was discussed later.

In ANSYS FLUENT, size of mesh in each flow domain is very important, affecting to calculation results. For deciding proper sizes of mesh, various versions of mesh have to be tested. Normally, grid tests in numerical studies compare result error, reducing size of mesh (increasing a number of mesh). However, key properties selection should be done first to secure the decision of mesh size. For instance, temperature can’t be selected as key property in isothermal model. Plus, if pressure analysis was planned, pressure should be included in key properties.

In this study, velocity, pressure, current density and oxygen molar

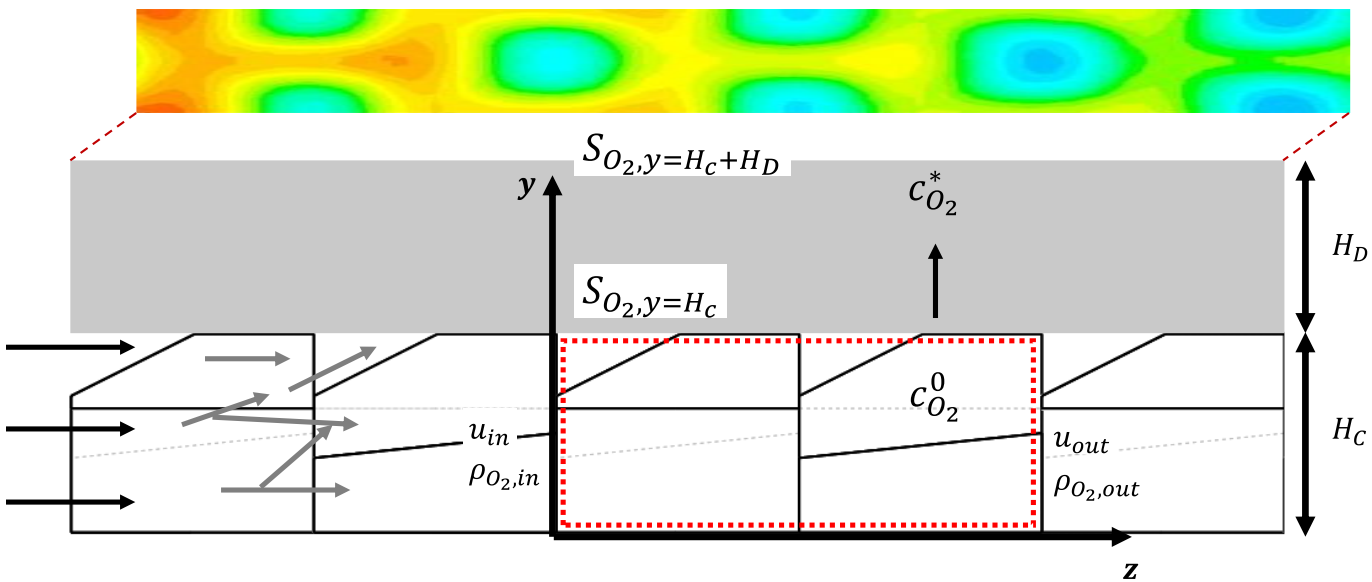

Figure 3.1 Schematic of flow and 3D structure inside a fuel cell

concentration on catalyst layer were selected as key properties. **Figure 3.1** shows simplified diagram with properties, channel geometry and contour of oxygen molar concentration on the interface between GDL and catalyst layer. Black arrows indicates initial flow direction and gray arrow indicates changed flow direction through 3D structure. In this process, reactants and products are transported through 3D structure, GDL and catalyst layer. According to electro-chemical reaction, concentration of reactants such as oxygen is much higher at channel compared with catalyst layer. Concentration loss occurs when this concentration difference goes large. Relations between reactants concentration and overvoltage are expressed in Eq. (3.22) to Eq. (3.24)

$$\eta_{conc} = E^0_{Nernst} - E^*_{Nernst} \qquad \text{Eq. (3.22)}$$
$$= \left(E^0 - \frac{RT}{nF} ln \frac{1}{c^0_R}\right) - \left(E^0 - \frac{RT}{nF} ln \frac{1}{c^*_R}\right)$$
$$= \frac{RT}{nF} ln \frac{c^0_R}{c^*_R}$$

$$\eta_{conc} = \eta^*_{act} - \eta^0_{act} \qquad \text{Eq. (3.23)}$$
$$= \left(\frac{RT}{\alpha nF} ln \frac{j c^{0*}_R}{j^0_0 c^*_R}\right) - \left(E^0 - \frac{RT}{nF} ln \frac{j c^{0*}_R}{j^0_0 c^0_R}\right)$$
$$= \frac{RT}{\alpha nF} ln \frac{c^0_R}{c^*_R}$$

$$\eta_{conc} = \left(1 + \frac{1}{\alpha}\right) \frac{RT}{nF} ln \frac{c^0_R}{c^*_R} \qquad \text{Eq. (3.24)}$$

Eq. (3.22) indicates relation between concentration and Nernst voltage. Eq.

(3.23) indicates relation between concentration and reaction rate. Therefore, total concentration overvoltage can be expressed as Eq. (3.24). As current density increases, reactants concentration on catalyst layer decreases so concentration loss is dominant in high current density. Plus, water accumulation in cathode channel blocks reactants flow and impedes mass transfer. As a result, oxygen concentration on catalyst layer have to be the most important property during computational study, related with high current density.

Oxygen distribution along the channel be written as follows:

$$\rho_{O_2}\big|z = Z, y = H_c + H_D = \rho_{O_2,in} - M_{O_2}\frac{j}{4F}\left(\frac{H_c}{Sh_f D_{O_2}} + \frac{H_D}{D_{O_2}^{eff}} + \frac{Z}{u_{in}H_c}\right) \quad \text{Eq. (3.25)}$$

where H_c and H_D are thickness of channel and GDL, Z is position along flow channel, Sh_f is Sherwood number and u_{in} is initial velocity. If flow rate for unit channel volume is fixed, reducing of H_c can be favor of molar concentration on catalyst layer and if H_c is equal along the channel, increasing u_{in} can be favor of fuel cell performance. This means non-uniformity in width and slope can affect fuel cell performance and velocity of flow can be important factor, analyzing flow characteristics related with performance enhancement. In chapter 2, pressure analysis was conducted and pressure, so pressure difference can be included in key properties. Therefore, grid test comparing

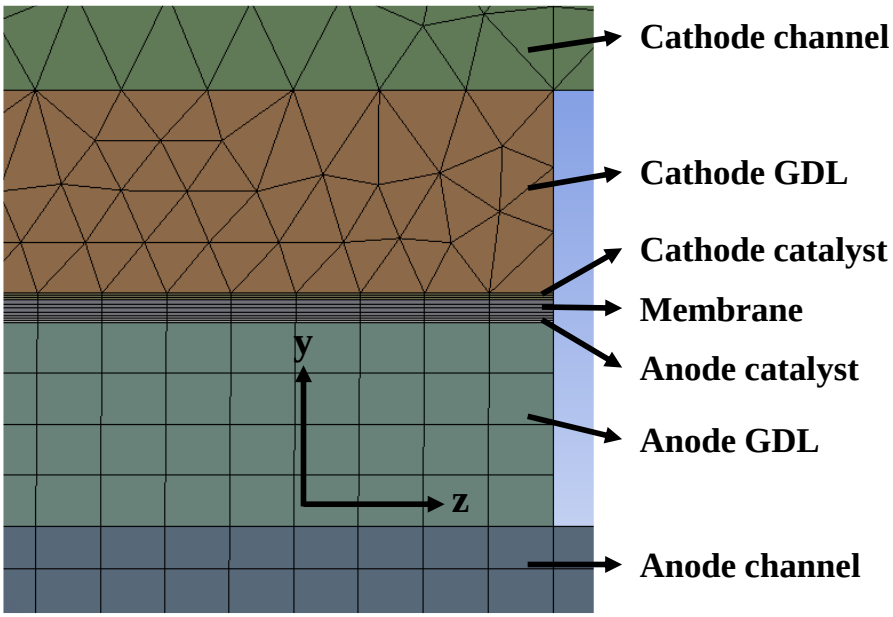

Figure 3.2 Schematic of mesh at various components

Table 3.2 Specifications of mesh

Component \ Version	1	2	3	4
Membrane	15060	20040	30060	44080
Cathode catalyst layer	11295	15030	22545	30060
Anode catalyst layer	11295	15030	22545	30060
Cathode GDL	66065	99903	278883	396656
Anode GDL	15060	20040	30060	44080
Cathode channel	103063	361619	385471	519840
Anode channel	11040	11360	22044	28056
Cathode bipolar plate	199921	337538	352795	539269
Anode bipolar plate	22590	31730	37575	62124

velocity, pressure, current density and oxygen molar concentration on catalyst layer should be done before computational analysis.

Next, mesh size should be verified since rough composition of mesh can't draw accurate results and excessively dense mesh would consume plenty of time and computing power. Therefore, deciding proper sizes of mesh is quite important. Cathode channel, GDL of both side, catalyst layer of both side and membrane have to be considered important fluid domain since complex electro-chemical reaction and flow occur through these. **Figure 3.2** shows configurations of mesh at each component. Reducing size of mesh on important domain, various versions of mesh were built. Of course, mesh sizes of anode channel and bipolar plate of both sides were also reduced since all of the node in mesh were connected. **Table 3.2** shows specific number of each version of mesh according to the components in fuel cell and **Figure 3.3** shows four versions of mesh. Considering the fourth version of mesh as a standard, result errors of key properties are plotted in **Figure 3.4**. As shown, all errors between fourth and third mesh were under 1%, so fourth mesh was selected as proper version of mesh, securing reliability of result and saving computing power and time.

For model validation, unit cell for long straight channel with 3D structure was prepared. **Figure 3.5** shows BPP of unit cell and single-unit arranged 3D

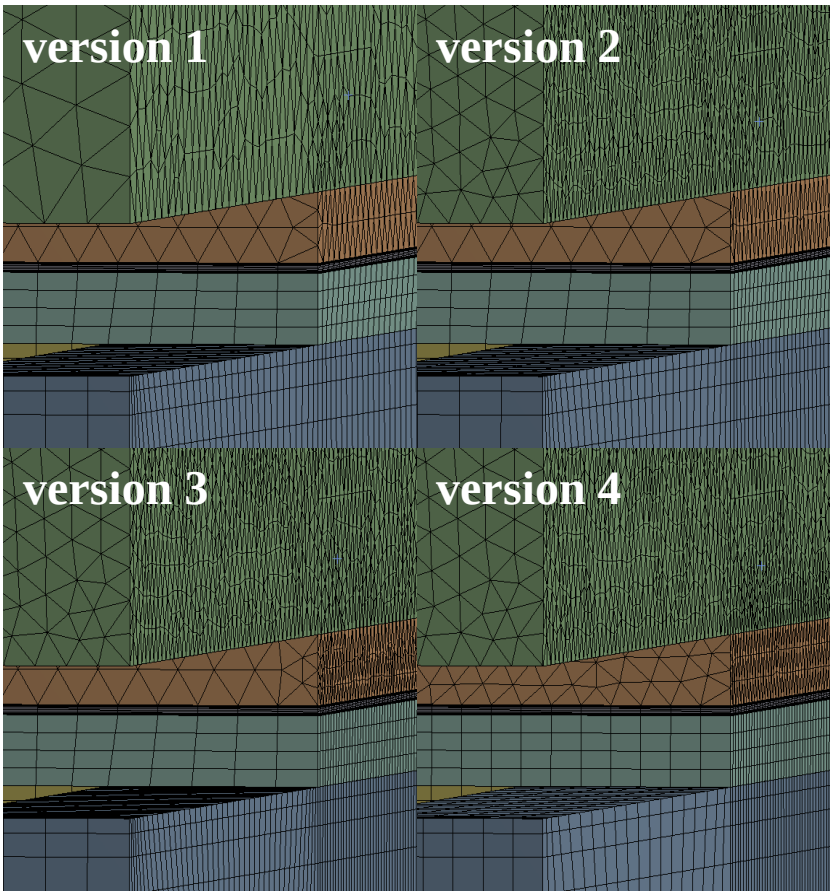

Figure 3.3 Formations of mesh

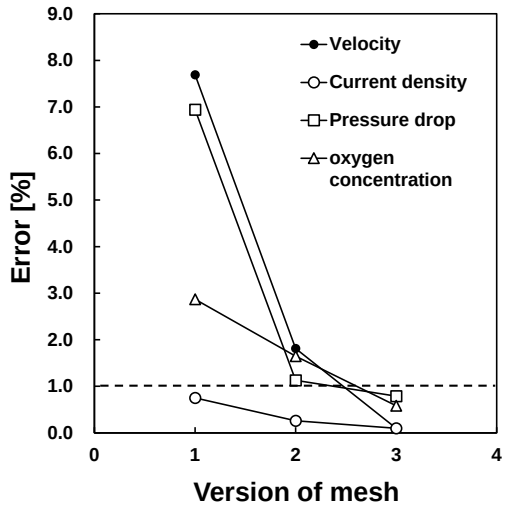

Figure 3.4 Errors in key properties among different versions of mesh

structure. Test conditions for experiment and computational analysis are listed in **Table 3.3**. According to Eq. (3.10), current density difference between anode and cathode side needs to be converged to zero. Therefore, current density difference between two adjacent steps and both side could be selected as convergence criterion. Methods for measuring I-V curve in experiments was the same with chapter 2. **Figure 3.6** shows comparison between experimental and numerical results. Open circuit voltage (OCV) measured in experiment was applied to input value in FLUENT model. Errors were below 5% from open circuit voltage (OCV) to about 0.5 V but increased until 0.3 V. This errors were thought to be occurred due to water droplet accumulation. By means of Eq. (3.12) to Eq. (3.14), water blockage effect was only considered in GDL and catalyst layer domain. In real world, water droplet accumulation along the channel, especially near outlet of cathode block GDL surface, impeding reactants mass transfer through GDL. However, 0.5 V could be considered as low enough to assume high current density region since driving range under 0.5 V causes severe decline of fuel efficiency and life time [104]. For this reason, 0.5 V was selected as test condition.

Experiments were conducted on 20 cm^2 unit cell and computational analysis were conducted on 1.01cm^2. In other words, at 777 arrangement, seven unit structures were aligned in width direction and 51 structures were aligned in

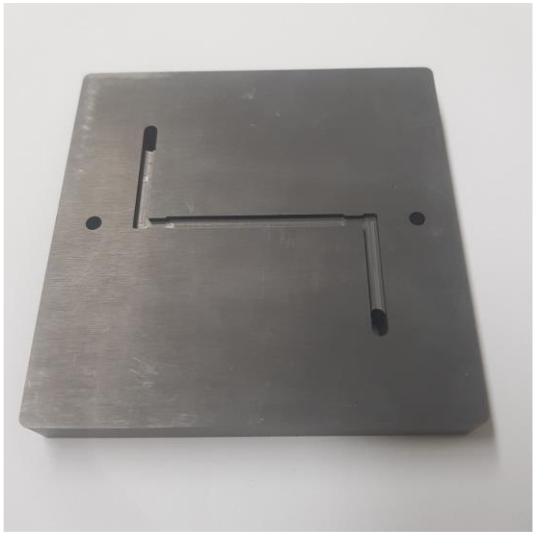

(a)

(b)

Figure 3.5 (a) Carbon BPP and (b) 3D structure for model validation

Table 3.3 Experimental and numerical boundary conditions

Parameter	Value
Temperature of the inlet gas [K]	333
Temperature of the cell [K]	333
Relative humidity (anode/cathode) [%]	0 / 100
Stoichiometric ratio (anode/cathode)	1.5, 2
Current density for mass flow rate [A/cm^2]	1.2
Voltage (on-circuit)	0.5
Voltage (open-circuit)	0.95
Operating pressure (anode/cathode) [bar]	1, 1
Channel width [mm]	2.8
Channel length [mm]	36
Version of single structure	SS-7(0)
Convergence criterion [%]	$\pm$0.1

length direction (20 cm^2). Instead, at the first step of computational analysis, one unit structure was positioned in width direction and 18 structures were aligned in length direction. Due to limitation of computing capability, scale of computing domain was reduced. Except for this reason, numerical study on 3D structure with single structure arranged was essential since sole effects from non-uniform arrangement in length direction was needed to be discussed. In chapter 2, long rectangular active area was chosen instead of square since the object of experiment was prove the effect of non-uniform arrangement in length direction, minimizing mass transfer along width direction.

Starting this chapter, fifth steps of model validation, geometry modification were introduced. In experimental study, channel width was controlled by a number of unit, arranged in width direction (6, 7 and 8). If the geometric parameters were not modified, unit structure of SS-6(0), SS-7(0) and SS-8(0) had different channel width which made 678 arrangement of single row had width difference according to the position of structure. **Figure 3.7** (a) shows 678 arrangement with no geometric modification, which was not appropriate to be analyzed and **Figure 3.7** (b) shows desirable transformation. The reason of this difference was manufacturing limitation of thickness, 0.6 mm. In computational analysis, however, thickness limitation could be solved. Through proper modification, results of key properties had to be similar and the most

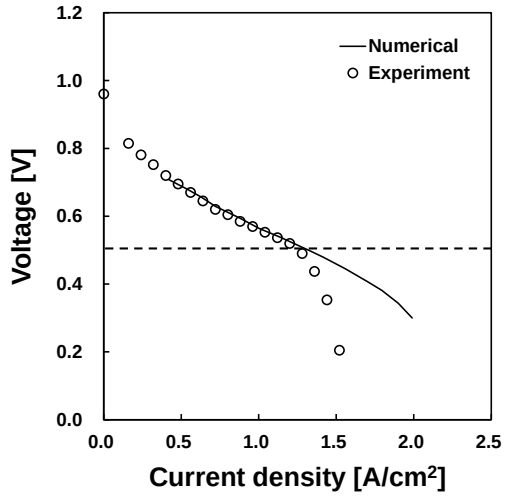

Figure 3.6 I-V curve comparison between numerical and experimental results

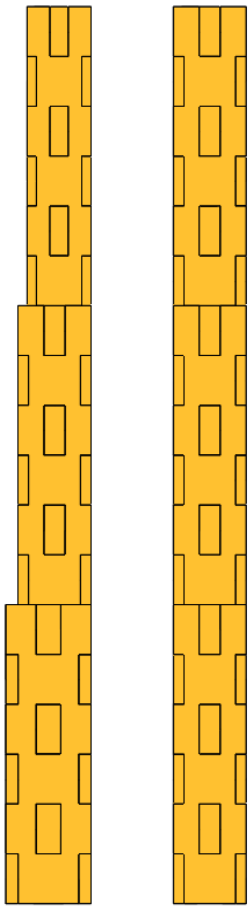

(a) **(b)**

Figure 3.7 678 arrangement of single row of unit structure; (a) experiments, (b) numerical

importantly, similarity should be secured between structures used in experimental and computational study.

Reminding that volume of structure, contact area between GDL and structure and volume fraction of inclined structure were considered as important variable deciding geometric parameter of SS-6(0), SS-7(0) and SS-8(0), these should be maintained to minimize modification error. **Table 3.4** shows geometric parameters of 3D structures used in experiments and numerical modeling. Decreasing and increasing wall thickness of unit structure of SS-7(0), modified SS-6(0) and SS-8(0) could be formed. Through this process, width of unit structure, volume fraction, GDL contact area and volume fraction of inclined surface of each unit structure were maintained. **Figure 3.8** shows error in modification results of key properties and non-dimension numbers through modification. Reynolds number (Re) and the transversal Peclet number (Pe_y) can be expressed as follow [105]:

$$\mathrm{Re} = \frac{\rho u L}{\mu} \qquad \text{Eq. (3.26)}$$

$$\mathrm{Pe}_y = \frac{time_{Diff\_y}}{time_{Res\_y}} \qquad \text{Eq. (3.27)}$$

$$time_{Diff\_y} = \frac{{H_C}^2}{D_{O_2}} \qquad \text{Eq. (3.28)}$$

$$time_{Res\_y} = \frac{H_C}{u} \qquad \text{Eq. (3.29)}$$

Both are non-dimensional number that represent the ratio of inertial forces

Table 3.4 Specific parameters of uniform 3D structure arrangements for numerical study

	Parameter				
Type	Volume [%]	GDL contact area [%]	Inclined volume [%]	Width [mm]	Wall thickness [mm]
6-exp	54.81	31.85	28.41	3.33	0.60
6-m	54.81	31.85	28.41	2.86	0.51
7-exp	58.09	34.79	37.46	2.86	0.60
7-m	58.09	34.79	37.46	2.86	0.60
8-exp	61.37	37.73	51.22	2.50	0.60
8-m	61.36	37.73	51.22	2.86	0.68

* N-exp : Unit structure of SS-'N' used in experiment * N-m : Modified unit structure of SS-'N' used in model

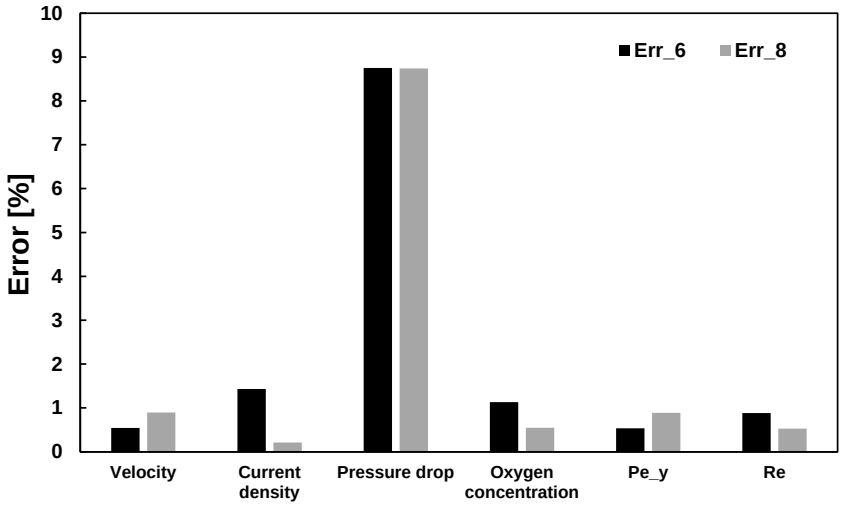

Figure 3.8 Errors in key properties through modification

to viscous forces and the characteristic time for diffusion to that for convection. According to Reynolds number flow characteristics such as flow regime are differed and Peclet number can help to reveal dominant factor at mass transfer. According to geometry of channel, average velocity and density along the channel, and mass transfer dominance can be differed. Therefore, analysis on two non-dimensional numbers was needed to secure validity of model modification. However, the only problem was error of pressure. It was occurred due to decrease of cross-sectional area with the same channel length. Instead, **Figure 3.9** shows deviation between modified 666 pattern and 888 pattern, compared with modification result. Ratio between modified results and geometry deviation could be newly defined as follow:

$$\mathrm{Dev_m} = \left| \frac{X_{6\_m} - X_{8\_m}}{X_{6\_m} - X_{6\_exp}} \right| \quad \text{Eq. (3.30)}$$

$$\mathrm{Dev_{exp}} = \left| \frac{X_{6\_exp} - X_{8\_exp}}{X_{6\_m} - X_{6\_exp}} \right| \quad \text{Eq. (3.31)}$$

where X means various properties result of computational analysis. If the difference through modification are much smaller than deviation between two types of flow channel, it can be considered minor in terms of key properties. According to result, structure modification could be used to analyze flow characteristics along 3D structure in fuel cell.

Table 3.5 lists detail results of models. Result of experimental and numerical

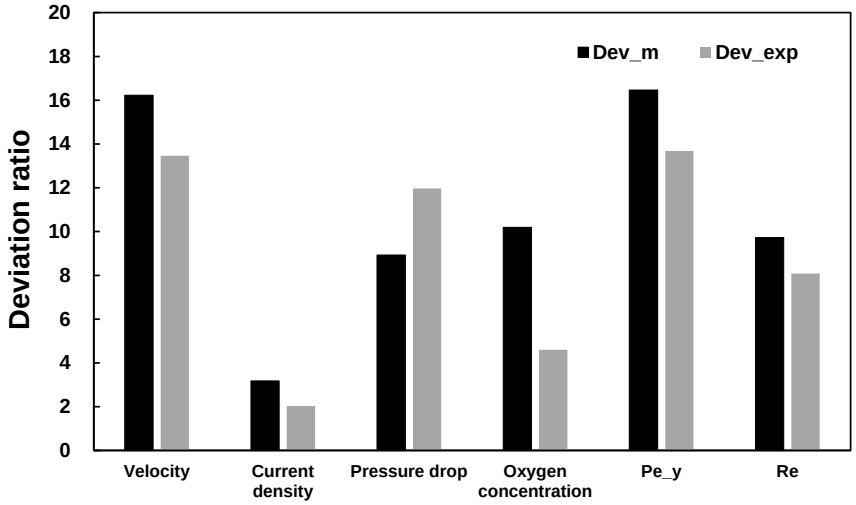

Figure 3.9 Deviation ratio of key properties

Table 3.5 Specific values of key properties

	Properties					
Type	u [m/s]	j [A/cm^2]	dP [Pa]	$c^*_{O_2}$ [mol/m^3]	Pe	Re
6-exp	0.34	1.29	29.56	1.53	21.14	1.45
6-m	0.34	1.30	32.14	1.54	21.03	1.44
7-exp,m	0.35	1.27	38.57	1.45	21.83	1.49
8-exp	0.37	1.25	60.52	1.45	22.69	1.56
8-m	0.37	1.25	55.23	1.44	22.89	1.56

model of SS-7(0) was equal since there was no parameter modification on unit structure of SS-7(0), considering it as standard in chapter 2.3.1. In this chapter, instead of maintaining name of 3D structure like SS-7(20), new terms such as ‘normal’, ‘thick’, ‘thin’ and ‘steep’ were used since numbering structure by number of units along width direction was no longer valid through structure modification. Since wall thickness was changed to numerical study, the name of structure for CFD was corrected. **Table 3.6** shows various types of structure arrangements for numerical study. For width non-uniformity, structure with thick and thin wall were substituted in outlet region. N-T represented 778 pattern on experiments in previous chapter. In order to focus on flow characteristic near the outlet region, calculation on N-t was also conducted to compare flow properties between thickening and thinning wall. Likely, N-t represented 776 pattern. For revealing the cause of performance difference between 778 and 877 pattern, T-N case was selected. On the same hand, N-S and S-N were selected to verify similar performance between 777(0-10-20) and 777(20-10-0) pattern.

Table 3.6 Specific parameters of non-uniform 3D structure arrangements for numerical study

	Parameter		
Pattern	Volume [%]	GDL contact area [%]	
N-N (normal)	58.09	34.79	
T-T (thick)	61.36	37.73	
t-t (thin)	54.81	32.10	
N-T	59.18	35.77	Width = 2.86 mm
N-t	57.00	33.89	Length = 35.29 mm
T-N	59.18	35.77	
N-S (steep)	58.99	34.79	
S-N	58.99	34.79	

3.3. Results and discussion

3.3.1. General characteristics of 3D structure as flow channel

Firstly, comparison between parallel and 3D structure as flow channel for PEMFC was conducted. **Table 3.7** lists geometric parameters of standard uniform 3D structures arrangement and two parallel flow channels. The rib size of first parallel flow channel was set to make GDL contact area equal with N-N. Plus, the rib size of second parallel flow channel was set to reference in experimental study. It had rib and channel width ratio of 0.9:1 and this value is on proper range of conventional parallel flow channel. In this chapter, x, y and z-plane and direction were used to briefly explain domains position of analysis. Each of direction means width, perpendicular with GDL surface and length direction respectively. Therefore xy-planes are perpendicular with inlet-outlet, yz plane shows flow characteristics from inlet to outlet at the middle of flow channel and zx-planes are parallel with GDL, catalyst layer and membrane surfaces. **Figure 3.10** shows oxygen molar concentration contour on yz-plane passing through middle of flow channel. From inlet to outlet, oxygen molar concentration was continuously declined since reactants are continuously consumed along flow direction in PEMFC. Plus, concentration near GDL was smaller than that on middle of flow channel since reactants molecular diffusion

Table 3.7 Specific parameters of 3D structure and reference parallel flow channel

	Parameter		
Pattern	Volume [%]	GDL contact area [%]	Rib width [mm]
N-N	58.09	34.79	2.86
Parallel 1	34.79	34.79	1.00
Parallel 2	45.00	45.00	1.29

* Width = 2.86 mm / Length : 35.29 mm

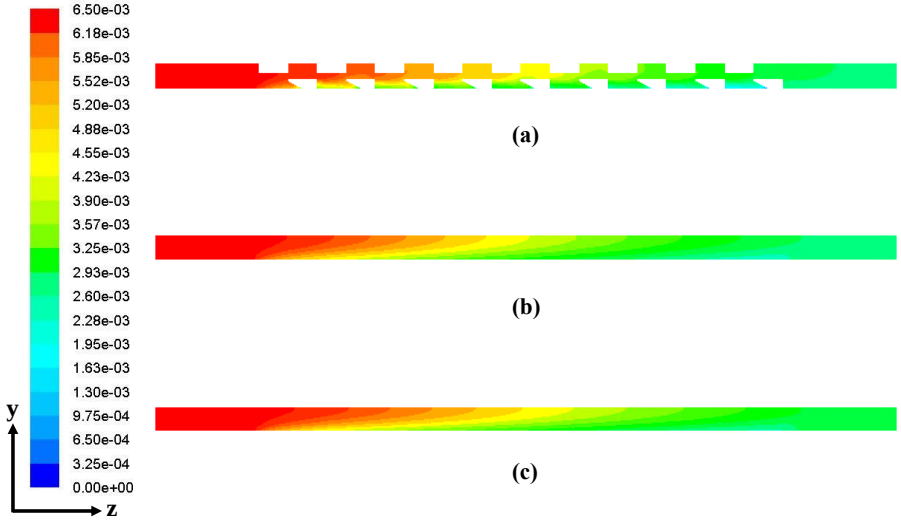

Figure 3.10 Contour of oxygen molar concentration along flow channel; (a) N-N, (b) Parallel 1, (c) Parallel 2

through GDL surface. Generally, molar concentration in flow channel, so called bulk concentration, is continuously decreased in y-direction until catalyst layer. This concentration gradient forces species to diffuse to low concentration region. Written phenomena is occurred regardless of type of flow channel geometry. **Figure 3.11** shows oxygen concentration contour on interface between GDL and catalyst layer. In fuel cell, high concentration of reactants on this surface have to be secured to develop a high performance fuel cell. Unlike with parallel flow channel, 3D structure had staggered arrangement of unit structures, allowing reactants and products flow via unit to unit. Meanwhile, flow along parallel needs to pass under rib to reach to adjacent channel. If ratio of rib width to channel width increases in parallel flow channel like from the Parallel 1 to 2, overall flow velocity was expected to be increased. Also, oxygen diffusion was expected to be decreased due to increased GDL-rib contact area. Comparing **Figure 3.11**(b) and (c), result shows that non-uniformity of oxygen concentration on catalyst layer of second parallel channel was higher than that of the first parallel channel. **Figure 3.12** shows specific values about three types of channel. Thickening width of rib on parallel channel resulted in decreasing molar concentration on catalyst layer and increasing standard deviation meaning non-uniform chemical reaction is expected to be harsh. Comparing N-N and the first parallel channel, 3D structure brought lower oxygen

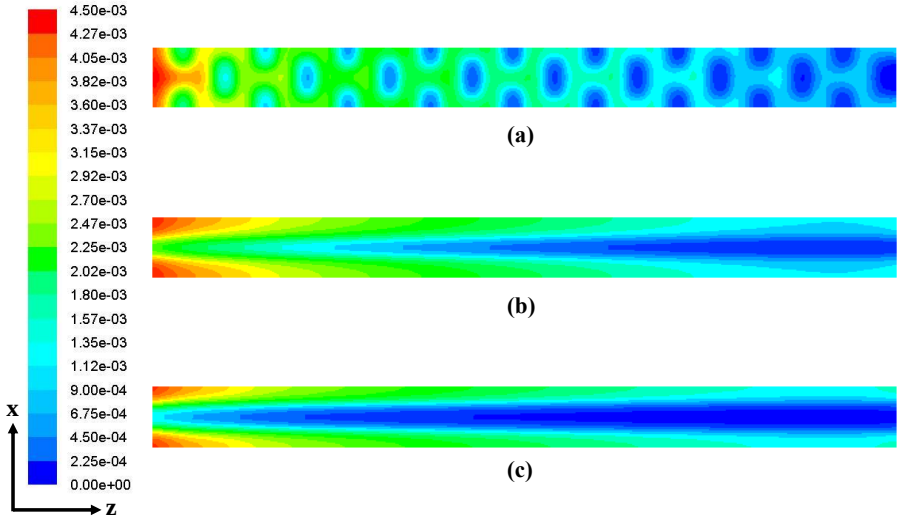

Figure 3.11 Contour of oxygen molar concentration on interface between GDL and catalyst layer; (a) N-N, (b) Parallel 1, (c) Parallel 2

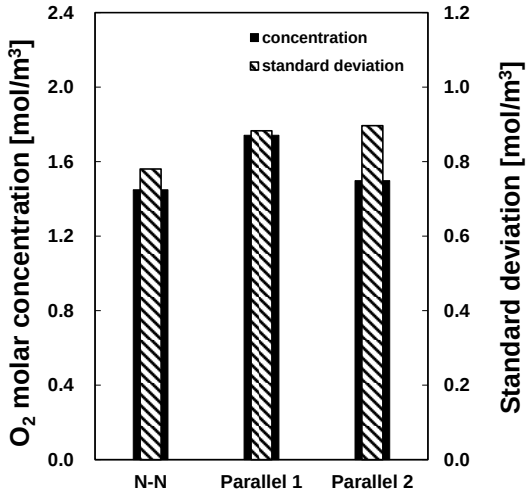

Figure 3.12 Oxygen molar concentration value on interface between GDL and catalyst layer and standard deviations

concentration, however, more uniform distribution was obtained. Moreover, this analysis was on assumption that flow channels had ideal inlet. The biggest problem in parallel flow channel, especially in multichannel situation, is non-uniform distribution of reactant gas due to non-ideal header design [68].

Figure 3.13 shows velocity contour on yz-plane in flow channel. Parallel flow channel can perform higher average velocity by reducing channel width or height according to **Figure 3.13** (b) and (c). Even if flow velocity through parallel flow channel is supposed to be increased by manipulating geometry of channel, velocity fluctuation via grooved and staggered structures was one of the most unique characteristics of 3D structure as flow channel. Locally accelerated velocity profile was expected to enhance mass transfer of reactants and this point was discussed in **chapter 3.3.2.**

Through these basic analysis, several advantages of 3D structure could be stated, compared with conventional channel and metal foam as flow distributor. For example, flow can easily reach to adjacent channel unit along 3D structure, not blocking reactants and accumulated water and this characteristic is similar with metal foam as flow distributor [57]. Due to this feature, more uniform distribution of reactants on GDL-catalyst interface could be observed in **Figure 3.12**. The biggest difference between metal foam and 3D structure is sloped structure. Metal foam can't manipulate flow direction and control velocity

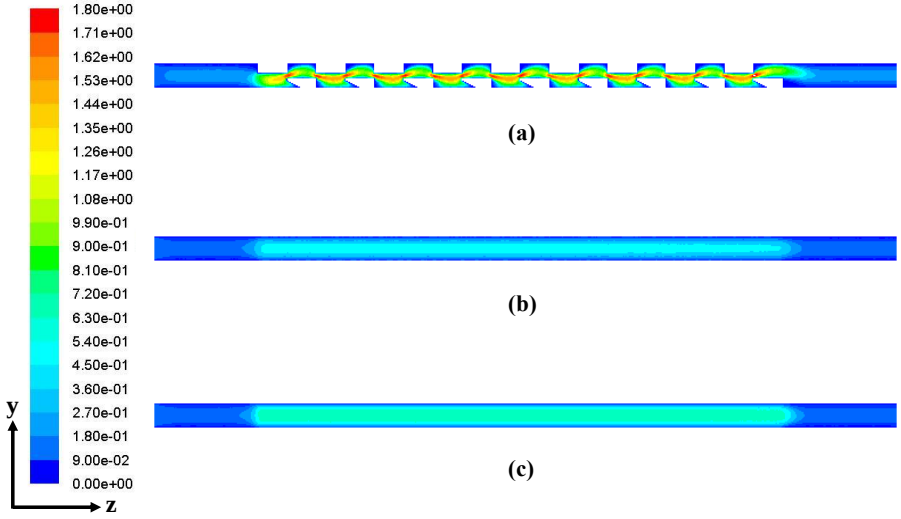

Figure 3.13 Contour of velocity magnitude along flow channel; (a) N-N, (b) Parallel 1, (c) Parallel 2

magnitude easily. Even if some studies tried to control flow velocity through metal foam [59, 96], acceleration directions were limited. Not only the velocity fluctuation in y-direction, which could be observed in **Figure 3.13**, diversified flow acceleration was possible through 3D structure and this was discussed in chapter 4.

Furthermore, additional analysis of Peclet number was conducted to decide appropriate domain of key properties. According to Eq. (3.27)~Eq. (3.29), the Peclet number along the channel and GDL can be calculated. Diffusivity of oxygen, length of flow path can be differed as calculation domains. The Peclet number along the channel and GDL with N-N arrangement was 21.8 and 0.026 respectively. When the Peclet number is way bigger than 1, mass transfer driven by flow velocity is much dominant than diffusion due to concentration gradient. On the contrast, if the Peclet number is way smaller than 1, mass transfer driven by concentration gradient is much dominant. Therefore, along the flow channel, velocity related indexes could be considered important in terms of mass transfer, and along the GDL, oxygen concentration related indexes could be considered important.

For the next step, **Figure 3.14** shows additional analysis domain in flow channel. Flow path through 3D structure can be divided in two region, upper and lower. Flow through below structure was expected to participate more on

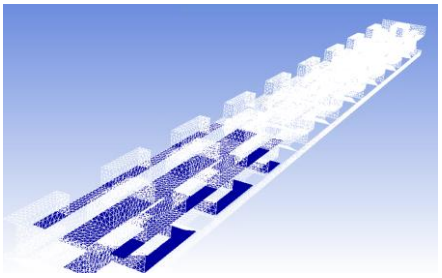

(a)

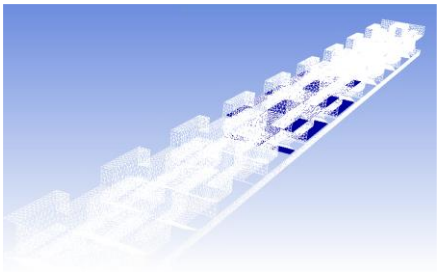

(b)

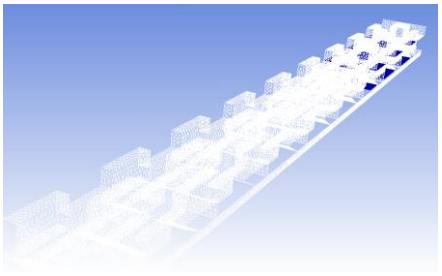

(c)

Figure 3.14 Schematic of zx-plane near GDL surface and middle of upper flow path; (a) inlet (position 1), (b) middle (position 2), (c) outlet (position 3)

mass transfer through GDL. Upper domain was set to pass middle of upper channel and its distance from GDL surface was 1.1 mm. Lower domain was set to pass right above the GDL surface and its distance from GDL surface was 0.1 mm. In addition, each plane was divided into three parts, inlet, middle and outlet. For convenience, each parts were indicated as 'Position 1, 2 and 3' in results. This separation was needed since non-uniform arrangements were planned to be applied on CFD analysis.

Figure 3.15 shows changes in three different properties along the flow direction. As wall thickness increased, average velocity and pressure drop were increased. **Figure 3.15** (a) indicates velocity difference between upper and lower channel. Regardless of wall thicknesses, flow velocity in upper channel was higher than that in lower channel. If increase of flow velocity near GDL surface was in favor of mass transfer, performance with T-T should be higher than that of t-t. However, **Figure 3.15**(c) proves not. According from Eq. (3.22) to Eq. (3.24) ratio of bulk oxygen molar concentration to oxygen molar concentration on catalyst layer decides concentration loss. According to results, higher oxygen molar concentration could be obtain utilizing t-t instead of T-T. This result accords with two different parallel flow channel in **Figure 3.12**. Both results indicated that mass transfer through GDL was good at thin wall (rib) than thick wall (rib) although overall velocity was high at T-T.

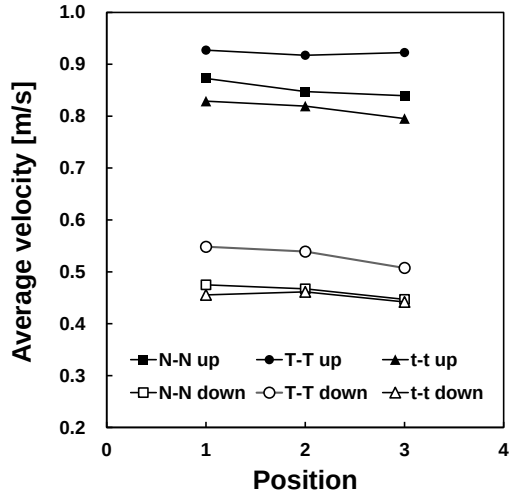
Average velocity [m/s]
1.0
0.9
0.8
0.7
0.6
0.5
0.4
0.3
0.2
0
1
2
3
4
Position
N-N up
T-T up
t-t up
N-N down
T-T down
t-t down

(a)

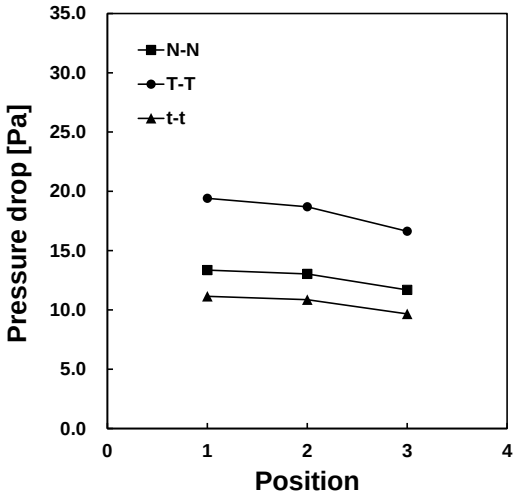
Pressure drop [Pa]
35.0
30.0
25.0
20.0
15.0
10.0
5.0
0.0
0
1
2
3
4
Position
N-N
T-T
t-t

(b)

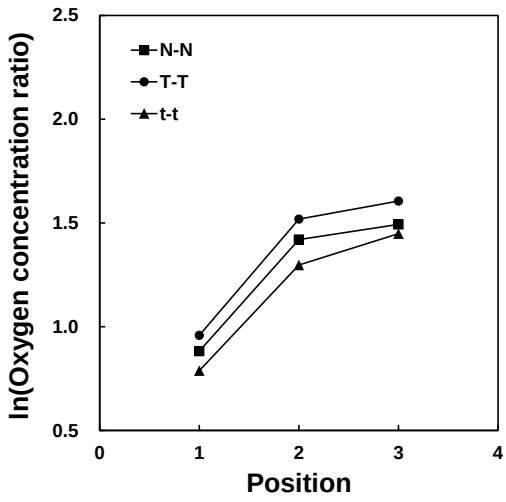

(c)

Figure 3.15 Property changes along flow direction through various uniform 3D structure arrangements; (a) average velocity, (b) pressure drop, (c) concentration term in overvoltage

Arato et al. [105] revealed relation between GDL-rib contact area and oxygen mean flux on catalyst layer.

$$\text{u} \approx 0, \text{Diffusive flux} \approx \left(\frac{\rho D_{O_2}}{GDL - rib\ \ width}\right)\left(m_{f-O_2}\right) \qquad \text{Eq. (3.32)}$$

In Eq. (3.32), m_{f-O_2} indicates mass fraction of oxygen and flow velocity along GDL could be neglected according to the Peclet number comparison between channel and GDL. Even if GDL was set to be isotropic, having equal permeability in all direction, flow path in y-direction is much smaller than the other direction due to length of path (thickness of GDL). In view of GDL, T-T and the second parallel channel provided larger contact area with GDL compared with t-t and the first parallel channel. Shown in **Table 3.6**, T-T had larger GDL-structure contact area, meaning that larger blockage participated in mass transfer. This result has been revealed through various studies in chapter 1.2. In summary, larger GDL-rib contact area could reduce oxygen diffusive flux, leading increased concentration loss.

These characteristics could also be observed by analyzing diffusion of oxygen through GDL, along the rib direction. **Figure 3.16** showed oxygen molar concentration contour on xy-plane, in the middle of flow channel. With N-N, 35.1% of oxygen molar concentration was transferred from center to side. On the other hand, with T-T, 34.7% could be transferred. Larger rib thickness could impede reactants mass transfer through GDL along rib direction. This

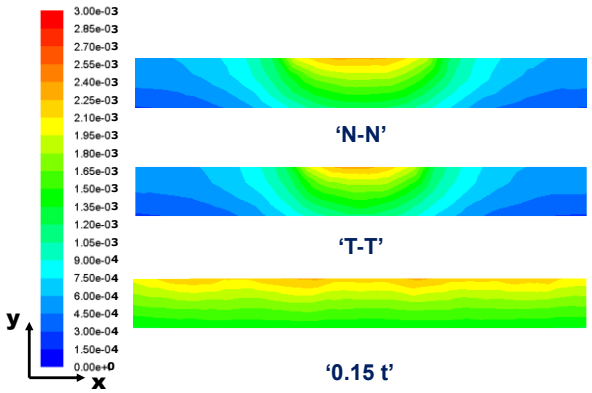

Figure 3.16 Contour of oxygen concentration at GDL (xy-plane) with different wall thickness

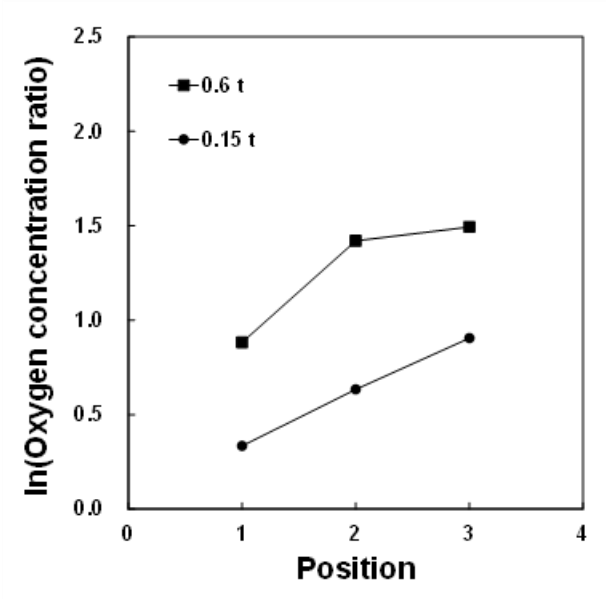

Figure 3.17 Difference at concentration term in overvoltage, comparing N-N with 0.6 mm and 0.15 mm wall thickness

difference could be neglected, however, if the rib thickness reduced by 75%, about 85% of oxygen molar concentration could be conserved and this was directly related with concentration overvoltage and performance. **Figure 3.17** shows reduce in concentration loss through thinning wall by 75%. Due to this result, under the operation at 0.5 V, 33.9% of current density enhancement could be obtained.

Meanwhile, if minimizing GDL-rib contact area is always in favor of fuel cell performance, there was no need to find optimal design for flow channel of fuel cell. Contact resistance and water droplet dynamic were not considered in this CFD model, therefore, additional explain about this is necessary.

In general metallic bipolar plate has higher contact resistance with GDL compared with graphite and carbon based composites [106]. Clamping pressure, surface roughness and material can affect to contact resistivity [107]. If size of rib in parallel flow channel is too small, contact resistance increases and mechanical crack can be occurred on GDL and catalyst layer.

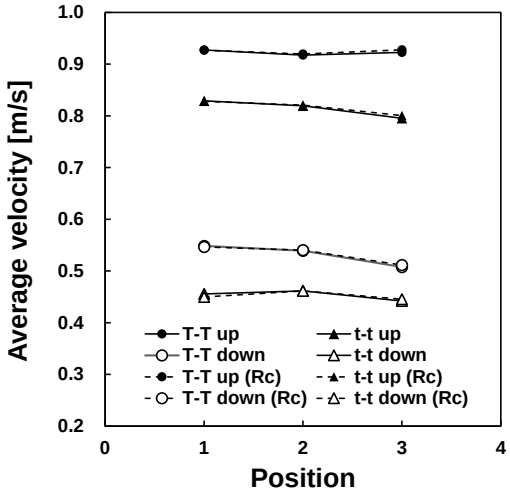
Average velocity [m/s]
1.0
0.9
0.8
0.7
0.6
0.5
0.4
0.3
0.2
0
1
2
3
4
Position
T-T up
t-t up
T-T down
t-t down
T-T up (Rc)
t-t up (Rc)
T-T down (Rc)
t-t down (Rc)

(a)

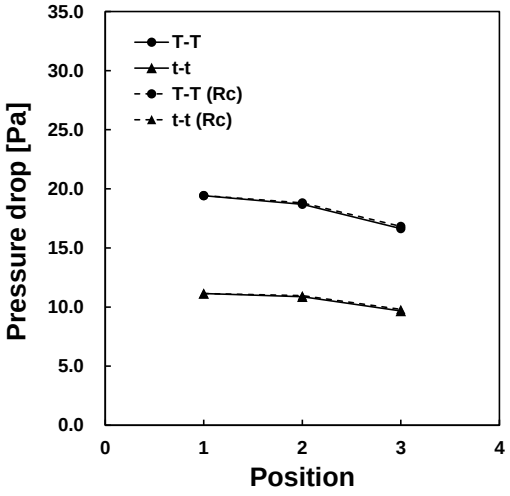
Pressure drop [Pa]
35.0
30.0
25.0
20.0
15.0
10.0
5.0
0.0
0
1
2
3
4
Position
T-T
t-t
T-T (Rc)
t-t (Rc)

(b)

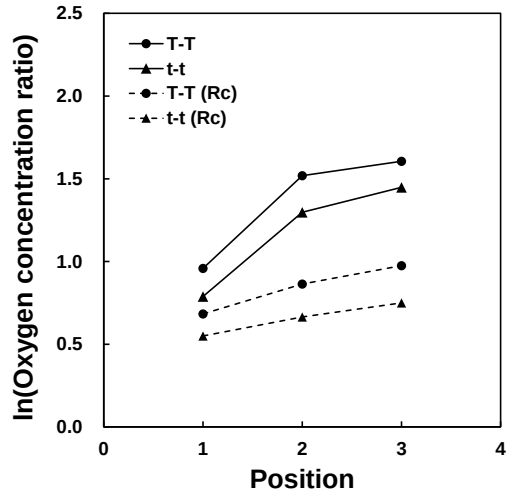

(c)

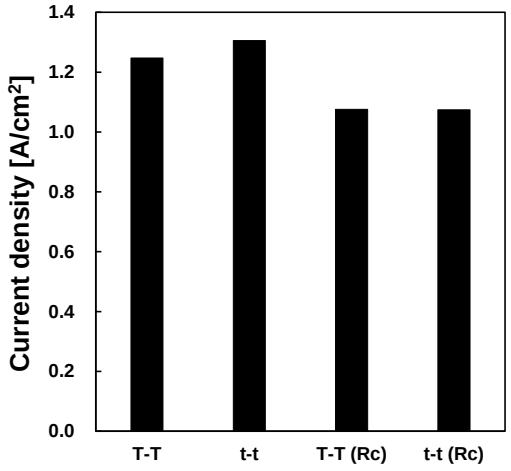

(d)

Figure 3.18 Property changes along flow direction through various uniform 3D structure arrangements with contact resistance; (a) average velocity, (b) pressure drop, (c) concentration term in overvoltage, (d) overall current density

According to previous study, contact resistivity between metallic bipolar plate and GDL surface can be varied 10~30 $m\Omega \cdot cm^2$ [108]. **Figure 3.18** shows alteration of various properties when 20 $m\Omega \cdot cm^2$ of contact resistivity was applied between 3D structure and GDL surface. Flow velocity and pressure drop was almost equal. Total voltage loss was maintained to 0.45 V, therefore, due to increased ohmic voltage loss, concentration voltage loss decreased at both 3D structure. According to **Figure 3.18** (d), current density magnitude decreased more at t-t, meaning smaller contact area between 3D structure and GDL increased contact resistance, elevating ohmic overvoltage. However, further numerical results were calculated except contact resistance since trend of average velocity, pressure drop and concentration ratio were maintained and contact resistance dependency was decreased at further study. In the next section, non-uniform arrangement of 3D structure was studied. In width non-uniformity, only the structure near the outlet was changed, dropping contact area difference into one-third. Moreover, in slope non-uniformity, there were no differences of contact area.

The second difference between CFD model and real world was water droplet dynamic. Amara et al. [109] adopt Capillary number (Ca) which reflects the competition between viscous forces and capillary forces. The capillary number can be expressed as follows:

$$\mathrm{Ca} = \frac{\mu u}{\sigma}$$ Eq. (3.33)

and **Figure 3.19** shows droplet detachment trends according to the Capillary numbers. With the same GDL contact angle, surface tension could be considered as equal, therefore, with high flow velocity, water droplet detachment on GDL surface could be accelerated, meaning that mass transfer resistance from flooding effect could be expected to be alleviated.

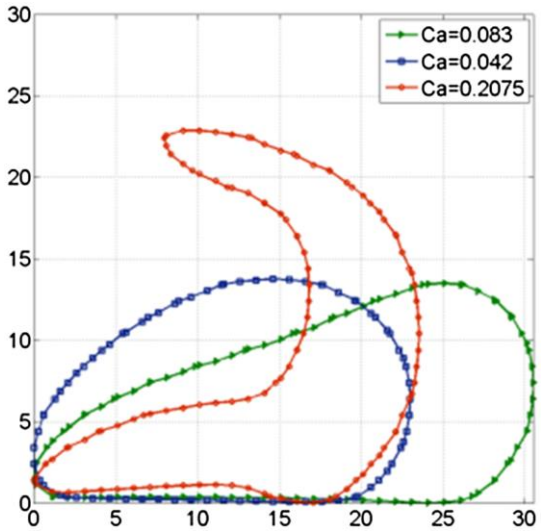

Figure 3.19 Evolution of the interfaces of droplets for different capillary numbers (Ca) [109]

3.3.2. Local characteristics in different geometrical parameters

For investigating causes of experimental results in chapter 2, one structure in outlet region was shifted to another structure at non-uniform arrangements. Meanwhile, middle and outlet structure were shifted to another structure at slope variation. **Figure 3.20** shows three different properties along flow direction by uniform 3D structure arrangements. Properties at inlet and middle regions were slightly changed according to the arrangements, however, these were minor enough to neglect compared with that at outlet region. Same with previous results from **Figure 3.15** and **Figure 3.18**, each structure with different wall thickness showed their own characteristics near outlet. First, N-t arrangement could reduce concentration overvoltage near outlet. Compared with N-N arrangement, concentration overvoltage was not increased near outlet, maintaining similar quantity of ratio between bulk and catalyst layer oxygen molar concentration. Bulk concentration and catalyst layer concentration were smaller in outlet region compared with middle region (general phenomenon in fuel cell). However, enhancing mass transfer through thinning wall could compensate concentration reduction partially. The weaknesses of thinning wall are shown in pressure drop and velocity. According to pressure analysis in chapter 2, extra compressor power to overcome increased pressure drop was minor compared with enhanced performance of fuel cell. In that case, low

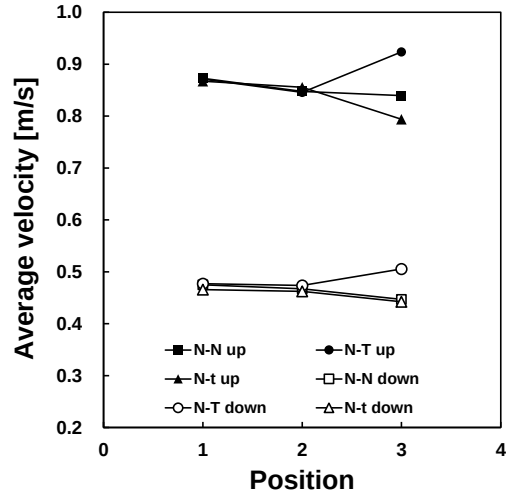
Average velocity [m/s]
1.0
0.9
0.8
0.7
0.6
0.5
0.4
0.3
0.2
0
1
2
3
4
Position
N-N up
N-T up
N-t up
N-N down
N-T down
N-t down

(a)

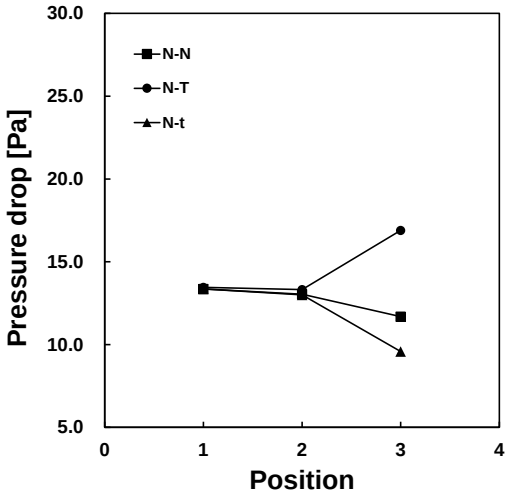
Pressure drop [Pa]
30.0
25.0
20.0
15.0
10.0
5.0
0
1
2
3
4
Position
N-N
N-T
N-t

(b)

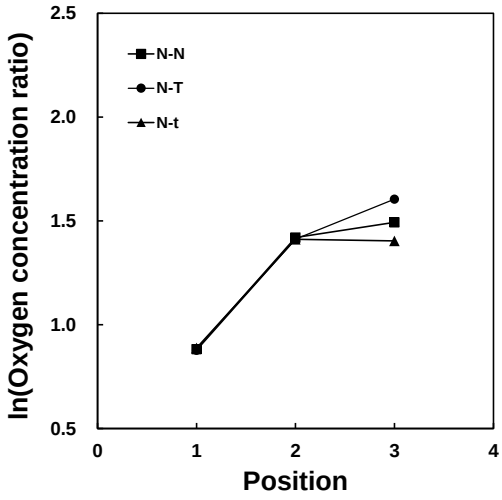

(c)

Figure 3.20 Property changes along flow direction through various non-uniform 3D structure arrangements with width variation; (a) average velocity, (b) pressure drop, (c) concentration term in overvoltage

velocity and pressure drop can hardly achieve uniform distribution of flow and removal of accumulated water droplet [72]. According to velocity plots, average velocity along both upper and lower channel were decreased in N-t arrangement. Second, N-T arrangement showed opposite results with N-t arrangement. Concentration overvoltage near outlet region became severe and pressure drop and velocity along both parts of channel were increased near outlet. **Figure 3.21** shows properties change along N-S arrangement comparing with N-N and N-T structure since both N-T and N-S arrangement in experiment showed better performance than N-N arrangement. N-S arrangement had 10% of bottom-rear channel depth decrease at middle structure and 20% of decrease at outlet structure. Pressure drop was increased along both N-T and N-S arrangements, however, velocity profiles were revealed different. N-T arrangement increased velocity along upper and below channel together but N-S arrangement increased velocity only along below channel. Moreover, velocity along upper channel was even decreased although volume of structure was increased at outlet. According to **Figure 3.21** (c), concentration overvoltage was lower than that of N-N and N-T. In **Table 3.6**, N-N and N-S arrangements had the same GDL-structure contact area, therefore, there were another reasons in performance enhancement compared with N-t arrangement. Velocity acceleration through below channel could be considered as a main cause of

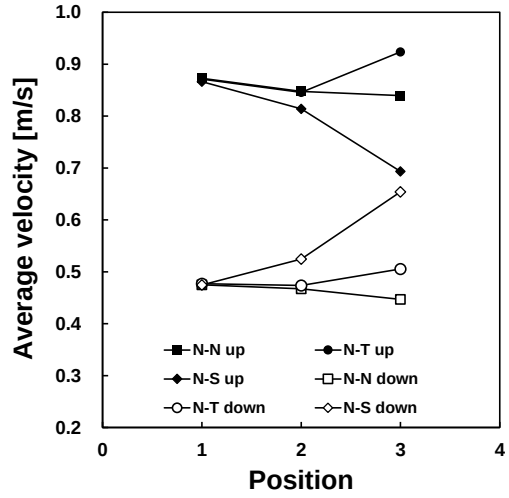
Average velocity [m/s]
1.0
0.9
0.8
0.7
0.6
0.5
0.4
0.3
0.2
0
1
2
3
4
Position
N-N up
N-T up
N-S up
N-N down
N-T down
N-S down

(a)

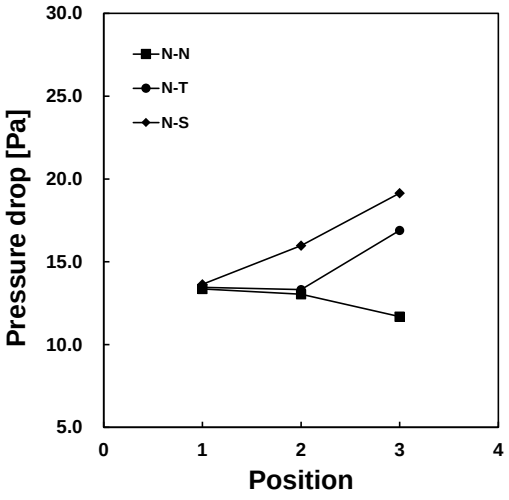
Pressure drop [Pa]
30.0
25.0
20.0
15.0
10.0
5.0
0
1
2
3
4
Position
N-N
N-T
N-S

(b)

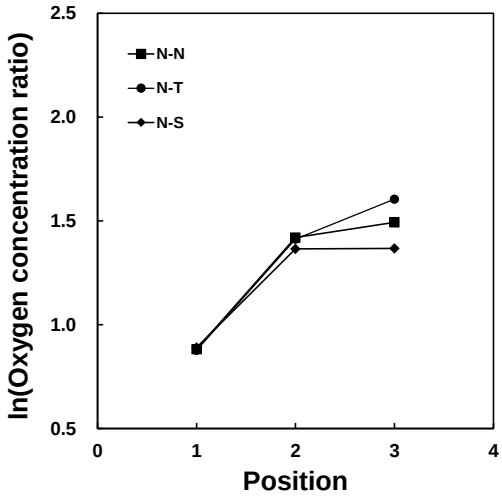

(c)

Figure 3.21 Property changes along flow direction through various non-uniform 3D structure arrangements with slope variation; (a) average velocity, (b) pressure drop, (c) concentration term in overvoltage

performance enhancement. Plus, flow direction could be a major factor in performance analysis. Even if basic tapered structure was applied to N-N structure also, the most of flow passes through 'path A' in **Figure 2.2**. **Figure 3.22** shows velocity and density contour in xy-plane at the outlet structure. Tapered structure was formed along 'path A' by reducing bottom-rear channel depth. Therefore, flow acceleration along path A was expected and flow direction could be forced to GDL surface. Moreover, due to staggered arrangement of 3D structure, some portion of outflow from 'path A' went through 'path B', basic tapered structure contacted with GDL. And this effect could be verified by calculating effective mass transfer coefficient (EMTC).

Shen et al. [39] introduced various evaluation criterions for flow channel in PEMFC. EMTC can be expressed as follow:

$$\text{EMTC} = \left| u_y \frac{\partial c}{\partial y} \right| \qquad \text{Eq. (3.34)}$$

where y-direction accords with y-direction in this chapter, perpendicular with GDL surface. In PEMFC flow channel reactants and products are transferred diffusion and advection. Diffusion is related with concentration gradient and advection is related with flow velocity. More importantly, velocity and concentration through GDL direction can be more important than bulk properties. EMTC value reflects both terms, so EMTC values were calculated.

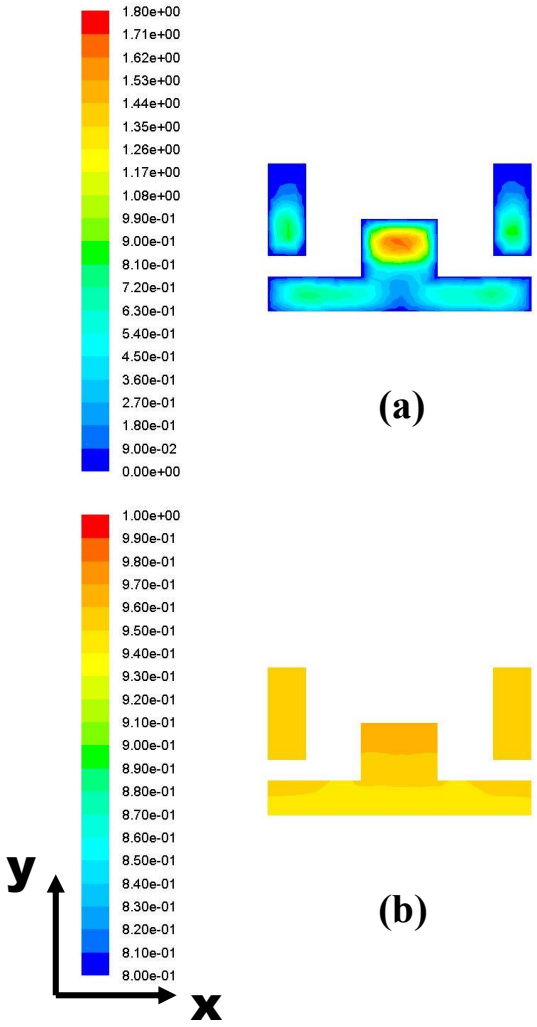

Figure 3.22 Contour of (a) velocity and (b) density on xy-plane near outlet of 3D structure

Oxygen molar concentration was measured on zx-plane near GDL surface in **Figure 3.14** and GDL surface, and y component of velocity was calculated.

Figure 3.23 (a) shows EMTC value in four different arrangements including width and slope non-uniform patterns. Except N-S, EMTC value decreased continuously along flow direction. When bottom-rear channel depth was decreased by 10%, reduction rate of EMTC value became gradual and when decrease ratio was increased to 20%, like outlet structure of N-S arrangement, EMTC value was increased. According to steepness of slope structure, average value of EMTC could be increased and value at outlet region was noticeably increased. Comparing among width varied arrangements, N-T arrangements showed higher EMTC value near outlet than N-N and N-t arrangement. For basic analysis, **Figure 3.23** (b) shows EMTC value on uniform arrangements. According to these results, velocity acceleration via wall thickening had a positive effect to EMTC value, however, it did not overcome narrow contact area between reactants flow and GDL surface as it shown in **Figure 3.15** (c) and **Figure 3.20** (c). Plus, adding slope structure on 'path A' was more effective to enhance EMTC value and to lower concentration overvoltage. Previous mentioned, unique characteristics of slope structure was not only accelerating flow velocity along below channel but also enhancing velocity direction was also reinforced toward GDL.

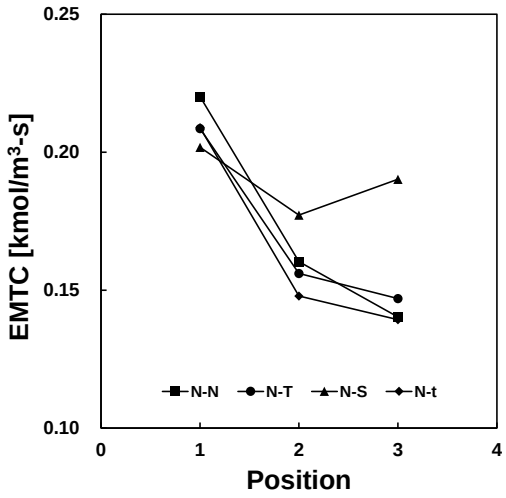

(a)

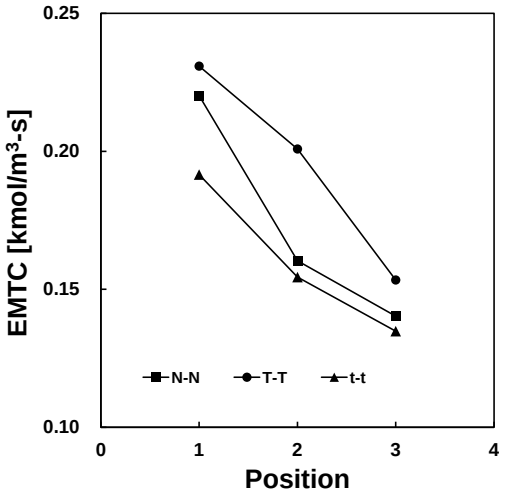

(b)

Figure 3.23 EMTC value at (a) non-uniform arrangements and (b) uniform arrangements with different channel width

If velocity enhancement through y-direction via sloped structure was valid, advection mass transfer could be expected to be enhanced through GDL. **Figure 3.24** shows y-velocity profile on zx-plane which was positioned 5 μm below from GDL surface. Comparing parallel and N-S arrangement, velocity fluctuation in y-direction could be formed through sloped structure. Although the Peclet number through y-direction through GDL was 0.2 (overall value) which indicated that diffusion mass transfer was still dominant through GDL, velocity fluctuation at the GDL surface could be considered as one of the reason of performance enhancement through slope application.

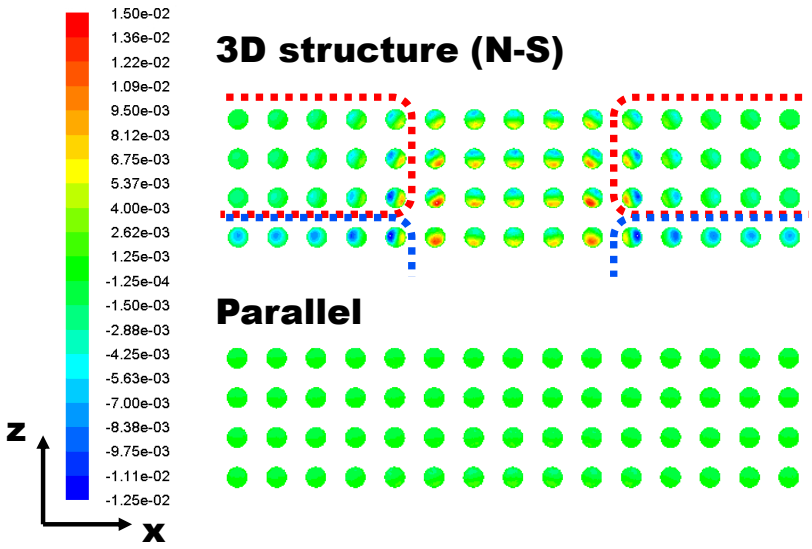

Figure 3.24 Contour of y-velocity at zx-plane (5 μm under from GDL surface)

Revealed effects of each geometric parameters could be summarized as follow:

- Thinning wall
  - ✓ Reduced overall velocity (upper and below)
  - ✓ Low pressure drop
  - ✓ High oxygen concentrate on catalyst layer due to narrow contact area between structure and GDL surface
- Thickening wall
  - ✓ Enhanced overall velocity (upper and below)
  - ✓ High pressure drop
  - ✓ Low oxygen concentrate on catalyst layer due to board contact area between structure and GDL surface
- Adding slope structure
  - ✓ Separately changed velocity (enhancing below and reducing upper)
  - ✓ The highest pressure drop
  - ✓ No contact area varied between structure and GDL surface
  - ✓ The highest oxygen concentrate on catalyst layer due to enhanced velocity forward GDL direction
  - ✓ Velocity fluctuation in y-direction could be observed

Using only these characteristics, performance enhancement utilizing 778 pattern could not be explained. Additional reasonable characteristics in experiment could be listed as follow:

- Thickening wall
    - ✓ Reduced contact resistance between metallic 3D structures and carbon based GDL surface.
    - ✓ Enhanced water droplet dynamic via flow velocity acceleration

The first reasonable characteristics could be considered minor since ohmic resistance difference was not noticeable according to **Figure 3.18**. The second could be possible difference between experiment and numerical results. Previously mentioned, properly enhanced pressure drop and velocity are necessary in fuel cell operation. Thickening wall near outlet could enhance pressure drop and overall velocity. Therefore, positive experimental results from 778 pattern could be explained.

3.3.3. Arrangement direction effects on fuel cell performance

In experiment, opposite direction of 3D structure arrangements showed different performance. Considering this, T-N and S-N arrangements were studied for comparison with N-T and S-N arrangements respectively. **Figure 3.25** shows various properties along four different arrangements. Comparing between two wall thickening cases, N-T and T-N, trend of velocity along flow direction was opposite. Therefore, EMTC value near inlet region was higher at T-N arrangement than N-T. If flow characteristics such as oxygen molar concentration were equal regardless of channel position, EMTC value near outlet region should be higher at N-T arrangement. However, in general, reactants are actively participated in electro-chemical reaction at inlet region compared with outlet region, especially highly humidified cathode inlet gas condition and low voltage operation [110]. As a result, EMTC value was affected stronger by inlet channel geometry compared with that of outlet. Therefore, overall EMTC value was higher at T-N arrangement compared with N-T arrangement. Meanwhile, EMTC reduction rate was lower at N-T arrangement due to flow acceleration near outlet.

Similarly, S-N and N-S arrangements showed opposite velocity trend and rapid reduction of EMTC value was observed in S-N arrangement. Inlet structure of S-N arrangement and outlet structure of N-S arrangement was

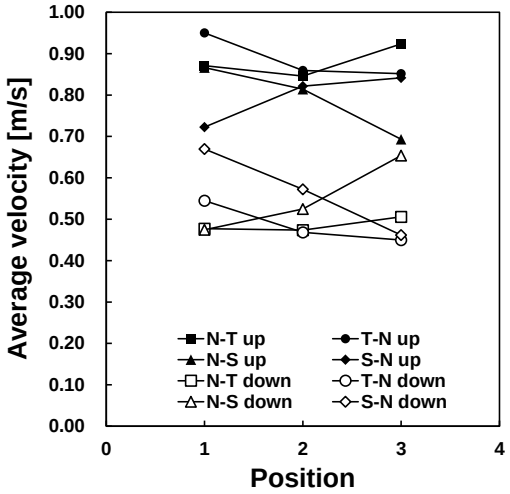
Average velocity [m/s]
1.00
0.90
0.80
0.70
0.60
0.50
0.40
0.30
0.20
0.10
0.00
0
1
2
3
4
Position
N-T up
T-N up
N-S up
S-N up
N-T down
T-N down
N-S down
S-N down

(a)

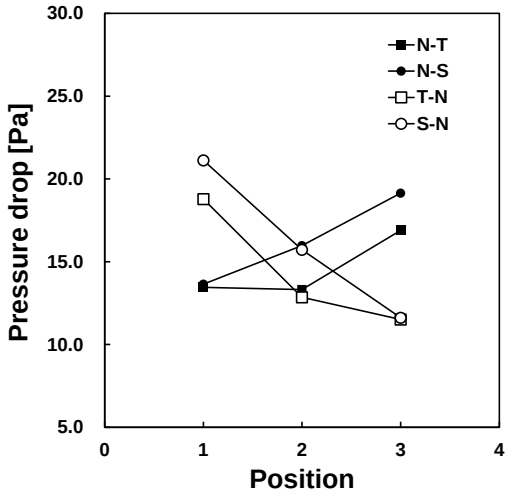
Pressure drop [Pa]
30.0
25.0
20.0
15.0
10.0
5.0
0
1
2
3
4
Position
N-T
N-S
T-N
S-N

(b)

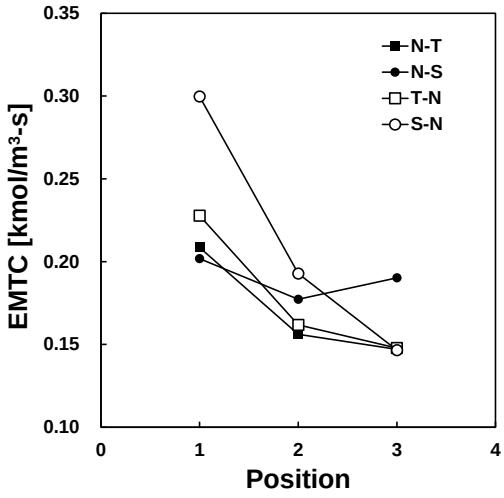

(c)

Figure 3.25 Property changes along flow direction through various non-uniform 3D structure arrangements and theirs reverse; (a) average velocity, (b) pressure drop, (c) EMTC value

equally tapered, however, EMTC value near inlet was more susceptible to channel geometry, the same result with comparison between N-T and T-N arrangements. Changes in wall thickness controlled overall velocity regardless of relative flow position with GDL surface and changes in slope intensity controlled velocity ratio between upper and below channel. Therefore slope structure on path A was more efficient to enhance mass transfer through GDL. Velocity acceleration near outlet could be expected in N-T and N-S arrangement. If faster water droplet detachment due to accelerated flow velocity was valid, experimental results between N-S and S-N arrangements should show noticeable difference alike with N-T and T-N. However, maximum power density of unit cell was slightly different between S-N and N-S arrangement, not according with N-T and T-N arrangements in experiments. In other words, if velocity acceleration effect of S structure on water removal was effective as similar as T structure, N-S arrangement should outperformed S-N arrangement, same as N-T arrangement. However, water removal effect through outlet of N-S structure did not exceed current density enhancement in inlet of S-N, resulting in similar maximum power density in experiments. On the other hand, water removal effect from N-T arrangement could exceed current density enhancement effect from T-N arrangement, resulting in noticeable difference in maximum power density between two width non-uniform arrangements. The

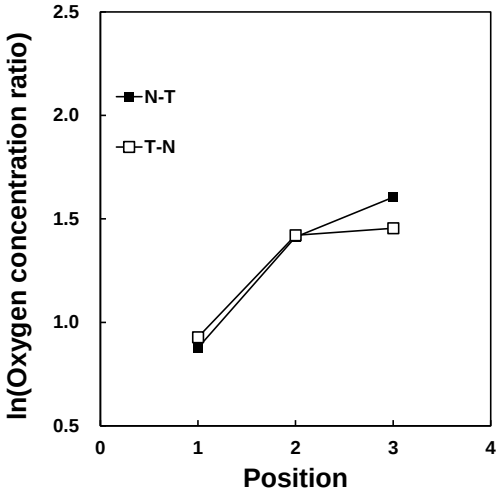

(a)

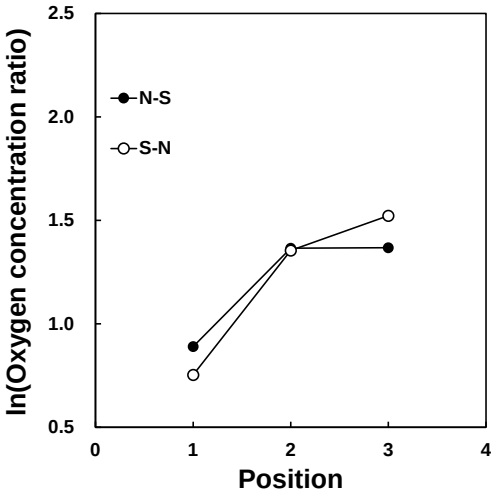

(b)

Figure 3.26 Concentration term in overvoltage changes along flow direction through non-uniform 3D structure arrangements with (a) width variation and (b) slope variation

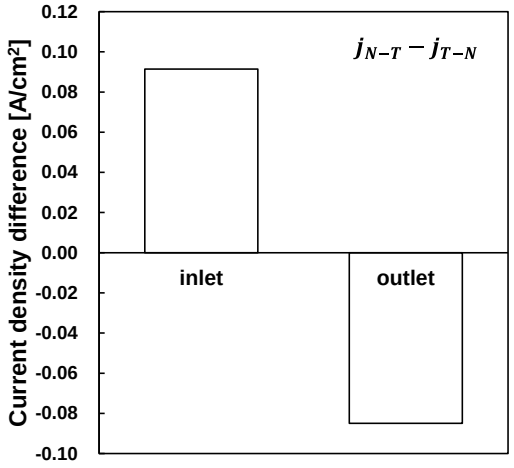

(a)

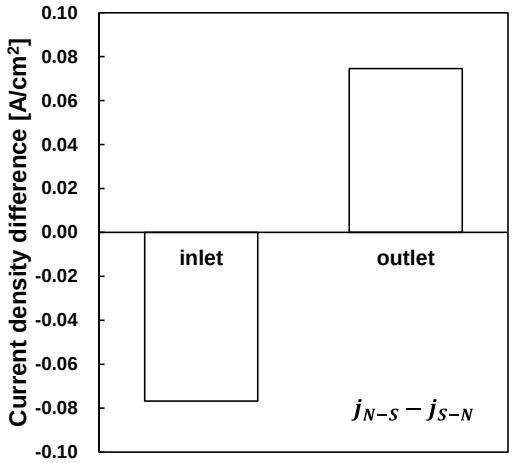

(b)

Figure 3.27 Current density difference between two different arrangements according to position on fuel cell; (a) width variation, (b) slope variation

noticeable between S and T unit structures was difference characteristic in velocity acceleration. Overall velocity enhancement rather partial velocity acceleration could be considered as major solution of water droplet removal.

In terms of concentration overvoltage, N-T arrangement showed larger loss near outlet and smaller loss near inlet compared with T-N arrangement. Similarly, S-N arrangement showed larger loss near outlet and smaller loss near inlet compared with N-S arrangement. Moreover, larger difference between concentration losses was observed at outlet in comparison between different arrangement directions as it shown in **Figure 3.26**. In addition current density difference between inlet and outlet was similar although concentration overvoltage differences were larger in outlet according to **Figure 3.27**. With smaller reduction of concentration overvoltage near inlet, comparatively larger current density enhancement could be achieved. In other words, to achieve current density enhancement near outlet, more efforts to decrease concentration overvoltage near outlet should be required.

In summary, current density enhancement was more efficient through slope structure and it could be maximized in inlet region. Also, water removal enhancement was expected to be more efficient through overall velocity enhancement by thickening wall and it could be maximized in outlet region. Combining these characteristics S structure near inlet and T structure near outlet

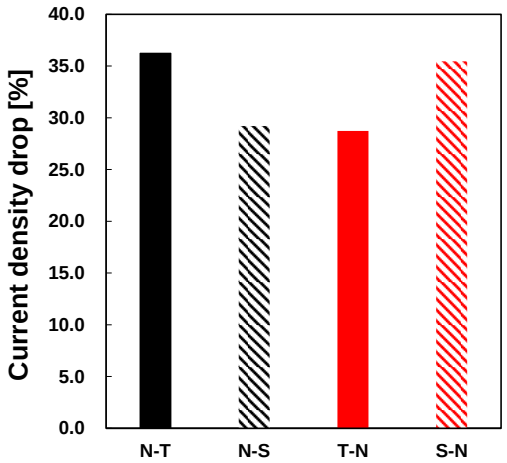

Figure 3.28 Current density difference between inlet and outlet of various non-uniform arrangements

could be thought as ideal arrangement for fuel cell performance enhancement. However, **Figure 3.28** indicates another perspective in terms of uniformity. Only with strategy for effective performance enhancement, current density distribution can be biased since EMTC value enhancement and reduction of concentration overvoltage were revealed more efficient near inlet in terms of current density. Generally, current density near inlet is higher than that of near outlet. If current density near inlet is more enhanced by modified flow channel, durability problem can be occurred severely [68]. In the next chapter, modifications of 3D structure arrangement focusing on flow and current density uniformity were conducted in larger CFD domain.

3.4. Summary

In this chapter, changes in flow characteristics at different arrangements of 3D structures were studied to figure out relations between fuel cell performance and geometric parameters. Basic characteristics of flow through 3D structure and general tendency of changes in flow properties along length direction were firstly analyzed. Then, changes in flow characteristics with outlet structure modification were studied to figure out which points affect the performance of fuel cell in experimental studies. Finally, susceptibility of flow characteristics according to position along flow direction and performance uniformity issues were discussed to find specific differences between two opposite direction of arrangements.

Compared with conventional parallel flow channel, velocity fluctuation and uniform distribution of oxygen molar concentration on catalyst layer were observed at fuel cell with 3D structure. Among the various structure with different geometric parameters, flow characteristics could be summarized as follow:

1. Large contact area between structure and GDL surface could ensure high overall velocity and low contact resistance, but mass transfer through GDL was impeded due to narrowed interface.
2. Small contact area between structure and GDL surface could obtain

high oxygen molar concentration on catalyst layer according to CFD results, however, decreased overall velocity near outlet could be obstacle in water removal.

3. Sloped structure along the ‘path A’ accelerated flow velocity near GDL surface and decreased flow velocity far from GDL surfaces, in other words, velocity difference along the y-direction could be strengthen.
4. Slope structure was efficient in velocity acceleration along y-direction and thicker-wall structure was better at overall velocity acceleration which could be expected to be positive in water removal.
5. EMTC and oxygen concentration ratio were more susceptible near inlet due to high bulk molar concentration of oxygen.
6. To secure uniform distribution of current density, excessive performance enhancement near inlet had to be avoided.

According to these results, more complex strategy in arrangements of 3D structure could be considered. In next chapter, non-uniform arrangement design would be widen, considering geometric parameter changes along width direction.

Chapter 4. 3D structure arrangements for large active area

4.1. Introduction

In previous chapter, CFD analysis on single row of 3D structure to figure out channel width and slope structure effect on various flow characteristics along fuel cell. Although meaningful insights were obtained through analysis, there were some limits in terms of scale of CFD. In experiments, 20 cm^2 of active area was selected and six to eight single units were arranged in width direction. However, in CFD, single unit structures were arranged in length direction.

Figure 4.1 shows difference between utilized structure arrangements in experiments and CFD analysis. Along a single row of 3D structure, reactants and products flow through length direction and this flow pattern is similar with that of single long straight channel with baffle structures. One of the strengths of 3D structure and porous media as flow channel is that staggered or opened structures of them allow flows to transport to adjacent channel unit not only through under-rib convection. In a single row of 3D structure, this strength and unique characteristic which make different compared with parallel and serpentine flow channel couldn't be realized. Plus, PEMFC with large active area can be utilized as commercialized energy conversion system. In this perspective, multi-row arrangement of 3D structures have to be analyzed to

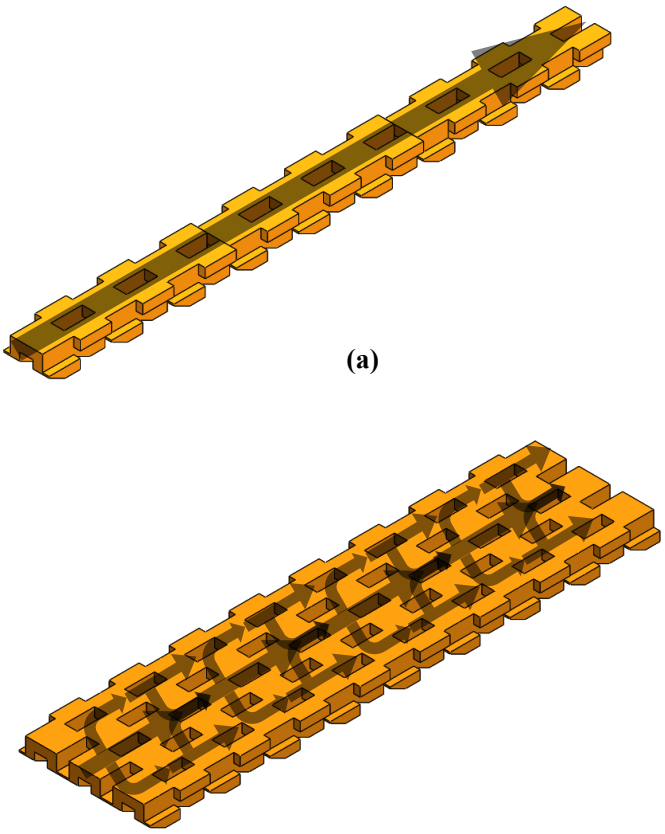

(a)

(b)

Figure 4.1 3D structure arrangement; (a) a single row, (b) three rows

figure out unique characteristics of opened flow channel and to apply to commercialized PEMFC with large active area.

In fuel cell with large active area, uniform distribution of flow and prevention of dead-zone are very important issues. **Figure 4.2** shows potential problems can be occurred when non-uniform distribution of inner flow goes severe [111]. Uneven flow distribution is same as uneven reactants distribution on catalyst layer which can bring uneven chemical reaction. In fuel cell, various chemical reactions occur on catalyst layer and they produce reaction heat, liquid water and chemical byproducts like radical. If reaction heat is produced unevenly, local hot spot can be generated. According to temperature, reaction rate, water content on membrane, electronic conductivity and so on can be changed. Similarly, liquid water accumulation can affect mass transfer of reactants through GDL, therefore, unevenly distributed liquid water can reinforce locally biased current density. In terms of current density, more chemical radicals such as peroxide can be produced more actively on high current density area and chemical byproducts can accelerate durability degradation such as corrosion, mechanical deformation and crack, etc. Moreover, these problems can't be considered separately since various problems are normally occurred in the same time and they accelerate faults of each other. Finally, in water accumulation case, it can be not only problem to fuel cell performance itself but also

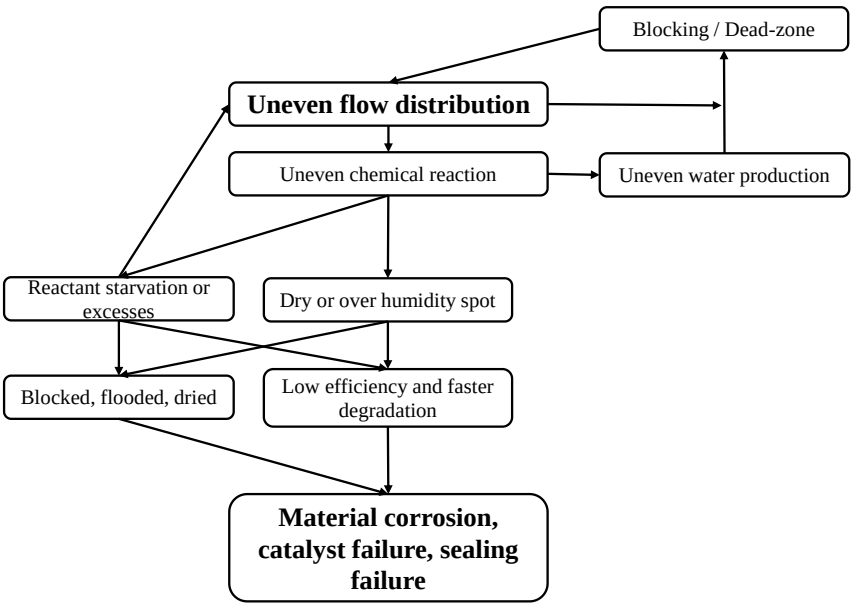

Figure 4.2 Various problems came from uneven flow distribution [111]

accelerator of uneven water accumulation. Therefore, if uneven flow distribution is not considered, aggravated problems would be remained, decreasing fuel cell performance and durability.

Non-uniform distribution of flow can be generated by various results. Poorly designed header, not optimized channel configuration and bad design of stack manifold result in severe flow mal-distribution along single channel, among each channel and cell. To overcome this problem, various header, manifold, channel shape and configuration have been invented, however, excessively complicated design can increase pressure drop along channel and stack. Of course, too low pressure drop can't secure uniform distribution of flow along fuel cell. On contrast, too high pressure drop can also generate general problems and it can be listed like **Figure 4.3**. High pressure drop can damage mechanically to membrane, sealing gasket and GDL and increase parasitic operating power. In summary, without increasing pressure drop excessively, uniform flow distribution has to be secured to enhance fuel cell performance and durability.

Wilberforce et al. [112] proposed various housing design for fuel cell utilizing metal foam as flow distributor and examined dead-zone generation along the active area. According to design of header, different location on active area can be formed as dead zone. Dead zones are generated when flow velocity

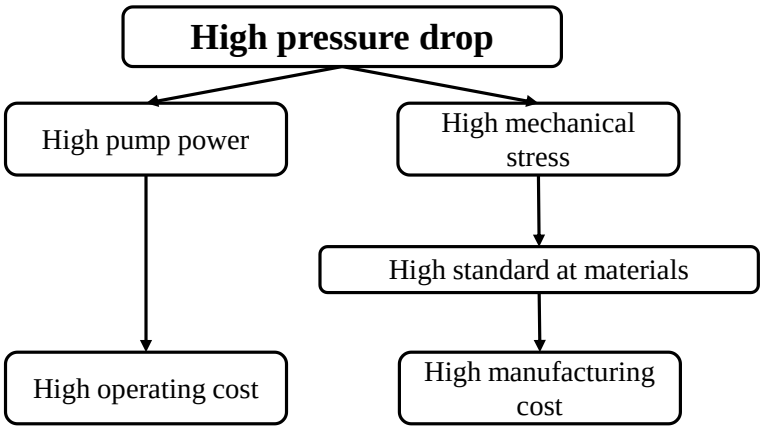

Figure 4.3 Various problems came from high pressure drop [68]

is unevenly distributed along the fuel cell. During operation, produced water is accumulated locally, especially on low-velocity region, increasing flow resistance again. The result indicated that corner of active area and location positioned far from inlet or outlet are vulnerable to dead-zone generation and **Figure 4.4** indicates results. This study was conducted on porous media as flow distributor, not on parallel and serpentine flow channel, therefore, analysis on 3D structure arrangement for flow channel in fuel cell also have to consider dead-zone generation in order to overcome scaling up problem.

In this chapter, in order to realize opened characteristic of 3D structure and to consider possible dead-zone, numerical studies on various multi-row arrangements of 3D structures including channel width and slope variations were conducted. Due to limitation on computing power and time, three rows arrangements were selected. However, if non-uniformity along flow channel are observed in relatively small scale without water droplet accumulation, far more flow non-uniformity can be concerned in real fuel cell systems. Also, if numerical results are revealed that problems can be solved by non-uniform arrangement of 3D structures, results can be expected to suggest meaningful insights and strategies in high efficiency, long durability and large scale fuel cell system development. Lastly, experiment studies on larger active area was conducted, verifying designing strategy for dead-zone formation. Comparison

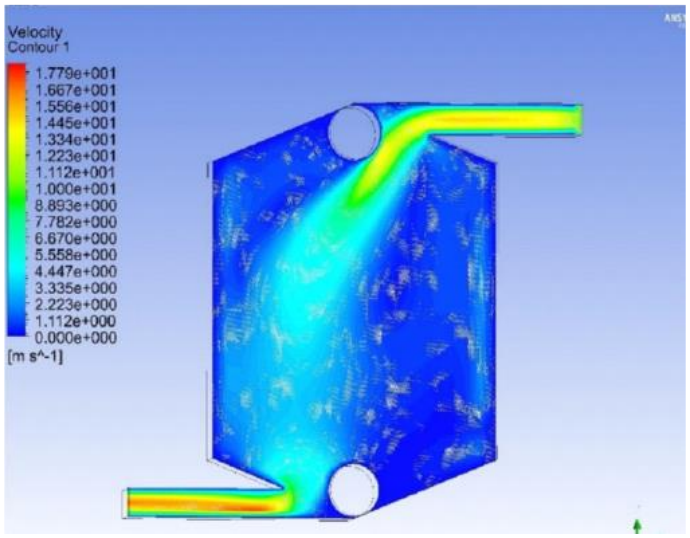

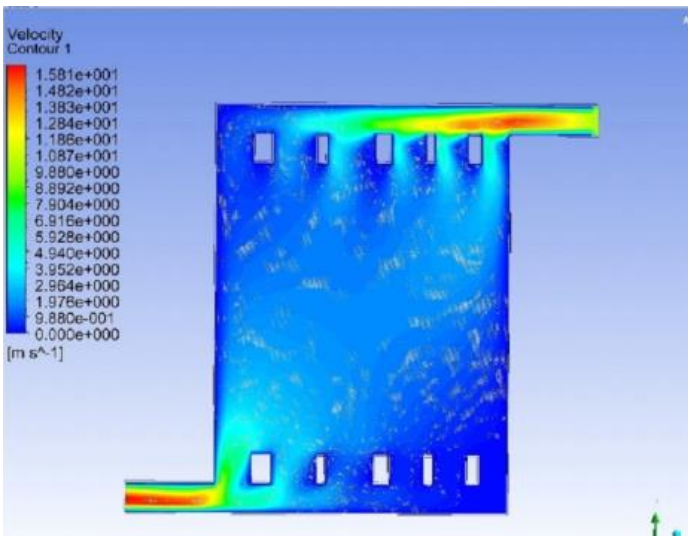

Figure 4.4 Formation of velocity dead-zone along metal foam as flow distributor [112]

between uniformly and non-uniformly arranged 3D structure was conducted through measuring I-V curve and EIS data. To verify flow uniformity along the non-uniformly arranged 3D structure, accelerated stress test was performed, measuring performance degradation.

4.2. Design strategies for fuel cell scaling up

4.2.1. Width varied non-uniform pattern along width direction

Numerical scale was widen to three row of arrangement, triple times larger than original scale. **Figure 4.5** shows contour of oxygen molar concentration along cross section of flow channel. **Figure 4.5** (a) indicates outlet of second row and (b) indicated outlet of the first row. Even if uniform ideal header was assumed and liquid water accumulation was not considered, flow non-uniformity could be occurred in three rows arrangement of 3D structure. Compared with commercialized fuel cell, 3D structure arrangement with three rows was quite small scale since its width and length was about 1.4mm and 36 mm respectively. With presence of liquid water in channel at large scale fuel cell, flow non-uniformity can be severe. Header design was not target of this study. Instead, assuming velocity decline and mass transfer reduction were occurred in the corner of outlet, enhancement of performance uniformity via manipulating arrangement strategy was tried.

Comparing **Figure 4.6** (a) and (b), performance indexes such as current density and term related with concentration overvoltage were not largely diverged at the outlet of fuel cell, however, velocity related indexes such as EMTC and average velocity were different according to the position of

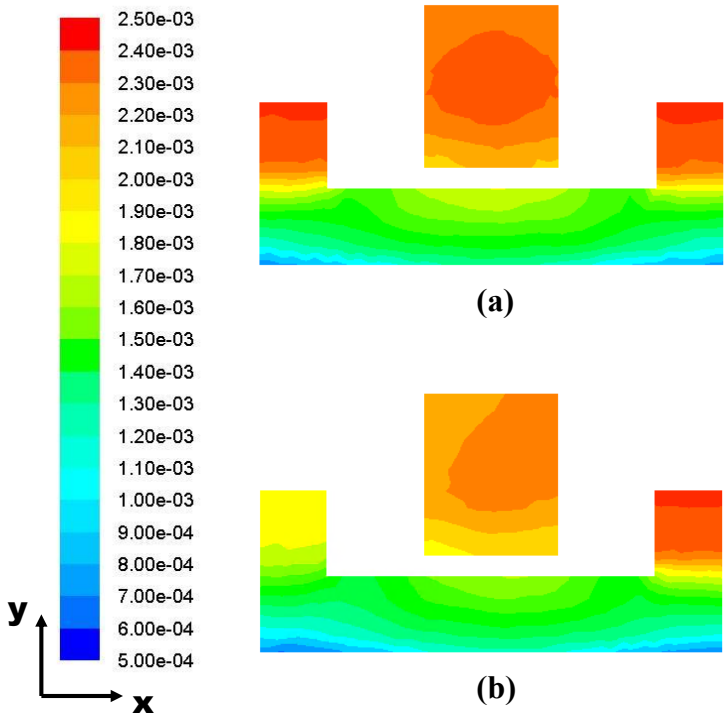

Figure 4.5 Contour of oxygen molar concentration on xy-plane near outlet; (a) row on center, (b) row on side

measurement. N-N(1) was uniform arrangement with single row of normal unit structure and N-N(3) was uniform arrangement with three rows. Plus, ‘c’ and ‘s’ indicated center and side, in other words, the first and the third row were the same with ‘s’ and the second row was the same with ‘c’. EMTC value on N-N(3-s) was rapidly reduced compared with N-N(3-c). Velocity index difference with minor change in performance index was similar with performance comparison between N-T and T-N arrangements in chapter 3. Considering experimental results and previous studies, reduction of velocity index near outlet might affect to fuel cell performance in negative way. Therefore, targeting velocity enhancement near outlet, new strategy was proposed.

Reviewing the numerical results in previous chapter, each of geometric characteristics had their own strengths. Originally, only non-uniform arrangements along length direction were considered in experimental and numerical studies. Width non-uniformity and non-uniformity along width direction were different concepts. For example, N-T arrangement was designed to vary width along length direction. Possible flow non-uniformity on larger fuel cell was that of width direction. Be contingent upon position of structure, varying width of channel gave difference impact. In a single row, thickening wall near outlet could increase overall velocity both upper and below channel. If only the structure at the center row near outlet was changed from N to T, flow

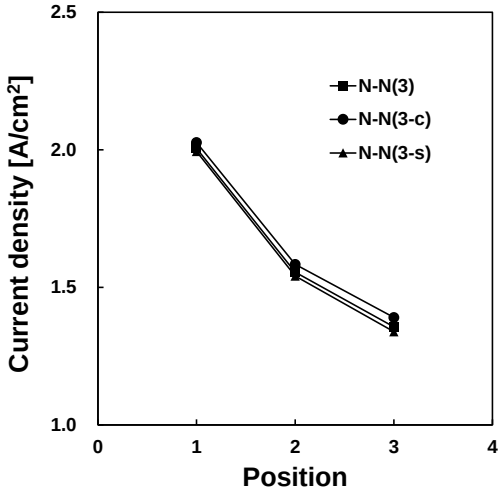
2.5
2.0
1.5
1.0
Current density [A/cm²]
N-N(3)
N-N(3-c)
N-N(3-s)
0
1
2
3
4
Position

(a)

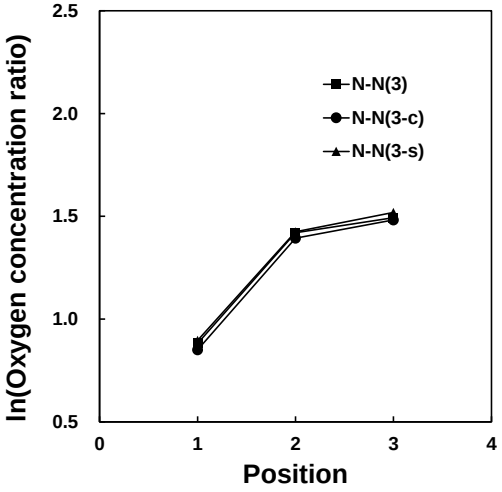
2.5
2.0
1.5
1.0
0.5
ln(Oxygen concentration ratio)
N-N(3)
N-N(3-c)
N-N(3-s)
0
1
2
3
4
Position

(b)

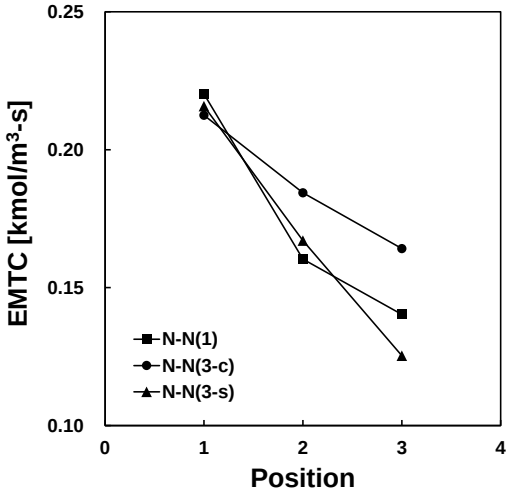

(c)

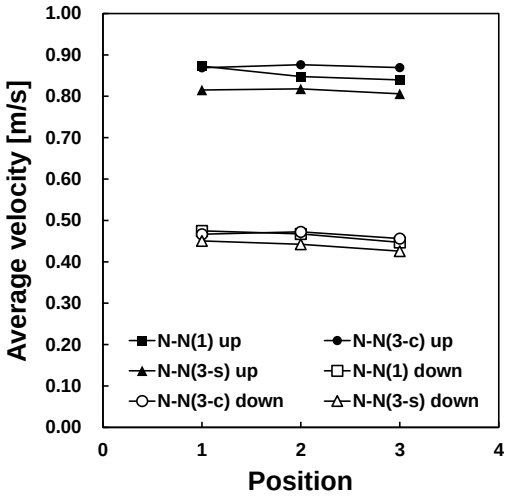

(d)

Figure 4.6 Performance and velocity index difference between single row and three rows; (a) current density, (b) concentration term in overvoltage, (c) EMTC value, (d) average velocity

resistance along center channel would be increased, accelerating velocity along two side rows instead of increasing its own velocity.

Table 4.1 compares two different strategies, ‘Type t’ and ‘Type T’, related with width variation along width direction and ‘tt’ and ‘TT’ means thinner and thicker walled structure compared with ‘t’ and ‘T’ respectively. Type t was designed for velocity enhancement on the side of flow channel. Two rows at side of active area were similar with N-t arrangement in chapter 3. Therefore, enhanced oxygen concentration at side and outlet region could be expected. However, in terms of overall velocity, reduced volume fraction of structure would decrease overall velocity, worsening water accumulation along dead zone. Plus, if wall thickness of 3D structure went way below of standard structure (N), manufacturing failure could be generated. Moreover, narrow contact area between structure and GDL could be cause of high contact resistance. On the other hand, Type T had no problem in manufacturing via enough wall thickness to be made by 3D printer. Also, enhanced overall velocity would be in favor of water removal and large contact area between GDL and structure would be good at contact resistance. However, excessively increased contact area between GDL and 3D structure could hinder mass transfer through GDL and non-uniform distribution of current density near outlet could be expected since a major portion of mass flow rate would be

Table 4.1 Non-uniform arrangements along width and length direction, wall thickness varied

Pattern	Features
Type t **tt** **N** **tt** **t** **N** **t** **N** **N** **N**	✓ Mass flow rate enhancement at sides ✓ Small contact area (GDL-structure) ✓ Reduced overall velocity ✓ Manufacturing limitation due to wall thickness ✓ Small pressure drop
Type T **TT** **N** **TT** **T** **N** **T** **N** **N** **N**	✓ Biased mass flow rate at center ✓ Large contact area (GDL-structure) ✓ Enhanced overall velocity ✓ Large pressure drop

Type 1

t	T	t
t	N	t
N	N	N

- ✓ Higher average velocity than Type t
- ✓ No manufacturing limitation
- ✓ Similar with Type t

Type 2

T	t	T
T	N	T
N	N	N

- ✓ Lower pressure drop than Type T
- ✓ Similar with Type T

focused on center of flow channel and wider GDL-flow interface would help more activated mass transfer on center of active area.

For obtaining flow uniformity and water removal capability at the same time, ‘778’ pattern in chapter 2 could be applied to Type t. If wall thickness of each outlet of row are increased like transformation from N-N to N-T arrangement, overall average velocity would be compensated and manufacturing limitation would be overcame. On contrast, applying transformation from N-N to N-t arrangement, Type 2 could be made as opposite model with Type 1. As a result, Type 1 could be suggested as refined non-uniform arrangement for fuel cell with large active area. Moreover, Type 2 had to be analyzed also to verify this assumption.

Figure 4.7 (c), (d) and (e) show velocity related indexes difference between N-N, Type 1 and Type 2 arrangements. Without any modification on arrangement, EMTC value gap between center and side of active area increased. Through modification, EMTC converged to similar value, compensating mass transfer capability to the side, expectable dead-zone along fuel cell and also, sacrificing mass transfer along the center. Due to overall flow velocity acceleration through Type 2 could enhance EMTC value near outlet, the gap between center and side of arrangement became severe. Smaller overall velocity along Type 1 was obtained since 24 and six single N units were

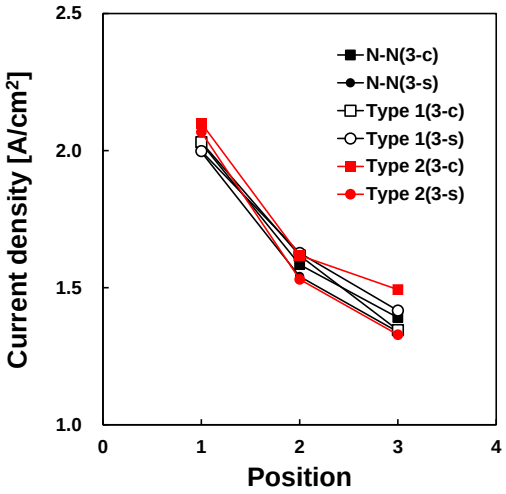
Current density [A/cm²]
Position
N-N(3-c)
N-N(3-s)
Type 1(3-c)
Type 1(3-s)
Type 2(3-c)
Type 2(3-s)
2.5
2.0
1.5
1.0
0
1
2
3
4

(a)

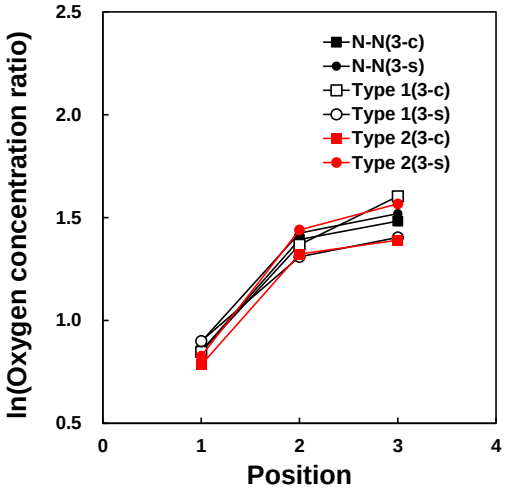
ln(Oxygen concentration ratio)
Position
N-N(3-c)
N-N(3-s)
Type 1(3-c)
Type 1(3-s)
Type 2(3-c)
Type 2(3-s)
2.5
2.0
1.5
1.0
0.5
0
1
2
3
4

(b)

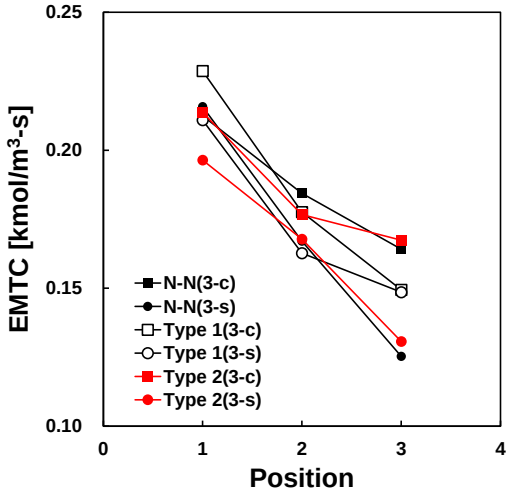
0.25
0.20
0.15
0.10
EMTC [kmol/m3-s]
0
1
2
3
4
Position
N-N(3-c)
N-N(3-s)
Type 1(3-c)
Type 1(3-s)
Type 2(3-c)
Type 2(3-s)

(c)

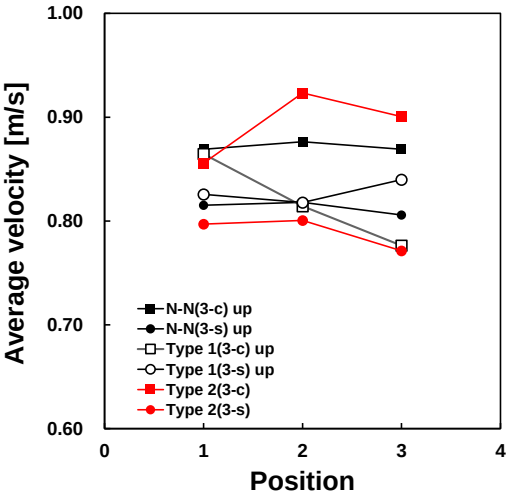
1.00
0.90
0.80
0.70
0.60
Average velocity [m/s]
0
1
2
3
4
Position
N-N(3-c) up
N-N(3-s) up
Type 1(3-c) up
Type 1(3-s) up
Type 2(3-c)
Type 2(3-s)

(d)

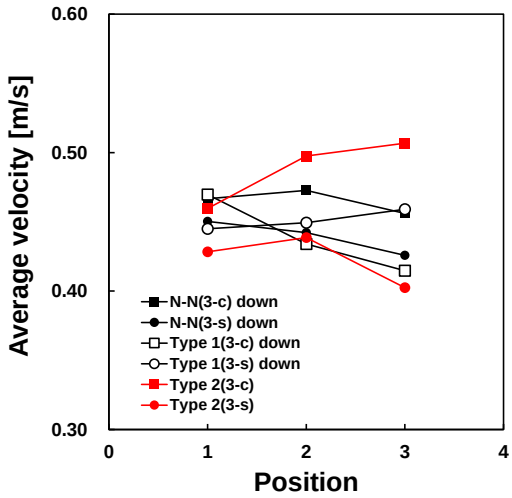

(e)

Figure 4.7 Velocity index difference among N-N, Type 1 and Type 2; (a) EMTC value, (b) average velocity (upper), (c) average velocity (lower)

substituted with t and T unit respectively, reducing integral structure volume. Instead, upper and below channel velocity along Type 1 were enhanced along the side of fuel cell which could be beneficial in reducing dead-zone. **Figure 4.7** (a) and (b) indicates current density and oxygen molar concentration index along the 3D structure arrangements. Along Type 1, current density and oxygen molar concentration were both increased at the side of fuel cell. However along Type 2, performance difference between center and side of flow channel became larger than N-N(3) arrangement which meant aggravated non-uniform distribution of current density could be expected. In terms of pressure drop, Type 1 had lower pressure drop than N-N(3) arrangement which meant without excessive pressure drop, non-uniform distribution of flow along the fuel cell could be overcome via applying non-uniform arrangement design on flow channel and this results was summarized in **Figure 4.12** in chapter 4.2.2.

4.2.2. Slope varied non-uniform pattern along width direction

The reason why considering width modification along the width direction rather than slope modification was that contact area between GDL and 3D structure arrangement could be differed through width changes. In order to minimize the other influences, width arrangements could firstly considered and then slope variation could be under consideration. Adding slope on path A of 3D structure could enhance velocity separately, dividing flow into upper and lower region and could efficiently increase mass transfer capability through GDL by strengthening velocity direction component to perpendicular with GDL surface. Reminding that slope variation was expected to give smaller impact on water removal than width variation, various patterns more focused on mass transfer capability were designed. **Table 4.2** lists four types of slope non-uniform arrangement and all of them were applied on 'Type 1' arrangement. To minimize impact of overall velocity, total channel volume fractions of four arrangements were equal achieved by controlling intensity of slope structure. Type 1A represented equally sloped arrangement. Without non-uniform application of slope structure, slope itself could enhance mass transfer capability. Type 1B was similar with N-S arrangement. From inlet to outlet, slope structure could be applied gradually, not varying with position in width direction. Through Type 1B, enhanced mass transfer capability near outlet

Table 4.2 Non-uniform arrangements along width and length direction, adding slope intensity variation

Pattern	
Type 1A	**Type 1B**
12% 12% 12% 12% 12% 12% 12% 12% 12%	24% 24% 24% 12% 12% 12% 0% 0% 0%
Type 1C	**Type 1D**
0% 20% 0% 10% 20% 10% 20% 20% 20%	17% 6% 17% 11% 6% 11% 6% 6% 6%

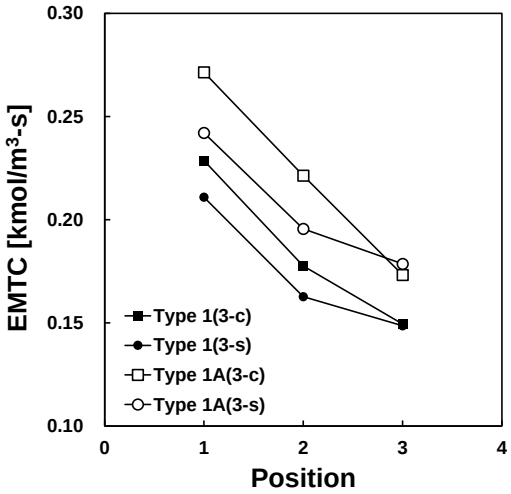
0.30
0.25
0.20
0.15
0.10
EMTC [kmol/m3-s]
0
1
2
3
4
Position
Type 1(3-c)
Type 1(3-s)
Type 1A(3-c)
Type 1A(3-s)

(a)

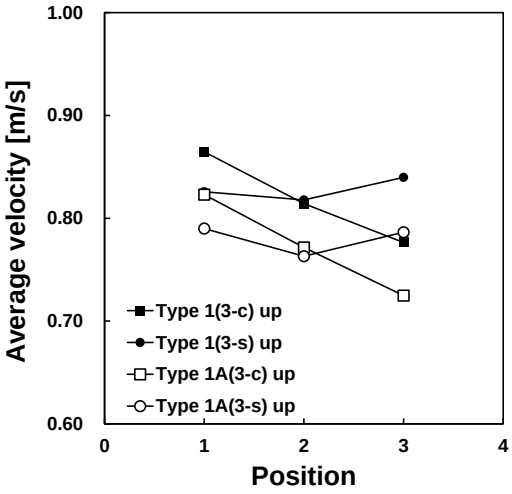
1.00
0.90
0.80
0.70
0.60
Average velocity [m/s]
0
1
2
3
4
Position
Type 1(3-c) up
Type 1(3-s) up
Type 1A(3-c) up
Type 1A(3-s) up

(b)

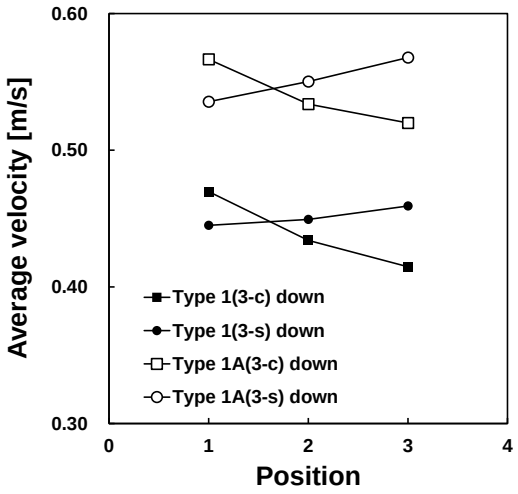

(c)

Figure 4.8 Velocity index difference between Type 1 and Type 1A; (a) EMTC value, (b) average velocity (upper), (c) average velocity (lower)

could be expected. Type 1C had equal design strategy with Type 1, reducing flow resistance at side. It could be expected to intensify change of flow characteristics which could be observed along Type 1. Type 1D had opposite design strategy with Type 1C. Balancing flow resistivity near outlet could be expected.

Figure 4.8 shows velocity related indexes comparing Type 1 and 1A. With slope added in all single unit of arrangement, all of velocity indexes increased together. The only problem could be increase in pressure drop and this was discussed at the end of this chapter. **Figure 4.9** shows velocity related indexes comparing Type 1A and 1B. Both had same channel volume fraction, therefore, validity of each strategy could be examined. Sacrificing EMTC value near inlet, mass transfer capability of outlet region was enhanced. However, decreased upper flow velocity and increased below velocity could be observed near outlet which could also be observed along N-S arrangement. **Figure 4.10** shows results from Type 1A, 1C and 1D. With Type 1C, more biased current density distribution than Type 1A was expected since mass transfer capability near inlet was increased, sacrificing capability at outlet. However, due to similar arrangement with S-N at the side row in arrangement, velocity along upper channel at side increased at outlet. Type 1D was expected to have more uniform distribution of current density than Type 1C since mass transfer capability

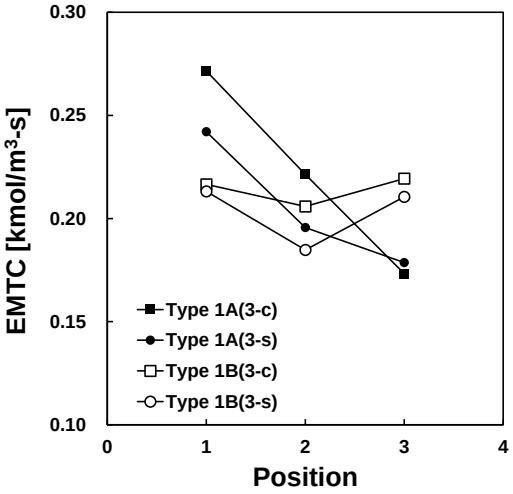
0.30
0.25
0.20
0.15
0.10
EMTC [kmol/m3-s]
0
1
2
3
4
Position
Type 1A(3-c)
Type 1A(3-s)
Type 1B(3-c)
Type 1B(3-s)

(a)

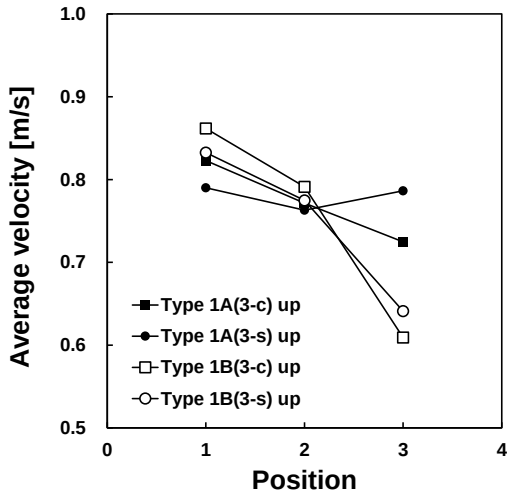
1.0
0.9
0.8
0.7
0.6
0.5
Average velocity [m/s]
0
1
2
3
4
Position
Type 1A(3-c) up
Type 1A(3-s) up
Type 1B(3-c) up
Type 1B(3-s) up

(b)

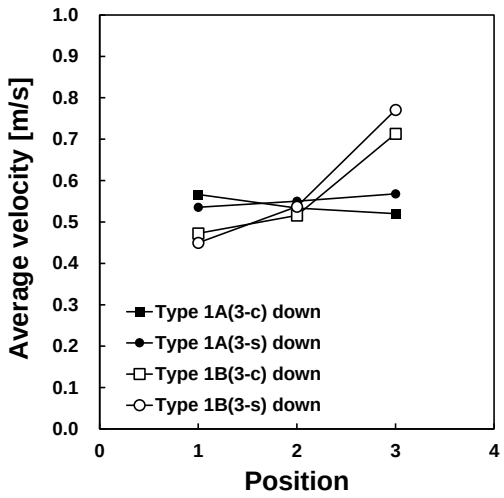

(c)

Figure 4.9 Velocity index difference between Type 1A and Type 1B; (a) EMTC value, (b) average velocity (upper), (c) average velocity (lower)

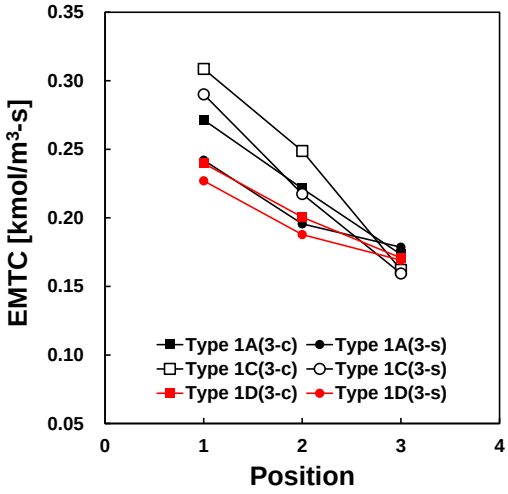
EMTC [kmol/m3-s]
0.35
0.30
0.25
0.20
0.15
0.10
0.05
0
1
2
3
4
Position
Type 1A(3-c)
Type 1A(3-s)
Type 1C(3-c)
Type 1C(3-s)
Type 1D(3-c)
Type 1D(3-s)

(a)

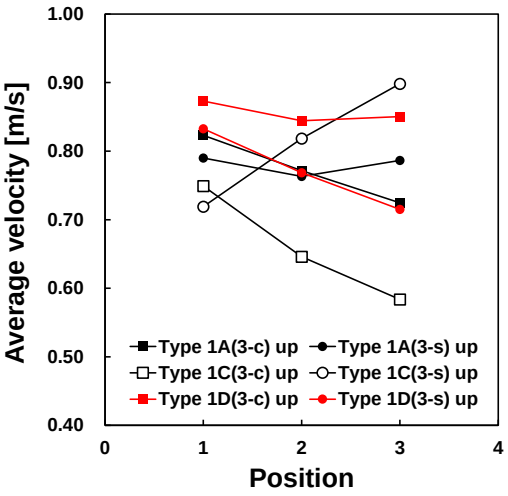
Average velocity [m/s]
1.00
0.90
0.80
0.70
0.60
0.50
0.40
0
1
2
3
4
Position
Type 1A(3-c) up
Type 1A(3-s) up
Type 1C(3-c) up
Type 1C(3-s) up
Type 1D(3-c) up
Type 1D(3-s) up

(b)

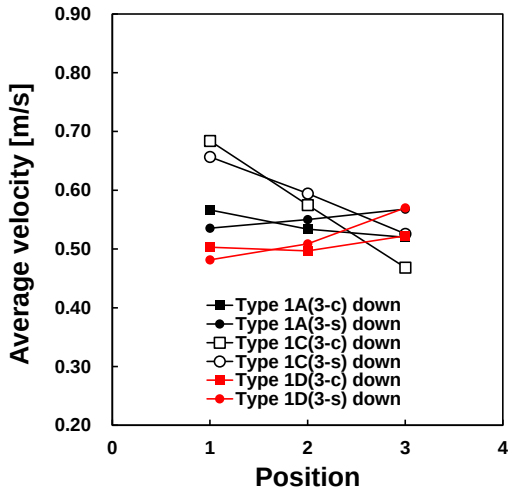

(c)

Figure 4.10 Velocity index difference among Type 1A, Type 1C and Type 1B; (a) EMTC value, (b) average velocity (upper), (c) average velocity (lower)

near outlet was increased. However, reduced upper velocity along the side channel near outlet could be a problem in water removal.

Current density distribution and pressure analysis were additionally conducted. **Figure 4.11** (a) shows current density decline ratio from inlet to outlet. In terms of current density difference between inlet and outlet region, Type 1B had the lowest difference. According to **Figure 4.11** (b), N-N(3) had the smallest current density difference between center and side of flow channel near outlet and Type 1B obtained second uniform current density distribution along the width direction. In fact, the values on **Figure 4.11**(b) were absolute values. In N-N(3) arrangement, current density on the center was higher than that of the side and in Type 1B, the opposite result could be observed. In other words, Type 1B was valid strategy to enhance performance on expected dead-zone along the fuel cell. **Figure 4.12** indicates Euler number of each arrangement. Lower Euler number at Type 1 compared with N-N(3) meant that modification of current density distribution could be obtained without pressure drop increase. Although from Type 1A to 1D had same channel volume fraction, average velocity, average density and pressure drop were different due to unique characteristics of their own design. Unfortunately, the best, Type 1B showed the highest Euler number which means that high pressure drop would

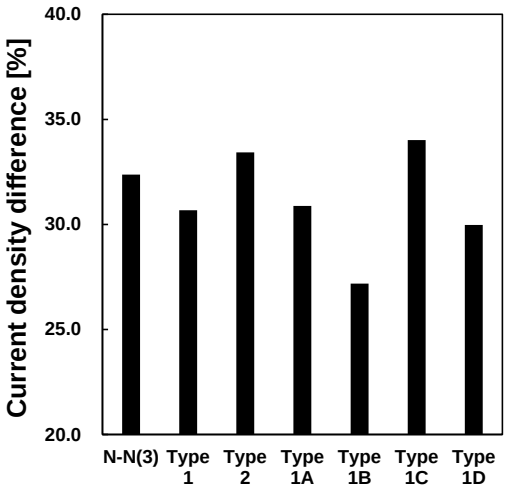

(a)

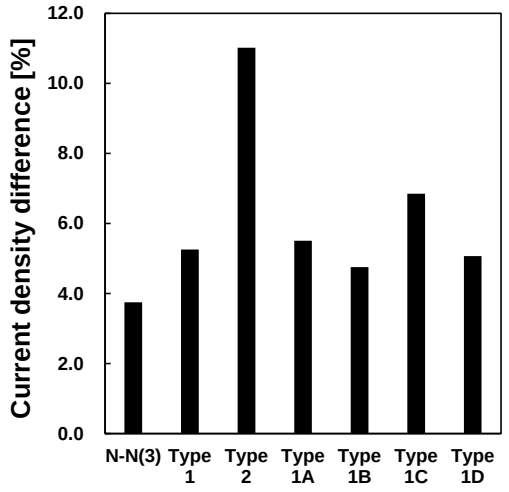

(b)

Figure 4.11 Current density difference in various arrangements; (a) decrease ratio from inlet to outlet, (b) difference ratio from center to side (near outlet)

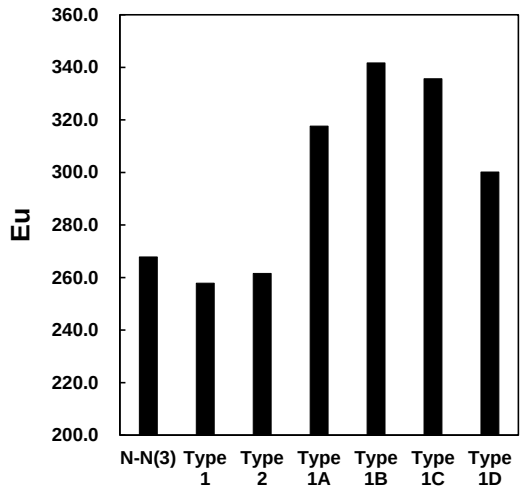

Figure 4.12 Euler number analysis in various arrangements

be required to operate fuel cell system with Type 1B. However, according to experimental results in chapter 2, additional compressor power consumption could be expected to be minor.

4.3. Durability test for fuel cell with large active area

Type 1B showed the lowest current density difference between inlet and outlet, plus, between center and side of active area near outlet, according to numerical results. In CFD, water droplet dynamics and water accumulated dead-zone formation were not considered, therefore, validation with experiments were necessary. In chapter 2, I-V curve and EIS data were measured to observe performance enhancement in terms of maximum power density. However, to verify alleviation of non-uniform distribution of reactants and current density, direct or indirect measurement should be added.

As previously mentioned, mal-distribution causes durability degradation since it brings local fuel starvation, local flooding, generation of hot and dry spot and so on. Assuming constant current density operation, the same amount of oxygen and hydrogen molecules participated in electro-chemical reaction to secure fixed current density. If formation of dead-zone becomes severe, specific portion of active area has to burden the most of the reaction to compensate poor reactants mass transfer through dead-zone. As a result, under the same current density, performance degradation rate can be differed by mass transfer capability of flow channel.

To reveal enhanced mass transfer capability of Type 1B, N-N arrangement and Type 1 were selected as references. In this chapter, unit cell with 40 cm^2

active area (40 mm of width and 100 mm of length) was selected. As total width of active area was doubled compared with that of chapter 2, design strategy considering mass transfer along the width direction was expected to affect fuel cell performance more. Experimental conditions were equal with **Table 2.3**. Durability test was conducted based on on-off stress test. Various versions of accelerated stress test have been performed to reduce testing time efficiently [106]. Among them, constant current on-off cycle was selected since uniformity of flow distribution had to affect fuel cell degradation in this case. For example, wet-dry cycle was not appropriate in verifying flow and current uniformity since the major factor in performance degradation in wet-dry cycle is mechanical stress on membrane. With constant current on-off test, the same amount of electro-chemical reactions could be expected. Therefore, if flow distribution could be enhanced along non-uniformly arranged 3D structure, degradation during on-off cycle could be alleviated since the gap between maximum and minimum current density would be reduced locally. 1 A/cm^2 of current density was applied for 4 seconds and OCV was measured for 4 seconds also. Total 60000 cycles were repeated and experimental data were measured interval of 30000 cycles.

Figure 4.13 shows I-V and I-P curve of three different arrangements. With no accelerated stress, Type 1B showed similar and 4.1% higher maximum

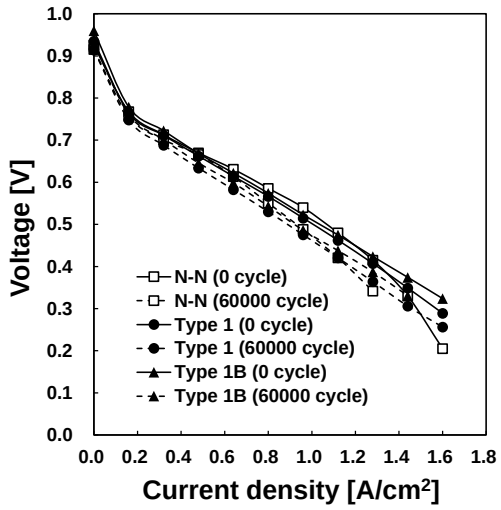

(a)

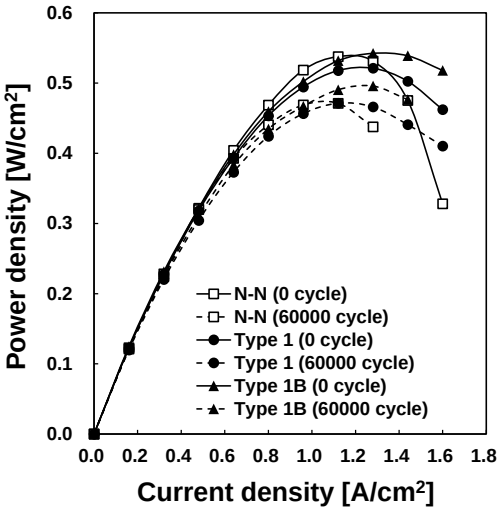

(b)

Figure 4.13 Performance degradation with different arrangements; (a) I-V curve, (b) I-P curve

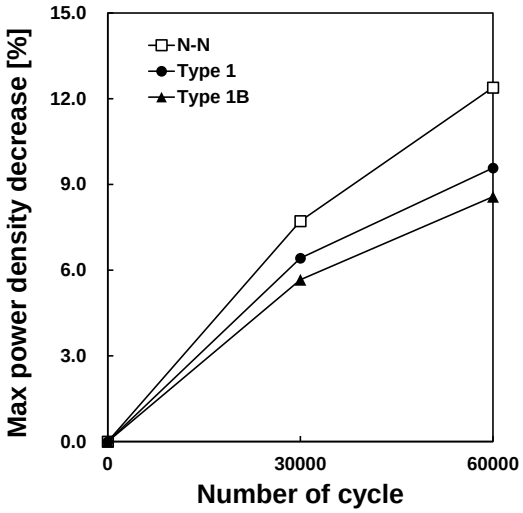

Figure 4.14 Decrease ratio of maximum power density among three different arrangements during accelerated stress test

power density with N-N arrangement and Type 1 respectively. Comparing Type 1B and N-N, N-N arrangement had larger GDL-structure contact area and higher structure volume fraction. Therefore, effect of non-uniform arrangement could be offset with reduced contact resistance and enhanced overall velocity. However, during accelerated stress test, N-N arrangement showed the fasted performance degradation ratio among the three arrangements. **Figure 4.14** shows decrease ratio of maximum power density. Compared with 8.6% and 9.6% maximum power density degradation during 60000 cycles with Type 1B and Type 1, N-N arrangement showed 12.4% of maximum power density degradation.

In terms of EIS data, **Figure 4.15** shows noticeable difference between non-uniformly and uniformly arranged 3D structure. According to **Figure 4.13 (b)**, rapid decline of power density could be observed along the N-N arrangement which meant uniformly arranged 3D structure had the lower limit current density compared with the other. EIS data were measured at current density of 1.2 A/cm^2 as same as **Figure 2.17 (b)**. Therefore, larger second arc could be observed in N-N arrangement.

Degradation of fuel cell is not belonged to a simple mechanism. Membrane, electrode, GDL, metal BPP and sealing can be damaged due to various complex and interactive process including mechanical stress, formation of radical,

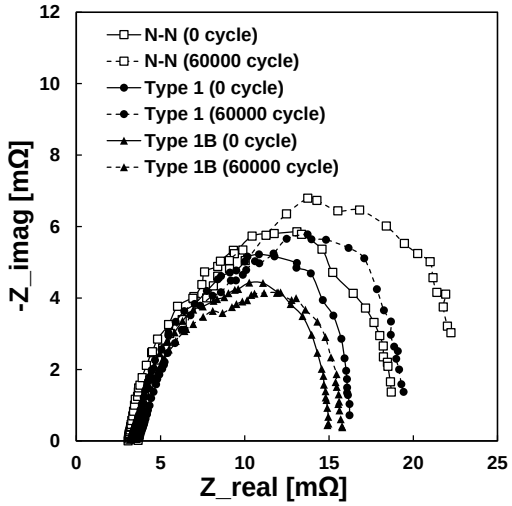

Figure 4.15 EIS data comparison among three different arrangements during accelerated stress test; 1.2A/cm^2

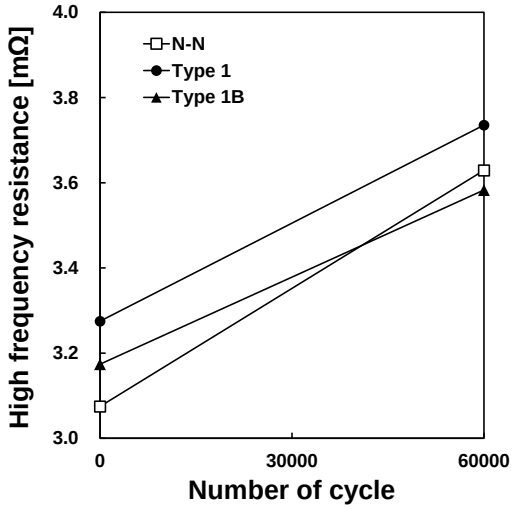

Figure 4.16 Increase of high-frequency resistance among three different arrangements during accelerated stress test

material corrosion, membrane thinning, gas crossover, catalyst dissolution and so on. Especially with metal based BPP, increasing high-frequency resistance can be observed which is related with ohmic loss [113]. **Figure 4.16** shows high-frequency resistance shifting during accelerated stress test. With Type 1B, 0.41 mΩ of high-frequency resistance was increased during 60000 cycles and 0.46 mΩ and 0.55 mΩ increases were observed at Type 1 and N-N respectively. Those were 12.6% and 35.6% higher increase compared with Type 1B. Through experimental tests, design strategy for large scale fuel cell could be verified.

4.4. Summary

In this chapter, to realize detailed characteristics of opened and staggered pattern of 3D structure, target of numerical and experimental analysis was widen. Until previous chapter, non-uniform arrangements with variation of two different parameters along length direction were covered. For large active area, changes of flow characteristics along width direction were additionally considered in this chapter. As a result, objective of this chapter was to find optimal design strategy, varying two geometric parameters along two different direction.

Since mal-distribution of reactants and formation of dead-zone became severe along large active area, the new strategy could be suggested that reducing flow resistance on potential dead-zone, accelerating flow velocity without increase total structure volume fraction. Maintaining contact area and channel volume ratio, increasing and reducing wall thickness at the center and side of active area respectively, overall velocity increase along the side channel was possible without increasing pressure drop. Moreover, the same strategy could be applied in slope intensity variation. Plus, enhancing mass transfer near outlet was still important issue, design strategy suggested in chapter 2 was also separately added. Through CFD analysis, mass transfer enhancement on potential dead-zone and uniform distribution of current density could be

obtained.

Even if the new design strategy showed better performance compared with uniform arrangement in CFD analysis, experimental test should be added to overcome several limitation of numerical study such as absence of water droplet accumulation. Through performance and durability measurement, Type 1B showed the highest maximum power during all process of accelerated stress test compared with Type 1 and N-N. Lower performance degradation and slower high-frequency resistance shifting were observed in Type 1B, therefore, design strategy for fuel cell with large active area could be verified through both numerical and experimental studies.

Chapter 5. Concluding remarks

Performance of fuel cell is sensitive with operating condition, design of component, configuration of external equipment and material. Of course, operating and manufacturing costs can be varied by these factors. Among them, metallic bipolar plate is one of the most important components in fuel cell since large portion of weight and volume of fuel cell stack comes from it and reactants pass through flow channel on bipolar plate. In this study, various attempts to develop novel design of metallic bipolar plate were conducted.

From conventional to new types of bipolar plate design, motivation of this study came from 3D mesh structure. Compared with conventional design, opened structure such as pin type bipolar plate and metal foam as flow channel have advantage that allowing reactants flow through adjacent channel unit without under-rib forced convection, enhancing mass transfer through GDL surface and reducing under-rib water accumulation. However, velocity modification could be done restrictively since specific geometric structure such as baffle design can’t be applied easily. To overcome this point, flow modification through non-uniform arrangement of unit structures of 3D mesh type flow channel was suggested in this study.

In chapter 2, experimental study was started with a single assumption that

velocity acceleration near outlet region of fuel cell can enhance performance and this could be achieved by controlling both channel width and slope intensity. For manufacturing 3D structure, metal 3D printer was utilized but several limits in geometric parameters were happened. Due to limitation in wall thickness and curvature, simplified design of 3D structure was needed. In this process, two geometric parameter could be selected, maintaining the other parameters as much as possible. Conventional parallel flow channel made with graphite and 3D printed material and uniform arrangement of 3D structure were tested as reference cases and various non-uniform arrangements based on initial assumption of chapter 2 were tested. To prove assumption, reverse arrangements of the best cases were tested also.

As a result, the best non-uniform arrangements with width and slope intensity varied were found. Plus, combining these two arrangement was tried. Among width varied cases, the reverse version of the best arrangement showed noticeable lower performance which had narrow channel width near inlet instead of outlet. Rough but positive relation between structure volume fraction and maximum power density could be observed, however, the best and its reverse pattern showed large performance gap even if those two had the same structure volume fraction. On the contrast, the best arrangement with slope intensity varied and its reverse pattern showed similar performance. Through

EIS data measurement, comparison between uniform arrangement and combined non-uniform arrangement was conducted and reduce of concentration loss could be observed through applying non-uniformity along the flow channel.

Although experimental results verified initial assumption about non-uniform arrangement of flow channel in fuel cell, optimized design was not found and detailed flow characteristics along the flow channel could not be analyzed through experimental methods. In chapter 3, therefore, numerical analysis on narrowed domain was conducted. Comparing with uniform arrangement, outlet structure was replaced with modified structure and the effects of geometry modifications and non-uniform arrangements were revealed. Thick wall thickness with narrow flow path could enhance overall flow velocity and lower contact resistance, however, narrowed contact area between GDL surface and flow hindered mass transfer, reducing oxygen molar concentration on catalyst layer. Sloped structure could separately enhance flow velocity under the structure which could increase mass transfer capability regardless of position of unit structure. Combining with experimental results, overall flow enhancement rather than separated enhancement could be expected to be in favor of water removal. EMTC value, pressure drop, current density distribution, velocity changes, oxygen molar concentration related index were

comprehensively discussed and causes in performance enhancement in chapter 2 were explained.

In chapter 4, computational domain was widen to realize characteristic of 3D structure as flow channel and to add additional consideration about dead-zone formation. As fuel cell becomes larger, uneven flow distribution and following problems from it can be worsen. Material corrosion, dissolution of catalyst, membrane thinning and formation of chemical radical could be generated during fuel cell operation especially with poorly designed flow channel design. To overcome this situation, new design strategy was suggested to enhance flow distribution uniformity along the active area. Although water droplet dynamics was not considered in CFD analysis, potential formation of dead-zone could be predicted through previous studies. Therefore, assuming near outlet and side of active area are vulnerable to water accumulation and fuel starvation, non-uniform arrangement along width direction was additionally suggested. Combining two different design strategies which include velocity and mass transfer enhancement near outlet and side active area, current density distribution could be improved. Through performance and durability measurement, the new design strategy with two geometric variables and two direction of non-uniformity was tested on large active area fuel cell. Compared with uniformly arranged 3D structure, it showed lower concentration loss and

performance degradation rate.

In conclusion, geometric parameter changes in channel unit were considered to form non-uniform arrangement and this result was investigated through experimental and numerical methods. Relations between geometric parameters and flow characteristics which can affect performance of the fuel cell were revealed numerically and advanced non-uniform arrangement for large scale fuel cell could be found. Lastly, through durability test, advanced non-uniform arrangement showed better durability compared with uniform arrangement.

To achieve high level of performance which can be competitive with commercialized fuel cell, several researches can be furtherly studied. In chapter 2, manufacturing limit on wall thickness was mentioned and in chapter 3, effect of wall thickness to oxygen mass transfer through GDL was examined. Without manufacturing limit, performance of fuel cell with 3D structure can be jumped like **Figure 3.16** and **Figure 3.17.** This manufacturing limit can be overcome by advanced methods. For example, thinner structure can be printed using plastic and this can be coated by metal with high conductivity. Plus, a mold for mass production can make stamping manufacturing possible, which can get thinner metallic bipolar plate.

Through this study, performance and durability enhancement through geometry modification on flow channel was possible. Combining additional

refinement on the other component such as catalyst layer and GDL, highly performed and long-lasting fuel cell system can be expected.

Reference

1. Meinshausen, M., et al., *Greenhouse-gas emission targets for limiting global warming to 2 degrees C.* Nature, 2009. 458(7242): p. 1158-62.
2. Momirlan, M., et al., *Current status of hydrogen energy. Renewable and sustainable energy reviews*, 2002. 6(1-2): p. 141-179.
3. Wang, Y., et al., *A review of polymer electrolyte membrane fuel cells: Technology, applications, and needs on fundamental research.* Applied Energy, 2011. 88(4): p. 981-1007.
4. Jiao, K. and Li, X., *Water transport in polymer electrolyte membrane fuel cells.* Progress in Energy and Combustion Science, 2011. 37(3): p. 221-291.
5. Aiyejina, A. and Sastry, M.K.S., *PEMFC Flow Channel Geometry Optimization: A Review.* Journal of Fuel Cell Science and Technology, 2012. 9(1).
6. Manso, A.P., et al., *Influence of geometric parameters of the flow fields on the performance of a PEM fuel cell. A review.* International Journal of Hydrogen Energy, 2012. 37(20): p. 15256-15287.
7. Bachman, J., et al., *Experimental investigation of the effect of channel length on performance and water accumulation in a PEMFC parallel*

flow field. International Journal of Hydrogen Energy, 2012. 37(22): p. 17172-17179.

8. Chen, J., *Experimental study on the two phase flow behavior in PEM fuel cell parallel channels with porous media inserts.* Journal of Power Sources, 2010. 195(4): p. 1122-1129.

9. Henriques, T., et al., *Increasing the efficiency of a portable PEM fuel cell by altering the cathode channel geometry: A numerical and experimental study.* Applied Energy, 2010. 87(4): p. 1400-1409.

10. Hossain, M.S., et al., *Enhanced gas flow uniformity across parallel channel cathode flow field of Proton Exchange Membrane fuel cells.* International Journal of Hydrogen Energy, 2017. 42(8): p. 5272-5283.

11. Lim, B.H., et al., *Numerical analysis of modified parallel flow field designs for fuel cells.* International Journal of Hydrogen Energy, 2017. 42(14): p. 9210-9218.

12. Atyabi, S.A. and Afshari, E., *A numerical multiphase CFD simulation for PEMFC with parallel sinusoidal flow fields.* Journal of Thermal Analysis and Calorimetry, 2018. 135(3): p. 1823-1833.

13. Saco, S.A., et al., *A study on scaled up proton exchange membrane fuel cell with various flow channels for optimizing power output by effective water management using numerical technique.* Energy, 2016. 113: p.

558-573.

14. Vazifeshenas, Y., et al., *Numerical investigation of a novel compound flow-field for PEMFC performance improvement.* International Journal of Hydrogen Energy, 2015. 40(43): p. 15032-15039.

15. Freire, L.S., et al., *Influence of operational parameters on the performance of PEMFCs with serpentine flow field channels having different (rectangular and trapezoidal) cross-section shape.* International Journal of Hydrogen Energy, 2014. 39(23): p. 12052-12060.

16. Li, W., et al., *Experimental and numerical analysis of a three-dimensional flow field for PEMFCs.* Applied Energy, 2017. 195: p. 278-288.

17. Kuo, J.K. and Chen, C.K., *Evaluating the enhanced performance of a novel wave-like form gas flow channel in the PEMFC using the field synergy principle.* Journal of Power Sources, 2006. 162(2): p. 1122-1129.

18. Shimpalee, S., et al., *The impact of channel path length on PEMFC flow-field design.* Journal of Power Sources, 2006. 160(1): p. 398-406.

19. Marappan, M., et al., *Scaling Up Studies on PEMFC Using a Modified Serpentine Flow Field Incorporating Porous Sponge Inserts to*

Observe Water Molecules. Molecules, 2021. 26(2).

20. Baik, K.D., et al., *Effect of multi-hole flow field structure on the performance of H2/O2 polymer electrolyte membrane fuel cells.* International Journal of Hydrogen Energy, 2019. 44(47): p. 25894-25904.

21. Baik, K.D. and Seo, I.S., *Metallic bipolar plate with a multi-hole structure in the rib regions for polymer electrolyte membrane fuel cells.* Applied Energy, 2018. 212: p. 333-339.

22. Manso, A.P., et al., *Numerical analysis of the influence of the channel cross-section aspect ratio on the performance of a PEM fuel cell with serpentine flow field design.* International Journal of Hydrogen Energy, 2011. 36(11): p. 6795-6808.

23. Baz, F.B., et al., *Enhancing under-rib mass transport in proton exchange membrane fuel cells using new serpentine flow field designs.* International Journal of Hydrogen Energy, 2019. 44(58): p. 30644-30662.

24. Hu, G., et al., *Three-dimensional numerical analysis of proton exchange membrane fuel cells (PEMFCs) with conventional and interdigitated flow fields.* Journal of Power Sources, 2004. 136(1): p. 1-9.

25. Yan, W.M., et al., *Experimental study on the performance of PEM fuel cells with interdigitated flow channels.* Journal of Power Sources, 2006. 160(1): p. 116-122.

26. Cooper, N.J., et al., *Investigation of the performance improvement in decreasing aspect ratio interdigitated flow field PEMFCs.* Energy Conversion and Management, 2017. 136: p. 307-317.

27. Cooper, N.J., et al., *Experimental optimization of parallel and interdigitated PEMFC flow-field channel geometry.* International Journal of Hydrogen Energy, 2016. 41(2): p. 1213-1223.

28. Chen, S., et al., *Numerical studies of effect of interdigitated flow field outlet channel width on PEM fuel cell performance*. Energy Procedia, 2019. 158: p. 1678-1684.

29. Lee, P. H., et al., *Performance characteristics of a proton exchange membrane fuel cell (PEMFC) with an interdigitated flow channel*. International Journal of Automotive Technology, 2007. 8(6): p. 761-769.

30. Mahmoudi, A.H., et al., *Effect of inhomogeneous compression of gas diffusion layer on the performance of PEMFC with interdigitated flow field.* Energy Conversion and Management, 2016. 110: p. 78-89.

31. Moreno, N.G., et al., *Approaches to polymer electrolyte membrane fuel*

cells (PEMFCs) and their cost. Renewable and Sustainable Energy Reviews, 2015. 52: p. 897-906.

32. Sauermoser, M., et al., *Flow Field Patterns for Proton Exchange Membrane Fuel Cells.* Frontiers in Energy Research, 2020. 8.

33. Jang, J.Y., et al., *Experimental and numerical study of proton exchange membrane fuel cell with spiral flow channels.* Applied Energy, 2012. 99: p. 67-79.

34. Juarez-Robles, D., et al., *Multiple concentric spirals for the flow field of a proton exchange membrane fuel cell.* Journal of Power Sources, 2011. 196(19): p. 8019-8030.

35. Monsaf, T., et al., *Unsteady three-dimensional numerical study of mass transfer in PEM fuel cell with spiral flow field.* International Journal of Hydrogen Energy, 2017. 42(2): p. 1237-1251.

36. Arvay, A., et al., *Nature inspired flow field designs for proton exchange membrane fuel cell.* International Journal of Hydrogen Energy, 2013. 38(9): p. 3717-3726.

37. Liu, S., et al., *Numerical simulation and experimental study on the effect of symmetric and asymmetric bionic flow channels on PEMFC performance under gravity.* International Journal of Hydrogen Energy, 2019. 44(56): p. 29618-29630.

38. Fan, W., et al., *Plant vs. Animal Prototype for Designing Bio-inspired PEMFC Flow Fields: Corn Veins or Murray's Law?* Journal of Bionic Engineering, 2022.

39. Shen, J., et al., *Evaluation criterion of different flow field patterns in a proton exchange membrane fuel cell.* Energy Conversion and Management, 2020. 213.

40. Han, S.H., et al., *Simulation and experimental analysis on the performance of PEM fuel cell by the wave-like surface design at the cathode channel.* International Journal of Hydrogen Energy, 2014. 39(6): p. 2628-2638.

41. Atyabi, S.A. and Afshari, E., *Three-dimensional multiphase model of proton exchange membrane fuel cell with honeycomb flow field at the cathode side.* Journal of Cleaner Production, 2019. 214: p. 738-748.

42. Wang, B., et al., *A dot matrix and sloping baffle cathode flow field of proton exchange membrane fuel cell.* Journal of Power Sources, 2019. 434.

43. Heidary, H., et al., *Experimental investigation of in-line and staggered blockages in parallel flowfield channels of PEM fuel cells.* International Journal of Hydrogen Energy, 2016. 41(16): p. 6885-6893.

44. Heidary, H., et al., *Numerical modelling of in-line and staggered*

blockages in parallel flowfield channels of PEM fuel cells. International Journal of Hydrogen Energy, 2017. 42(4): p. 2265-2277.

45. Perng, S.W. and Wu, H.W., *A three-dimensional numerical investigation of trapezoid baffles effect on non-isothermal reactant transport and cell net power in a PEMFC.* Applied Energy, 2015. 143: p. 81-95.

46. Houreh, N.B., et al., *Effect of inserting obstacles in flow field on a membrane humidifier performance for PEMFC application: A CFD model.* International Journal of Hydrogen Energy, 2019. 44(57): p. 30420-30439.

47. Heidary, H. and Kermani, M.J., *Performance enhancement of fuel cells using bipolar plate duct indentations.* International Journal of Hydrogen Energy, 2013. 38(13): p. 5485-5496.

48. Shen, J., et al., *Enhancement of mass transfer in a proton exchange membrane fuel cell with blockage in the flow channel.* Applied Thermal Engineering, 2019. 149: p. 1408-1418.

49. Yin, Y., et al., *Numerical investigation on the characteristics of mass transport and performance of PEMFC with baffle plates installed in the flow channel.* International Journal of Hydrogen Energy, 2018. 43(16): p. 8048-8062.

50. Tiss, F., et al., *A numerical investigation of reactant transport in a PEM fuel cell with partially blocked gas channels.* Energy Conversion and Management, 2014. 80: p. 32-38.

51. Barati, S., et al., *An investigation of channel blockage effects on hydrogen mass transfer in a proton exchange membrane fuel cell with various geometries and optimization by response surface methodology.* International Journal of Hydrogen Energy, 2018. 43(48): p. 21928-21939.

52. Wang, Y., et al., *Numerical study of a new cathode flow-field design with a sub-channel for a parallel flow-field polymer electrolyte membrane fuel cell.* International Journal of Hydrogen Energy, 2018. 43(4): p. 2359-2368.

53. Wang, Y., et al., *New design of a cathode flow-field with a sub-channel to improve the polymer electrolyte membrane fuel cell performance.* Journal of Power Sources, 2017. 344: p. 32-38.

54. Niu, Z., et al., *Numerical investigation of innovative 3D cathode flow channel in proton exchange membrane fuel cell.* International Journal of Energy Research, 2018. 42(10): p. 3328-3338.

55. Fan, L., et al., *Optimization design of the cathode flow channel for proton exchange membrane fuel cells.* Energy Conversion and

Management, 2018. 171: p. 1813-1821.

56. Karthikeyan, M., et al., *Adoption of novel porous inserts in the flow channel of pem fuel cell for the mitigation of cathodic flooding.* International Journal of Hydrogen Energy, 2020. 45(13): p. 7863-7872.

57. Tsai, B.T., et al., *Effects of flow field design on the performance of a PEM fuel cell with metal foam as the flow distributor.* International Journal of Hydrogen Energy, 2012. 37(17): p. 13060-13066.

58. Kozakai, M., et al., *Improving gas diffusivity with bi-porous flow-field in polymer electrolyte membrane fuel cells.* International Journal of Hydrogen Energy, 2016. 41(30): p. 13180-13189.

59. Shin, D.K., et al., *Effect of cell size in metal foam inserted to the air channel of polymer electrolyte membrane fuel cell for high performance.* Renewable Energy, 2018. 115: p. 663-675.

60. Kang, D.G., et al., *Performance enhancement of air-cooled open cathode polymer electrolyte membrane fuel cell with inserting metal foam in the cathode side.* International Journal of Hydrogen Energy, 2020. 45(51): p. 27622-27631.

61. Baroutaji, A., et al., *Design and development of proton exchange membrane fuel cell using open pore cellular foam as flow plate material*. Journal of Energy Challenges and Mechanics, 2014. 1(7).

62. Yoshida, T. and Kojima. K., *Toyota MIRAI fuel cell vehicle and progress toward a future hydrogen society. The Electrochemical Society Interface*, 2015. 24(2): p. 45.

63. Konno, N., et al., *Development of Compact and High-Performance Fuel Cell Stack.* SAE International Journal of Alternative Powertrains, 2015. 4(1): p. 123-129.

64. Zhang, G., et al., *Multi-phase simulation of proton exchange membrane fuel cell with 3D fine mesh flow field.* International Journal of Energy Research, 2018. 42(15): p. 4697-4709.

65. Bao, Z., et al., *Analysis of single- and two-phase flow characteristics of 3-D fine mesh flow field of proton exchange membrane fuel cells.* Journal of Power Sources, 2019. 438.

66. Cai, Y., et al., *Numerical study on a novel 3D cathode flow field and evaluation criteria for the PEM fuel cell design.* Energy, 2018. 161: p. 28-37.

67. Shen, J., et al., *Performance enhancement in a proton exchange membrane fuel cell with a novel 3D flow field.* Applied Thermal Engineering, 2020. 164.

68. Wang, J., *Theory and practice of flow field designs for fuel cell scaling-up: A critical review.* Applied Energy, 2015. 157: p. 640-663.

69. Guo, H., et al., *Temperature distribution on anodic surface of membrane electrode assembly in proton exchange membrane fuel cell with interdigitated flow bed.* Journal of Power Sources, 2015. 273: p. 775-783.

70. Siegel, C., *Review of computational heat and mass transfer modeling in polymer-electrolyte-membrane (PEM) fuel cells.* Energy, 2008. 33(9): p. 1331-1352.

71. Shen, J., et al., *Partial flooding and its effect on the performance of a proton exchange membrane fuel cell.* Energy Conversion and Management, 2020. 207.

72. Wang, J. and Wang, H., *Discrete approach for flow field designs of parallel channel configurations in fuel cells.* International Journal of Hydrogen Energy, 2012. 37(14): p. 10881-10897.

73. Kahraman, H. and Orhan, M.F., *Flow field bipolar plates in a proton exchange membrane fuel cell: Analysis & modeling.* Energy Conversion and Management, 2017. 133: p. 363-384.

74. Liu, H.C., et al., *Reactant gas transport and cell performance of proton exchange membrane fuel cells with tapered flow field design.* Journal of Power Sources, 2006. 158(1): p. 78-87.

75. Fontana, É., et al., *Study of the effects of flow channel with non-uniform*

cross-sectional area on PEMFC species and heat transfer. International Journal of Heat and Mass Transfer, 2011. 54(21-22): p. 4462-4472.

76. Mancusi, E., et al., *Numerical study of two-phase flow patterns in the gas channel of PEM fuel cells with tapered flow field design.* International Journal of Hydrogen Energy, 2014. 39(5): p. 2261-2273.

77. Fontana, É., et al., *Flow regimes for liquid water transport in a tapered flow channel of proton exchange membrane fuel cells (PEMFCs).* Journal of Power Sources, 2013. 234: p. 260-271.

78. Akhtar, N. and Kerkhof, P.J.A.M., *Dynamic behavior of liquid water transport in a tapered channel of a proton exchange membrane fuel cell cathode.* International Journal of Hydrogen Energy, 2011. 36(4): p. 3076-3086.

79. Song, J., et al., *Mass transfer and cell performance of a unitized regenerative fuel cell with nonuniform depth channel in oxygen-side flow field.* International Journal of Energy Research, 2019. 43(7): p. 2940-2962.

80. Min, C.H., *Performance of a proton exchange membrane fuel cell with a stepped flow field design.* Journal of Power Sources, 2009. 186(2): p. 370-376.

81. Ferng, Y. and Su, A., *A three-dimensional full-cell CFD model used to investigate the effects of different flow channel designs on PEMFC performance.* International Journal of Hydrogen Energy, 2007. 32(17): p. 4466-4476.

82. Kumar, R.R., et al., *Experimental investigation on PEM fuel cell using serpentine with tapered flow channels.* International Journal of Hydrogen Energy, 2020. 45(31): p. 15642-15649.

83. Chowdhury, M.Z. and Akansu, Y.E., *Novel convergent-divergent serpentine flow fields effect on PEM fuel cell performance.* International Journal of Hydrogen Energy, 2017. 42(40): p. 25686-25694.

84. Shin, D.K., et al., *Study on the performance improvement of polymer electrolyte membrane fuel cell with inclined channel shape.* Electrochimica Acta, 2019. 320.

85. Zehtabiyan-Rezaie, N., et al., *Effect of flow field with converging and diverging channels on proton exchange membrane fuel cell performance.* Energy Conversion and Management, 2017. 152: p. 31-44.

86. Wang, C., et al., *Effect of height/width-tapered flow fields on the cell performance of polymer electrolyte membrane fuel cells.* International

Journal of Hydrogen Energy, 2017. 42(36): p. 23107-23117.

87. Yan, W.M., et al., *Numerical study on cell performance and local transport phenomena of PEM fuel cells with novel flow field designs.* Journal of Power Sources, 2006. 161(2): p. 907-919.

88. Rahimi-Esbo, M., et al., *Improving PEM fuel cell performance and effective water removal by using a novel gas flow field.* International Journal of Hydrogen Energy, 2016. 41(4): p. 3023-3037.

89. Wang, X.D., et al., *An inverse geometry design problem for optimization of single serpentine flow field of PEM fuel cell.* International Journal of Hydrogen Energy, 2010. 35(9): p. 4247-4257.

90. Wang, X.D., et al., *Flow field optimization for proton exchange membrane fuel cells with varying channel heights and widths.* Electrochimica Acta, 2009. 54(23): p. 5522-5530.

91. Liu, M., et al., *Geometry optimization and performance analysis of a new tapered slope cathode flow field for PEMFC.* International Journal of Hydrogen Energy, 2021. 46(75): p. 37379-37392.

92. Lei, H., et al., *Numerical simulation of water droplet transport characteristics in cathode channel of proton exchange membrane fuel cell with tapered slope structures.* International Journal of Hydrogen Energy, 2020. 45(53): p. 29331-29344.

93. Perng, S.W. and Wu, H.W., *Non-isothermal transport phenomenon and cell performance of a cathodic PEM fuel cell with a baffle plate in a tapered channel.* Applied Energy, 2011. 88(1): p. 52-67.

94. Yan, X., et al., *Flow field design with 3D geometry for proton exchange membrane fuel cells.* Applied Thermal Engineering, 2019. 147: p. 1107-1114.

95. Chen, X., et al., *Performance investigation on a novel 3D wave flow channel design for PEMFC.* International Journal of Hydrogen Energy, 2021. 46(19): p. 11127-11139.

96. Kang, D.G., et al., *Study on the metal foam flow field with porosity gradient in the polymer electrolyte membrane fuel cell.* Renewable Energy, 2020. 156: p. 931-941.

97. Wu, Y., et al., *Effects of microporous layer on electrolyte flooding in gas diffusion electrodes and selectivity of CO2 electrolysis to CO.* Journal of Power Sources, 2022. 522.

98. Larminie, J., et al., *Fuel cell systems explained*. Chichester, UK: J. Wiley, 2003. 2.

99. Tao, W. Q., et al., *Parameter sensitivity examination and discussion of PEM fuel cell simulation model validation.* Journal of Power Sources, 2006. 160(1): p. 359-373.

100. Min, C. H., et al., *Parameter sensitivity examination and discussion of PEM fuel cell simulation model validation.* Journal of Power Sources, 2006. 160(1): p. 374-385.

101. Mazumder, S. and Cole, J.V., *Rigorous 3-D Mathematical Modeling of PEM Fuel Cells.* Journal of The Electrochemical Society, 2003. 150(11).

102. Fan, L., et al., *Characteristics of PEMFC operating at high current density with low external humidification.* Energy Conversion and Management, 2017. 150: p. 763-774.

103. Meng, H., *A two-phase non-isothermal mixed-domain PEM fuel cell model and its application to two-dimensional simulations.* Journal of Power Sources, 2007. 168(1): p. 218-228.

104. Shan, J., et al., *Local resolved investigation of PEMFC performance degradation mechanism during dynamic driving cycle.* International Journal of Hydrogen Energy, 2016. 41(7): p. 4239-4250.

105. Arato, E. and Costa, P., *Gas-phase mass-transfer resistance at PEMFC electrodes.* Journal of Power Sources, 2006. 158(1): p. 200-205.

106. Wu, J., et al., *A review of PEM fuel cell durability: Degradation mechanisms and mitigation strategies.* Journal of Power Sources, 2008. 184(1): p. 104-119.

107. Zhou, P. and Wu, C.W., *Numerical study on the compression effect of gas diffusion layer on PEMFC performance.* Journal of Power Sources, 2007. 170(1): p. 93-100.

108. Xu, Z., et al, *Fabrication of micro channels for titanium PEMFC bipolar plates by multistage forming process.* International Journal of Hydrogen Energy, 2021. 46(19): p. 11092-11103.

109. Amara, M.E.A.B. and Nasrallah, S.B., *Numerical simulation of droplet dynamics in a proton exchange membrane (PEMFC) fuel cell micro-channel.* International Journal of Hydrogen Energy, 2015. 40(2): p. 1333-1342.

110. Liu, Z., et al., *Behavior of PEMFC in starvation.* Journal of Power Sources, 2006. 157(1): p. 166-176.

111. Wang, J., *Barriers of scaling-up fuel cells: Cost, durability and reliability.* Energy, 2015. 80: p. 509-521.

112. Wilberforce, T., et al., *Computational Fluid Dynamic simulation and modelling (CFX) of flow plate in PEM fuel cell using aluminum open cellular foam material.* IEEE Texas Power and Energy Conference, 2017. p.1-6.

113. De Bruijn, F.A., et al., *Review: Durability and Degradation Issues of PEM Fuel Cell Components.* Fuel Cells, 2008. 8(1): p. 3-22.

국 문 초 록

고분자 전해질막 연료전지의 핵심 부품 중 하나인 양극 분리판은 그 설계에 따라 연료전지의 성능, 연료 효율, 내구성 그리고 운영 및 제조 비용을 변화시킨다. 연료전지 내부 화학반응의 고유한 특성에 따라 유로의 기하학적 특성이 개별적으로 연구되어야 고효율 및 높은 내구성을 가지는 연료전지 시스템을 개발할 수 있다. 반응물의 고갈과 물 배출 저하는 연료전지 성능 저하에 직접적인 영향을 미친다. 따라서 적정 수준의 압력 강하로 효율적인 물질전달을 이룰 수 있는 분리판 개발이 필수적이다. 일반적으로 양극 유로를 따라 물 축적이 심화되고 이로 인해 반응물이 제대로 전달되지 않는 영역이 발생하므로 본 연구에서는 양극 유로의 설계에 대하여 실험적, 해석적 연구를 진행하였다.

본 연구에서는 3D 프린팅 기술을 활용하여 양극 유로로써 사용될 수 있는 3D 구조체를 제작하고 이를 개선할 수 있는 방안을 도출하고자 하였다. 구조체의 기하학적 형상을 연료전지 성능에 친화적으로 변화시키기 위하여 유로 단위 폭과 경사도를 변화시킬 수 있는 형상 수치를 선정하고 3D 프린터로 제작될 수 있도록 그 구조를 단순화 시켰다. 유로의 단위 폭과 경사도를 유동 진행 방향에 따라 다르게 변화시켜 성능을 측정하였고 결과에 따라 각 형상 변수의 최적 배치를 찾았다. 이후 두 최적 배치를 하나로 결합한 경우 균일하게 배치된 대조 실험군과 비교하여 13.0%의 최대 출력 증가를 얻었

다. 전기화학임피던스분광법을 활용하여 해당 배치가 대조군과 비교하여 더 낮은 농도 손실을 가짐을 보였다.

성능 향상의 세부적인 원인을 밝히기 위하여 유동 해석 프로그램 중 하나인 ANSYS FLUENT를 활용하였다. 3차원 유동 해석의 시간을 줄이고, 단일 유닛 내의 유동 특성 변화를 독립적으로 분석하기 위하여 1열의 단일 유닛 배치를 기준으로 해석을 진행하였다. 출구부의 단일 유닛들을 실험으로 검증했던 배치들과 같은 경향을 가지도록 배열하고 해당 변화들이 연료전지 성능에 영향을 줄 수 있는 유동 특성에 어떠한 변화를 가져오는지 분석하였다. 두꺼운 벽 두께와 좁은 채널 폭은 낮은 접촉 저항과 향상된 유동 속도로 인해, 유로 내의 물 축적이 반영되는 실제 상황에서 성능 변화를 기대해 볼 수 있었지만, 유동이 기체확산층과 닿는 면적을 줄임으로써 다공성의 기체확산층을 통과하는 반응물의 물질 전달을 방해하는 것이 드러났다. 경사 구조는 특히 기체확산층과 수직 방향의 유속을 증가시키는 것으로 나타났으며 가장 효율적인 유로 내 물질 전달 능력 향상에 기여하였다. 전반적인 유속의 증가는 실제 실험 시 축적된 액적의 제거에 긍정적일 것으로 기대되었다. 더 나아가 실험에서 측정할 수 없었던 유동 영역 내의 성능 분포에 대한 결과도 얻을 수 있었는데, 비슷한 전류 밀도를 얻을 수 있더라도 배치의 방향에 따라 연료전지 입구와 출구 사이의 성능 편차가 변화하였다.

더욱 발전된 양극 유로 배치 전략에 대해 제시하기 위하여 더 큰 유동 영역에서 해석을 진행하였다. 잠재적으로 물 축적과 물질 전달 저해가 우려되는 영역이 유로의 주된 진행 방향과 수직한, 즉 유로의 폭 방향으로 형성되는 것이 예상되어, 유로 폭 방향으로도 불균

일한 유로의 형상 변화를 피할 수 있음을 시사했다. 구조의 벽 두께를 유로 폭 방향에 따라 변화를 줌으로써 중앙부의 유동 저항을 늘리고 주변부의 유동 저항을 감소시켜 성능 저하가 우려되는 영역에서 물질 전달을 강화시킬 수 있었다. 유동 해석을 통하여 전류밀도의 불균일함이 일정부분 해소됨을 보였으며 이를 실험적으로 추가 검증하기 위하여 내구성 실험이 진행되었다. 그 결과 폭과 길이 방향으로 모두 유로 형상이 불균일하게 변하는 설계 전략으로 유동 불균일로 인한 내구성 감소를 완화시킬 수 있음을 보였다.

주요어: 고분자 전해질막 연료전지, 금속 분리판, 불균일 설계, 전산 유동 해석, 성능 증가, 내구성 실험
학번: 2017-26437